VALIDATION OF A STRIP THEORY APPROACH TO ESTIMATING SHIP MOTION FROM SEA STATE

By

Funanya Martha Azimoh

Thesis submitted in fulfilment of the requirements for the degree

Master of Engineering in Mechanical Engineering

In the

Faculty of Engineering an the Built Environment

at the

Cape Peninsula University of Technology

Supervisor: **Prof Graeme John Oliver**

Co-supervisor: **Mr Butteur Ntamba Ntamba**

Bellville Campus

September 2023

DECLARATION

I, Funanya Martha Azimoh, declare that the contents of this dissertation/thesis represent my own unaided work, and that the dissertation/thesis has not previously been submitted for academic examination towards any qualification. Furthermore, it represents my own opinions and not necessarily those of the Cape Peninsula University of Technology.

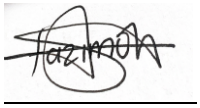

07/09/2023

Signature Date

ABSTRACT

A method to estimate the ship motion on board of a vessel underway is presented in this work. Oscillatory ship motions in four degrees of freedom (heave, surge, roll, and pitch) are measured using a low-cost combined gyro and accelerometer-based instrument placed near the center of mass of the vessel. Measurements were recorded from the SA Agulhas II, a South African Polar Supply and Research Vessel on a regular trip from Cape Town to the polar region in the Southern Ocean. The motion power spectra for different degrees of freedom are determined from time series. The electronic filter analogy is used in this study. Response Amplitude Operators are used to predict the ship motion response to the wave through various frequencies and directions. Response Amplitude Operators were computed numerically for roll and pitch as well heave and surge using a hydrodynamic strip code for seakeeping for different ship speeds. The ship motion obtained from the sensors are compared to motion spectra computed from visual observation entries recorded from the vessel's logbook using the Bretschneider Ansatz model and wave spectra computed from a re-analysis of remote sensing data from the European Centre for Medium Weather Forecast. In the conclusion, considering there were a certain margin of error in the visual observations, a good agreement was obtained for all degrees of freedom. A much better agreement was achieved when compared with the reconstructed sea state from a re-analysis of remote sensing data.

ACKNOWLEDGMENTS

A special thanks to God almighty because without him this would not have been possible.

Firstly, I would like to express my gratitude to my co-supervisor Mr Butteur Ntamba Ntamba from the Department of Maritime Engineering at the Cape Peninsula University of Technology. He dedicated his time to ensure that I finished this thesis. For the effort, patient, guidance, corrections and always being available whenever I needed assistance. I have learnt a lot from you and am super grateful.

Secondly, I would like to thank Cape Peninsula University of Technology for sponsoring my studies, especially the financial departments they probably got tired of receiving emails from me.

Thirdly, I would like to say a big thank you to brother and friend a PHD student Victory Opeolu for all the encouragement and support. Many times, I tried to give up, but you kept pushing me to move forward.

Then a special thank you to my husband, son and sister for always assisting, encouraging and supporting me in every obstacle that came my way. You are amazing.

Lastly, thank you to my supervisor Prof Oliver from the Department of Mechanical Engineering at the Cape Peninsula University of Technology.

TABLE OF CONTENTS

LIST OF FIGURES

LIST OF TABLES

ABBREVIATIONS

ECMWF - European Centre for Medium Weather Forecast

BCE – Before Common Era

ERA5 – Fifth Major Global Reanalysis

Deg - Degrees

DOF – Degree of freedom

Hz – Hertz

RAO - Response Amplitude Operator

PDStrip – Public Domain Strip

PSD – Power Spectrum Density

SA – South Africa

CHAPTER 1

INTRODUCTION

1.1 Introduction

Ships are the oldest form of water transportation, dating from 8040 to 7510 BC (Stilwell et al. 2020). Ships are essential in human society and have been used for thousands of years for travel, trade, and warfare. It is critical to comprehend and analyse the various motions of ships in various sea conditions. If sea conditions are not carefully monitored, they can be very unpredictable and dangerous for ships (Stilwell et al. 2020).

In this research, the aim is to investigate ship movement (act of moving body) and motion (state of progression from one place to another) of vessel. Ships typically move at a mean forward speed and oscillate in waves over a steady flow field. The ship is treated as a rigid body with six degrees of freedom when determining its motion in waves.

Degrees of freedom are often employed in engineering to explain the motion or behaviour of mechanical systems. They can be used to define the number of independent variables that control the behaviour of a dynamic system, or the number of independent coordinates needed to represent the position and orientation of a rigid body in space. Degrees of freedom can be used in maritime research to analyse and develop many features of ships and offshore structures. It can be used, for instance, to calculate how many separate motions a floating platform or vessel can experience under various environmental circumstances. (Hibbeler, 2004)

There are six degrees of freedom, and they are classified into three translational degrees (heave, sway and surge) and three rotational degrees (roll, pitch and yaw) (Menon, 2021). Translational motion is the movement of a body in which every point moves at the same rate (Menon, 2021). Rotational motion on the other hand refers to the movement of a body in which different points move at different speeds depending on their position. These concepts are discussed in more detail in the literature review chapter (Chapter Two).

In this research, the aim to understand and quantify ship motion through different approaches using the different degrees of freedom: heave, surge, roll, pitch, yaw, and sway. Note that while there are six degrees of freedom that the ship moves in, this research will focus primarily on the first four. Yaw is generally considered less detrimental to ships since it is primarily induced by wave coupling that acts perpendicular to the vessel's length, as noted by Menon in 2021. On

the other hand, sway has the potential to inflict damage, but its occurrence is less frequent due to specific wave conditions, as mentioned by Menon in the same source.

1.2 Problem Statement

Ships are bound to be affected by the effects of hydrodynamics while on the move. Consequently, the instability of ship movement has a profound effect on their navigational behaviour. Engineers can enhance ship design technology by comprehending ship motion, allowing them to optimize and improve existing systems. In this research, the aim to gain more insight from understanding ship motion using experimental results, providing a comparative analysis of the different experimental results.

1.3 Objectives and Aim

The primary aim of this research is to investigate ship motion of the SA Agulhas II. This is done using an electronic filter analogy[1] and experimental analysis of the ship. For the experimental analysis, data is collected using two gyroscopic sensors and processed the results using specialized software[2]. Note that the theory, our processes, and systems employed are explained further in the next few chapters. To successfully complete this research the following objectives, need to be achieved.

- Computing the ship motion. This involves the following:
    - Investigate ship motion by remote sensing. This is done by acquiring wave data (ERA5) from the European Centre for Medium-Range Weather Forecasts (ECMWF).
    - Evaluating ship motion by capturing data from visual observations, and further processing it using the Bretschneider spectrum.
- Determine ship motion using electronic filter analogy. This approach involves understanding the Response Amplitude Operator (RAO) of the ship.
- Evaluate the results provided from the sensors installed to understand if they provide accurate data of the ship's motion.

[1] The electronic filter analogy refers to a conceptual framework used to understand and analyse systems, by drawing parallels to the behaviour of electronic filters. By mapping the parameters and behaviours of the system to the components and characteristics of an electronic filter, can apply well-established principles and techniques from electronic filter theory to gain insights, design algorithms, and/or develop mathematical models for the system at hand (Oppenheim et al, 1997; Mitra, 2011; Svoboda and Dorf, 2013).

[2] Software includes Matlab and PDStrip.

- Perform a comparative analysis of the above approaches taken, providing feedback on how their results are consistent and/or conflicting. Will the ship motion measured from the sensors agree with the computed motion using wave data from ECMWF (satellite/remote sensing) and visual observations?

1.4 Background to Research

The earliest form of waterborne vessel dates to 4000 BC in Egypt, where boats were an important mode of transportation that evolved over time. Because the Egyptian boats were confined to the Nile and relied on the wind for navigation, they had sails and oars. Navigation by sea began in the third millennium BC with a voyage to Crete, followed by trade down to the eastern coast of Africa (Stilwell et al. 2020).

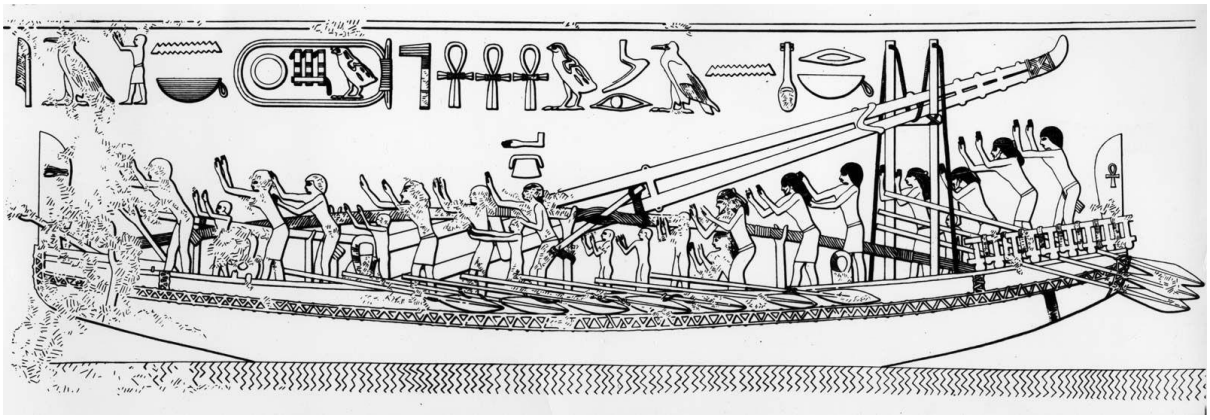

Figure 1: The Egyptian Sea Going Drawing 2600 BCE (Stilwell et al, 2020).

Ship design necessitates a wide range of engineering and technology. A good design is essential for effective and safe maritime operations. The Archimedes principle, which states that for a body to float, the weight of a static body must be equal to the weight of the volume of water it displaces, is used in the basic design of a vessel. This is also known as the buoyancy law. The hull determines a ship's ability to withstand moderate damage, sea conditions, and sink slowly. The hull is built in the shape of a rectangular box; it must be wide for adequate stability and strength, and it must be deep for beam bending in the longitudinal plane (i.e. have sufficient radius of gyration to resist bending) (Stilwell et al. 2020).

The dynamic interaction between the water and hull resistance to maintain forward motion governs the hull shape. The resistance to steady forward motion is affected by four factors: (1) water-hull surface friction, (2) wave energy impacting the hull, (3) energy dissipation due to swirl around the hull and rudder, and (4) air resistance for the ship parts above the water line.

All these factors are considered when designing the hull, and the resistance determines the propellant power (Stilwell et al. 2020).

Propulsive power is the amount of power required to propel the ship, and it is directly proportional to the ship's speed. Only when an external force or moment acting is required for the ship to deviate from its original course is it considered stable. It is considered unstable, however, when it deviates from its original cause without the assistance of external forces and its heading can only be maintained by manoeuvring (controlling) (Molland, 2008).

Manoeuvring is defined as a vessel's planned motion or action that involves yaw (rotation about a vertical axis) and sway (sideways motions). The ship in motion experiences all six degrees of freedom, all of which are undesirable except when changing course and yaw is required. As a result, being able to predict the ship motion will allow for better manoeuvring (Molland, 2008).

1.5 Related Literature

In this research, the aim to investigate ship movement and motion of vessels. Various methods have been used over the years to estimate ship motion. Some of these studies are summarized in this section.

Lewis (1929) determined the two-dimensional characteristic of the transverse unit using the hydrodynamic force, which was incorporated into the strip theory. He calculated a three-dimensional correction factor for an exact solution of a prolate spheroid. This was the first application of strip theory in ship hydrodynamics.

Ogilvie (1962) pointed out that when developing a theory of ship motion, one needed to include the general features of a damped resonant system. He reviewed attempts to describe a satisfactory perturbation theory for ship motions based on describing the associated boundary-value problem and the limitations of the various approaches various researchers have come up with.

Ogilvie used a qualitative analogy to show that a plot of heave amplitude versus wave height indicates the presence of a resonance condition that describes the spring-mass system over the resonance frequency. He also showed that, to successfully predict heave and pitch motion, the

equation of motion for a simple sinusoidal excitation must have coefficients that are frequency functions with the general characteristics of a damped resonant system (Ogilvie, 1969).

Because it is difficult to solve for the entire ship motion using hydrodynamics, most numerical algorithms rely on strip theory. The filter technique used to estimate ship motion in real-time simulations was invented by Kalman. This technique necessitates knowledge of the ship parameters, which are not always available (Triantafyllou, 1983).

Fournier (1986) used the wave model to determine ship motion by computing the height, pitch and roll of a ship using the sea surface height underneath the ship. The roll and pitch of the vessel is rotated to the tangent plane aligning it to the origin. This method is not flexible because only the sea surface height is taken into consideration. Therefore, ships of different shapes will all have the same response if the wave conditions are the same (Fournier, 1986).

Zhang et al. (2014) developed a mathematical model that calculates the total force acting on the ship in order to estimate the ship's motion. The differential equation between acceleration and force is derived using Newton's law. Because this method was designed primarily for harbour use, it can only determine yaw, sway, and surge. This method is untrustworthy and becomes inapplicable when the vessel is at sea (Zhang et al, 2004).

Chen et al. (2017) interpolated ship movements with a novel algorithm. The ship's course and speed are interpolated with an approach that forecasts the vessel position over an interpolated time period. This method employs the Automatic Identification System (AIS). For modelling, AIS data is collected and interpolated using software such as MATLAB. This method detects inaccurate ship motion data and can be used to overcome a loss of ship motion data (Chen et al. 2017).

Zhang et al. (2021) used an approach called the Long Short-Term Memory (LSTM) classic time series prediction, an approach that can capture the fundamentals of ship motion from each frequency range since wavelet transform is used to break down ship motion signals into different frequency scales. The weights of the various scales are then determined by the attention mechanism, which increases the sensitivity of the entire system by focusing attention on important information and reduces noisy signal interference. Data on ship motion are used to assess the viability and efficiency (Zhang et al.,2021).

Wu et al. (2022) used maritime radar with a multi-sensor fusion perception system. Where the first step is to build a hardware platform for the multi-sensor fusion ship motion perception

system, which consists of maritime radar, AIS, cameras, and other accessories. The ship motion data gathered from the three sensors is merged by using target detection and tracking algorithms and track association algorithms. Field studies conducted both during the day and at night serve as proof of the ship motion perception system's effectiveness (Wu et al., 2022).

Another approach that has been recently used by Meng et al. (2022), is a full-scale trial using a parameter identification scheme Support Vector Regression (SVR). SVR is used in the research of grey box identification modelling to generate the rough parameter reference values for the nonlinear whole-ship mathematical model and the ship response mathematical model. The modified grey wolf optimizer (MGWO) method and Firefly Algorithm are used to further improve these approximate reference values to provide the final parameter identification values. Recursive least squares with forgetting factor and the three algorithms' final parameter identification values are replaced into the mathematical model to get the predictions for ship motion state (Meng et al., 2022).

1.6 Delineation of Research

- The study will not be limited to zero speed but will account for forward speed.
- Water depth is considered as constant in space and time.
- Non-linear solutions to the hydrodynamic problem will not be considered.
- Propeller forces, wind forces, rudder forces and induced forces due to the shipping of water on the deck will all be ignored.

1.7 Thesis Outline

- Chapter 1: Introduction

This chapter gives a brief introduction about wave spectra and ship motion. This chapter defines what the problem statement is and the background to the study. Related literature, the objective and aim are also listed in this chapter.

- Chapter 2: Literature Review

In this chapter, a detailed summary of the literature is reviewed about the wave spectrum and previous studies of ship motion.

- Chapter 3: Experimental Setup and Performance

This chapter explains the experimental procedure and the data collection set-up.

- Chapter 4: Test Results and Discussion

The results obtained are discussed, numerical and experimental methods are compared.

- Chapter 5: Comparison

The chapter results from chapter 4 are compared and analysed.

- Chapter 6: Conclusion

This chapter concludes the thesis and future works are discussed.

CHAPTER 2

THEORY AND LITERATURE REVIEW

2.1 Description of a Wave

The current state of hydrostatics knowledge makes it relatively simple to design a vessel that meets the requirements for stability in calm water. However, ships rarely sail in calm water. Instead, they must contend with more difficult conditions subject to wind, current, and wave forces. The dynamic response of the ship to these forces will differ depending on the craft and loading conditions (Perez and Fossen, 2005).

Regular waves are known as ideal waves. They can be represented by a single sinusoidal section with a height, period, and direction (Lloyd, 1998). Regular waves do not occur in the sea environment naturally but can be generated in a towing tank for experimental purposes.

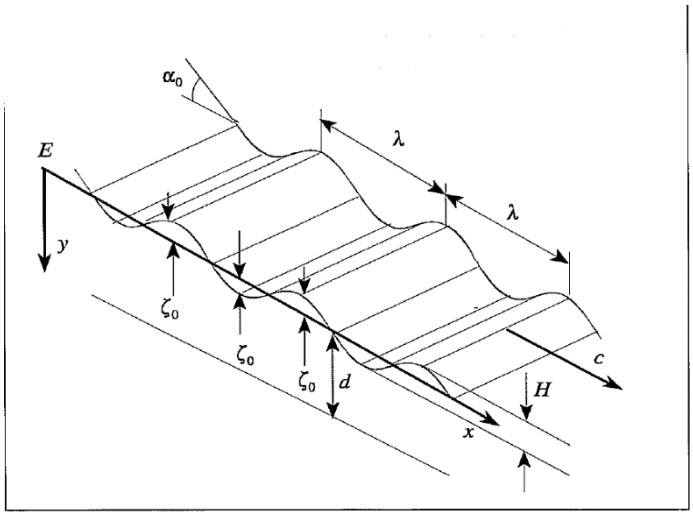

Figure 2: Regular Wave Train (Lloyd, 1998).

In figure 2 a two-dimensional regular wave train is shown at a constant depth *d*, moving on the water surface. The wave is two-dimensional, which means that it moves in the x-direction and has a crest that is perpendicular to the x-axis. The highest point on the wave is called the crest, and the lowest point is called the trough. The crest advances in an orderly manner at constant velocity *c*, wavelength λ and period *T* ensuring that the wave does not overlap. The amplitude a is calculated by measuring the distance from the water level to the crest or trough. Wave height *H* is measured from wave's trough level to the crest and can be twice the amplitude. The dimensionless wave steepness is defined as the ratio of wave height to wavelength. The shape

remains constant, and the train moves like a ridged sheet, with energy generated by changes in kinetic and potential energy (Lloyd, 1998).

Irregular waves that affect the behaviour of marine structures at sea can be represented by superimposing or adding a suitable assembly of regular waves (Lloyd, 1998). The nature of irregular waves exhibits a simplex sinusoidal wave pattern with varying wavelengths, height, and direction (Molland, 2008). Figure 3 shows a plot of recorded regular waves which sums up to an irregular wave.

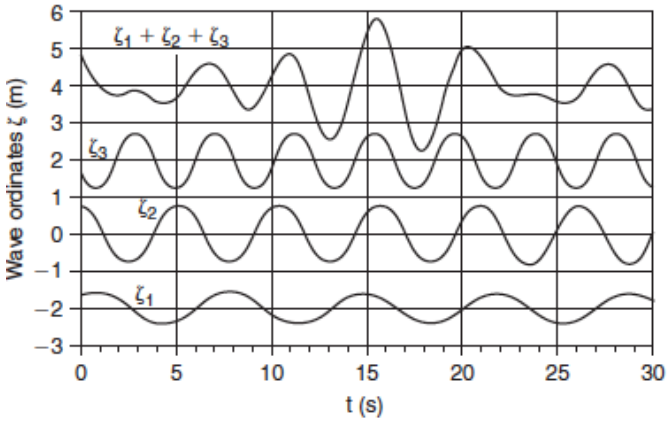

Figure 3: Irregular Wave from Sum of Regular Wave (Molland, 2008)

The main parameters associated with any type of wave are wavelength, wave height, wave period and wave propagation.

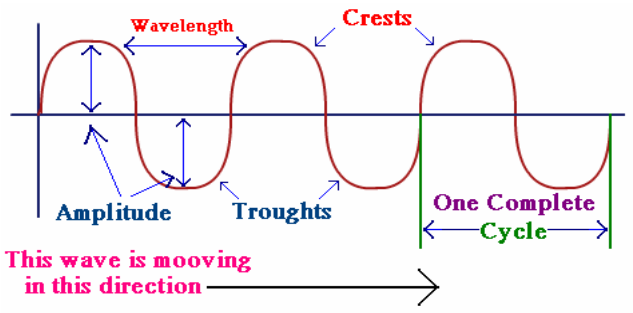

Figure 4: Wave Characteristics (Ju, 2021).

- Wave height: vertical distance from trough to crest, it is always referred to as two times the amplitude.
- Wavelength: distance from crest to crest of two consecutive waves in the direction of propagation,
- Wave period: time interval between the arrival of consecutive crests at a stationary point, and

- Wave propagation direction is the direction in which the wave is moving.

While wave height is one of the main wave parameters, in each area, waves have a range of heights. For scientific analysis of waves, the parameter or characteristic height over some time is expressed as significant wave height usually denoted by H_S. The significant height is the average height of the highest one-third of the waves in each period. During visual observation of the sea state, a trained observer (ship crew) will estimate the significant height. The maximum wave height, H_{max} is approximately 1.6 – 2 times the significant wave height (Molland, 2008).

2.1.1 Directional Wave Spectrum (DWS)

Directional Wave Spectrum (DWS) is the representation of ocean's wave energy, which sums up the water surface as sinusoidal waves with varying frequencies, amplitudes and directions as shown in figure 5. In other words, wave energy describes the energy of the waves distributed with frequency and direction. The area encompassed by the frequency and the directional range will be proportional to the total energy per square meter of the sea surface of all the wave components. The overall frequencies and directions of the total enclosed area by the wave spectrum are proportional to the total energy held by the wave field due to integration (Molland, 2008)

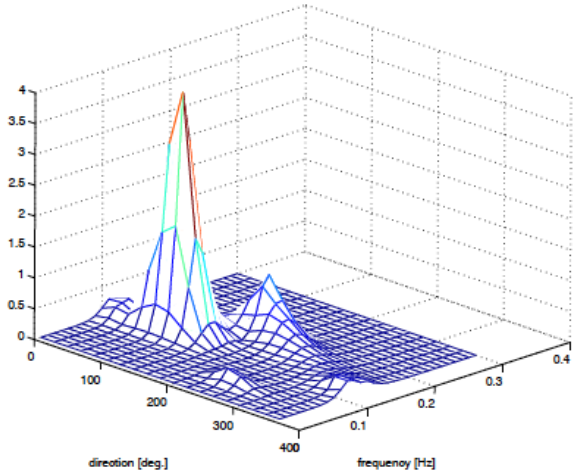

Figure 5: A 3-D Directional Wave Spectrum (Molland, 2008).

The spectrum of ocean waves can be estimated using parametric and non-parametric modelling. When the dimensions of a model are changed, parametric modelling can change the shape of the geometry. Non-parametric modelling frequently violates the normal distribution of a wave because it uses continuous data rather than discrete values. The term non-parametric, on the other hand, does not imply that the value lacks critical parameters; rather, the parameters are adaptable and can vary. The set-up conditions or equations related to the measured ship responses are similar in that both methods use linear spectral analysis (Munoz, 2014). For this research, the focus is on using parametric modelling to determine the ship motion.

Directional Wave Spectrum (DWS) and the cross spectra of ship motion time series (ϕ_{mm}) are related by Response Amplitude Operators (RAO) assuming linearity between waves and ship response. The ship motion ϕ shown through the following integral:

$$\phi_{mm}(\omega) = \int_{-\pi}^{\pi} RAO_m(\omega,\theta).RAO_n(\omega,\theta).S(\omega,\theta).d\theta \quad (1)$$

ϕ_{mm} – Cross spectra of ship motion time series

$\omega -$ Frequency

$\theta -$ incidence direction

$S(\omega) -$ Power spectrum

$n -$ the degree of freedom

The power spectrum can be obtained from directional spectrum by:

$$S(\omega) = \int_{-\pi}^{\pi} S(\omega,\theta)d\theta \quad (2)$$

The disadvantage of this method is that it generates a non-linear programming problem for the numerical solution, which is computationally costly. In practice, linearised theories are used to simulate irregular waves and obtain statistical estimates. The wave elevation of a wide area of irregular sea travelling along the x-axis can be given by the sum of many wave components (Faltinsen, 1993).

$$\zeta = \sum_{j=1}^{N} A_J \sin(\omega_j t - k_j x - \alpha_j) \quad (3)$$

where,

A_J: wave amplitude

ω_j: circular frequency of wave component *j*

k_j:wave number of wave component *j*

α_j: random phase angle of wave component *j*

N : number of wave component

x: position at the axis *x*

The wave amplitude A_J can therefore be expressed by a wave spectrum $S(\omega_j)$

$$\frac{1}{2}A_j^2 = S(\omega_j)\Delta\omega \tag{4}$$

where,

$\Delta\omega$ is a constant difference between successive frequencies.

$S(\omega_j)$: is the wave spectrum with respect to circular frequency

2.1.1.1 Definitions of Directional Wave Spectrum

Several definitions of directional wave spectrum under certain conditions have been proposed by scientists such as Pierson-Moskowitz, JONSWAP, and Bretschneider. These definitions have been accepted by the scientific community. Each of these spectra represents a domain, but all wave spectra can be identified using a general formula for the unknown wave model.

$$\left\{S(\omega) = \frac{A}{\omega^5}\ \exp\ \left(\frac{-B}{\omega^{-4}}\right)\right\} \tag{5}$$

Where:

$S(\omega)$: Spectral ordinate

A and B: Coefficients are parameters of wave factor

ω: Circular frequency

A brief explanation of each spectrum is written below.

Pierson-Moskowitz Spectrum: Is a theoretical ocean wave spectrum than can only be used in deep sea with an assumption that all waves begin at an equilibrium state with a long-lasting wind. The spectrum is dependent on the speed, height and period of a wave that are identified as one parameter. The spectrum was worked out using the general formula in equation 5 with slight modifications (Zwolan and Czaplewski, 2012).

$$A = \alpha g^2 (2\pi)^{-4} \qquad B = \frac{4\alpha g^2}{(2\pi)^2 H_S^2}) \tag{6}$$

where:

α: statistical fit parameter = 0.00810

g: acceleration of gravity

β: encounter angle = 0.74

U: Wind speed

H_s: Significant wave height

ω_p: Circular frequency at spectral peak

JONSWAP Spectrum: The Joint North Sea Wave Program known as JONSWAP was implemented to understand the wave spectrum in shallow waters and extreme sea conditions. This spectrum is mainly used for studies or analysis and is dependent on two input parameters: frequency and amplification coefficient (Zwolan and Czaplewski, 2012).

$$S(\omega) = \alpha g^2 (2\pi)^{-4} \omega^{-5} \exp\left[-\frac{5}{4}\left(\frac{\omega}{\omega_p}\right)^{-4}\right] \gamma^{\exp\left[\frac{(\omega-\omega_p)^2}{2\tau^2\omega_p^2}\right]} \tag{7}$$

$$\omega_p = 2\pi/T_p$$

$$\alpha = 0.0076\left(\frac{U_{10}^2}{F_g}\right)^{0.22}$$

where:

γ: Peakedness factor

α: Statistical fit parameter = 0.00810

g: Acceleration of gravity

ω: Circular frequency

Bretschneider Spectrum is a modified two-parameter version of the Pierson-Moskowitz spectrum based on research done in the North Ocean. This spectrum is based on the wave height and peak period from equation 5 (Zwolan and Czaplewski, 2012)

$$A = \frac{5H_S^2\omega_p^4}{16} \qquad B = \frac{5\omega_p^5}{4} \tag{8}$$

ITTC Spectrum: The International Towing Tank Conference, an organisation of voluntary associations which work with predicting the performance amongst marine ships, proposed a two-parameter wave spectrum, as shown in equation 5.

$$A = \frac{173H_S^2}{T_1^4} \qquad B = \frac{691}{T_1^4} \tag{9}$$

T: is the period

This spectrum is considered the same as the Bretschneider spectrum.

Wave Comparison Spectrum: Figure 6 shows a comparison between the different wave spectra presented for a significant wave height of 5m and the modal frequency of $\frac{2\pi}{9.7}$ rad/s.

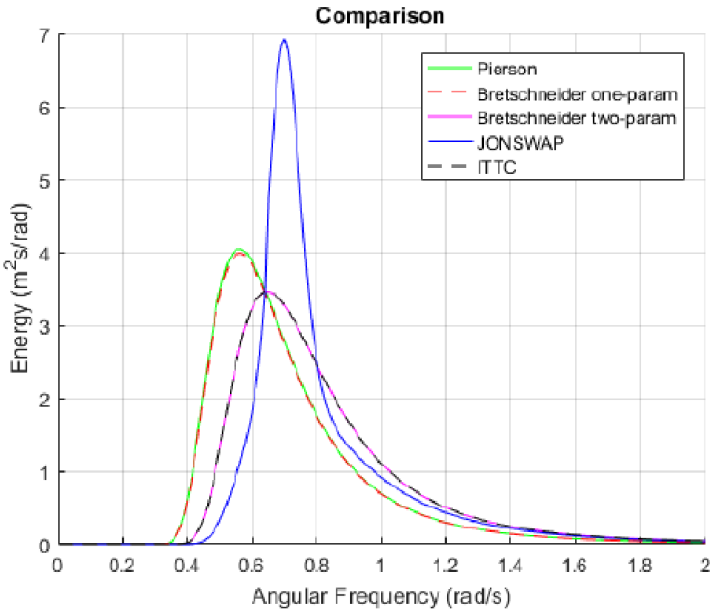

Figure 6: Comparison of two spectra (Molland, 2008).

Different spectra may be more appropriate for different ocean environments and types of structures or systems being designed. It is important to note that no single spectrum can fully

capture the complexity and variability of ocean wave behaviour, and each approach has its pros and cons.

For this thesis, Bretschneider Spectrum will be used to determine the sea state. This is because it is identical to the ITTC spectrum. Also, it is based on a more general statical analysis of the ocean wave data and can be applied to a wide range of ocean conditions with the JONSWAP spectrum and Pierson based on measurements from specific regions (the North Sea and Ocean generally) (Zwolan and Czaplewski, 2012).

2.2 Ship Motion

Vessels are built for transportation purposes and should meet certain requirements such as acquiring enough speed, floating upright and being able to be maneuverer as required. Hydrostatic knowledge makes it easier to meet these requirements in calm water, however, the ship rarely sails in calm water due to the various conditions at sea. In other words, in the seaway, the vessel's stability is severely affected by forces from wind, waves etc. The dynamic response to these forces will be determined by the loading condition for each vessel; thus, it is critical to design the vessel with capability against dynamic vulnerabilities (Tawfeek, 2018).

To prevent large amplitude motions in various conditions, comprehensive studies of dynamic instabilities must be conducted in order to provide the ship master with improved decision support tools. The advancement of computer technologies has made it easier to achieve this goal in real-time by installing numerical simulation programs onboard that produce easily interpretable output that will aid navigation in adverse weather conditions (Tawfeek, 2018).

Ship motion is described by movement in the six degrees of freedom. The six degrees of ship motion includes three translational DOF heave, sway, surge and three rotational roll, pitch and yaw. These motions are illustrated in figure 7 (Menon, 2021).

Translational:

- Heave: the linear up and down motion through the Z axis
- Sway: the linear left to right motion through the Y axis
- Surge: the linear front and back motion through the X axis fore-aft

Rotational:

- Roll: Refer to Figure 7 for the front and back rotation about its longitudinal X axis
- Pitch: the up and down rotation about its transverse Y axis

- Yaw: the turning rotation of the vessel about its vertical Z-axis (Zwart,2017)

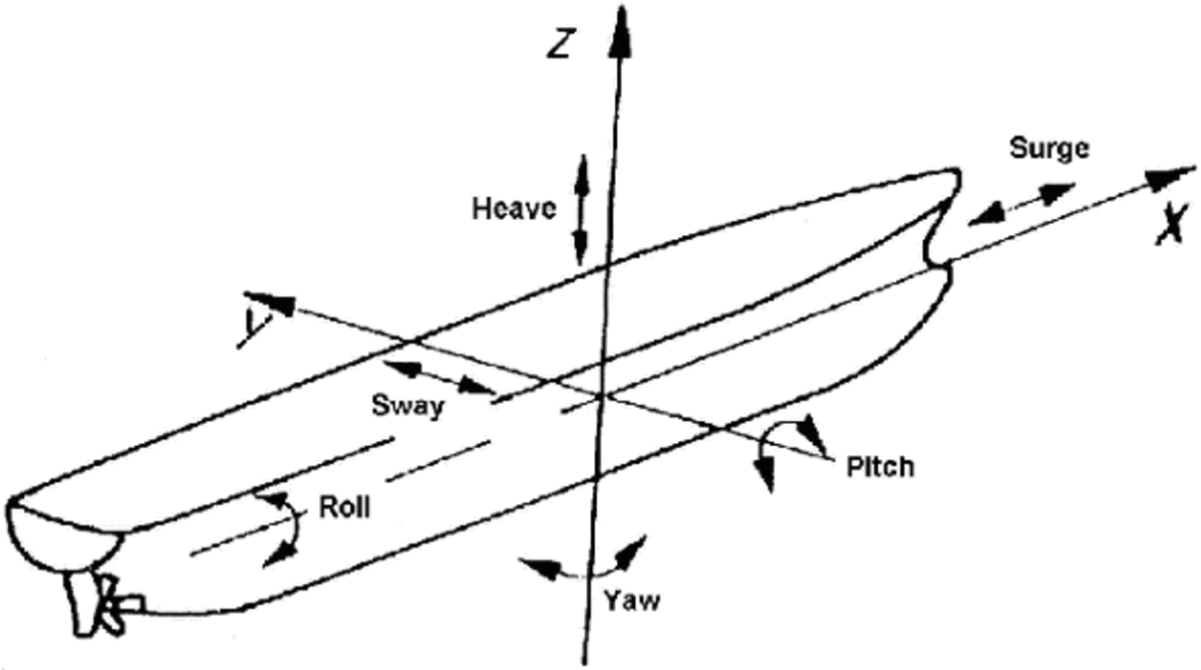

Figure 7: Ship motion notions (Prasanna, 2014).

All degrees of freedom (DOF) of a ship are affected in waves, and the most important ones are linked to a restoring force (OpenStax, 2023). Roll, surge, pitch, and heave are the four major DOF that predominantly affect the ship's stability (Menon, 2021).

The equations of motions of a ship in the water are derived from Newton's second law below:

$$\vec{F} = ma = \frac{d}{dt}mv$$
$$\vec{M} = \frac{d}{dt}\vec{H} \quad (10)$$

Where:

$\vec{F}$ is the external force applied to the centre of gravity

v is the velocity of the centre of gravity

m is the mass of the body

a is the acceleration of the centre of gravity

$\vec{M}$ is the external momentum applied at the centre of gravity

$\vec{H}$ is the angular momentum applied at the centre of gravity

The acceleration of a ship is calculated by Newton's second law of motion, it considers the ship to be a rigid body subjected to external forces due to the propulsion system, rudder, fins, the relative motion of the water and the environmental forces due to wind and waves. The accelerations are integrated twice to obtain the position and orientation as the ship manoeuvres (McCreight,1991). However, the flow velocity is categorized into two- or three-dimensional problems to be solved in the time or frequency domain using linear or non-linear methods.

The flow velocity around the ship is calculated as for an ideal fluid. The flow field can be represented by the scalar fluid velocity Φ which deals with the continuity equation and boundary value within the fluid domain. The fluid is ideal which means it is homogeneous, inviscid, incompressible and without surface tension, it is used to obtain the potential flow around the ship (Fonseca, 2010; Uzunoglu, 2011). The relationship for the conservation of mass reduce to the equation of continuity for an ideal fluid:

$$\frac{\partial u}{\partial x}+\frac{\partial v}{\partial y}+\frac{\partial w}{\partial z}=0 \tag{11}$$

where u, v and w are the fluid velocity vector components
If the fluid is inviscid then it is also irrotational (there is no vorticity, or it remains constant), therefore:

$$\vec{V}=\nabla\Phi \tag{12}$$

The fluid is taken as being inviscid and incompressible hence the fluid velocity potential can be defined as a scalar which reduces the continuity equation to the Laplace equation:

$$\nabla^2\Phi(\overrightarrow{x_0},t)=\frac{\partial^2\Phi}{\partial x^2}+\frac{\partial^2\Phi}{\partial y^2}+\frac{\partial^2\Phi}{\partial z^2} \tag{13}$$

According to the Bernoulli equation, the fluid pressure can be determined once the velocity potential is known:

$$p(\overrightarrow{x_0},t)=-\rho\left(\frac{\partial\Phi}{\partial t}+\frac{1}{2}|\nabla\phi|^2+gz_0\right) \tag{14}$$

$p(\overrightarrow{x_0},t)$ represents the fluid pressure, ρ the fluid specific mass and g is the acceleration of gravity. The integration of the fluid pressure over the hull wetted surface results in the hydrodynamics forces acting on the ship.

A fully non-linear solution to the hydrodynamic problem is difficult and the linearisation of the problem is convenient. The velocity potential $\Phi(\overrightarrow{x_0}, t)$ must be divided into two components, namely the steady flow (Φ) and the oscillatory flow ($\underline{\Phi}$) to linearise this boundary condition.

$$\Phi(\overrightarrow{x_0}, t) = \Phi\left(x + U_{x,y,z,t}\right) = \underline{\Phi}(\vec{x}) + \underline{\Phi}(\vec{x}, t) \tag{15}$$

The unsteady velocity potential is then decomposed further into incident (incoming) waves (Φ^I), diffracted waves (Φ^D) and radiated waves (Φ^R):

$$\underline{\Phi} = \Phi^I + \Phi^D + \Phi^R \tag{16}$$

Finally, the radiation potential is then decomposed into components related to each of the six oscillatory ship motions:

$$\Phi^R = \sum_{j=1}^{6} \Phi_j^R, j = |1 \dots 6| \tag{17}$$

Building on the assumption of small motions, the equation of motion is given by:

$$\{F_k^M\} = \left[M_{kj}\right]\{\ddot{\xi}_J\}, \quad kj = [1 \dots 6] \tag{18}$$

$\left[M_{kj}\right]$: the mass matrix

$\{\ddot{\xi}_J\}$: the acceleration ve2Dctors

$\{F_k^M\}$: is the summation of the radiation forces, exciting forces and restoring forces.

The final second order and homogeneous equation are presented as follows:

$$\sum_{j=1}^{6}\{\left(M_{kj} + A_{kj}\right)\ddot{\xi}_J + B_{kj}\dot{\xi}_J + C_{kj}\xi\} = F_k^E \tag{19}$$

Each of these equations can be linked to a mass-spring-damper system. The F_k^E term represents the exciting forces on the right side of the equation and the damping, inertia and the restoring terms are on the left. For the non-linear time domain case, the equations are solved with numerical procedures for each time step. The non-linear equations of motion domain are given by:

$$\sum_{j=1}^{6} \left\{\left(M_{kj}(t) + A_{kj}(\omega, t)\right)\ddot{\xi}_j + B_{kj}\dot{\xi}_j + C_{kj}\xi\right\} = F_k^I(t) + F_k^D(t) + F_k^P(t) + F_k^R(t) + F_k^W(t) + F_k^D W(t), \quad k = [1 \dots 6] \tag{20}$$

The $F_k^I(t)$ and the $F_k^D(t)$ are respectively Froude-Krylov forces and the diffraction forces as in the frequency domain case. The $F_k^P(t)$ is the force created by the propeller, $F_k^R(t)$ is the force due to the rudder, $F_k^W(t)$ is the force exerted by the wind and finally the $F_k^D W(t)$ term stands for the force induced due to the shipping of water on deck.

After the linearisation and the application of the boundary condition and the Bernoulli equation, the equations for the exciting forces (F^E), radiation forces (F^R) and the hydrostatic forces (F^H) are obtained (Fonseca, 2010; Uzunoglu, 2011). The equations are then solved using an appropriate method (e.g. strip theory).

2.3 Strip Theory

In strip theory a ship is represented by a finite number of transverse two-dimensional strips or cross sections that are rigidly attached to one another. The motion of this floating body in waves is typically treated as a linear problem. However, strip theory can be used for both linear and nonlinear strip theories. Results from two-dimensional hydro-mechanic coefficients and exciting wave loads can be used to determine strip theory, which describes the forces acting to produce the motions of a three-dimensional floating body. These values will be numerically integrated across the ship's length. The ship is taken to be a rigid body (Suandar, 2013).

In 1929 Lewis studied the hydrodynamic disturbance of the added mass connected to the hull vibrations in structural modes. The gravitational forces and wave effects are ignored due to dominant inertial effects created by large characteristic frequencies. This was the first time the strip theory was introduced in ship hydrodynamics (Newman, 1978).

The ship's hydrodynamic disturbance can be categorized into two or three dimensions and are solved in the time or frequency domain using linear and nonlinear methods.

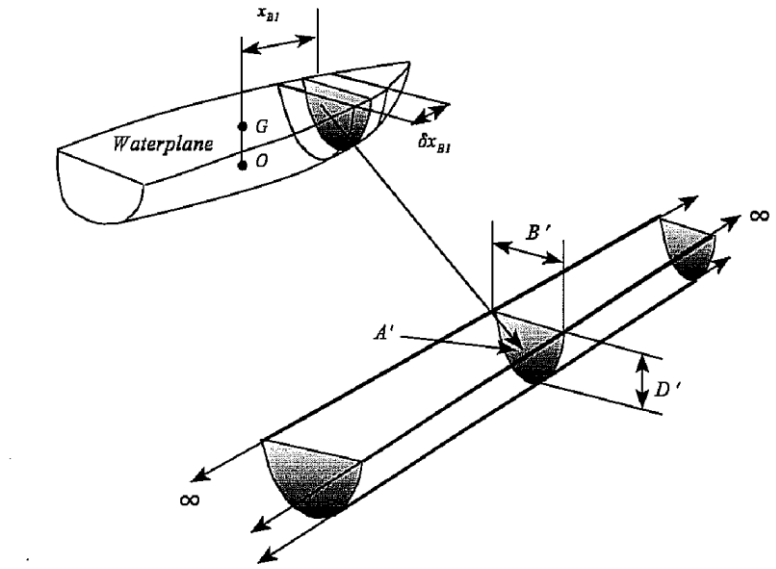

Figure 8: Representation of underwater hull section shape by an infinite cylinder (Llyod, 1998).

Figure 8 shows how the strip theory method analyses a strip of the ship's hull, assuming the length to be minor compared to the ship length and includes the local hydrodynamic properties such as mass, damping and stiffness which contributes to the coefficients for the complete hull in the equation of motion. The wave excitation experienced by the hull is composed of contributions from all the strips.

2.3.1 Linear Strip Theories

Strip theories are low-speed theories, so their applicability to fast ships is debatable (Newman, 1978). Linear strip theories have been used in naval architecture as the primary tool for estimating ship performance in waves due to their computational simplicity and general agreement with experiments. In irregular waves, the frequency-domain expression simplifies prediction and fatigue damage estimation. However, complications arise when there are nonlinear problems, such as extreme sea conditions, hull form optimization, and determining the maximum lifetime loads for the structural design. If the ship is designed to reduce both resistance and wave-induced motion, linear prediction of heave motion may lead to a different hull form optimization strategy (Newman, 1978).

2.3.2 Non-Linear Strip Theories

Model experiments and full-scale measurements have been conducted on nonlinear ship motions and structural measurements. In moderate seas, a nonlinear quadratic strip theory was expressed by Jensen and Pedersen (1976) to predict the wave load and ship response. Non-

linearity of exciting waves, flare-up the ship hull geometry and the distress of the two-dimensional hydrodynamic coefficient are caused by the quadratic terms.

There are many different types of strip theory used to predict the wave induced ship motion commercially. Some of these commercial software include AQWA, GL Rankine, MOSES, OCTOPUS, PDStrp and WAMIT. Gourlay et al. (2015) conducted a study that compared analyses from these commercial software on an experiment with three cargo ship models. The comparison was used to assess the suitability of each software for forward speed applications such as under-keel clearance in navigation channels as well as zero-speed applications such as berthed ship motion and under-keel clearance. The results showed that all the different software produced similar outcomes in wave induced motions and the model test results generally deviated from the numerical prediction for each in both directions. This means that we can anticipate reasonably accurate predictions of the motion response spectra and spectral properties of ship motions in irregular waves when integrating transfer functions of ship motions with energy spectra of irregular seaways. The strip method used in this thesis is PDStrip. (Gourlay et al. 2015)

2.4 Response Amplitude Operator (RAO)

Response Amplitude Operator (RAO) is the connection between the wave spectrum and the ship movements through implementation of a transfer function (Gjeraker, 2021). It is used to predict the expected forces and motion acting on the ship based on the wave activities. RAO is like a filter function which requires a wave spectrum as input and gives a motion spectrum as output. RAO has been separated into two sub-versions based on the findings for motifs and forces namely Force Response Amplitude Operator (FRAO) and Motion Response Amplitude Operation (MRAO) (Gjeraker, 2021).

The ship's response to waves is frequently considered linear and expressed in terms of RAO. The RAO is a frequency-dependent transmissibility function that provides the ratio to response input in the spectrum over the frequency range (Bell et al., 2018). The use of RAO necessitates that the relationship between the wave frequency and encounter frequency be considered. The two frequencies do not always have a mutual relationship (Bell et al., 2018).

The linearity between the wave excitation and the system response is based on the validation of this operator (RAO). To predict the ships motion response, RAOs are usually determined in regular seaways for various frequencies and directions either analytically, experimentally or through a numerical simulation (Gjeraker, 2021). Therefore, the RAO linearly relates the frequency component of one or more ship responses to the same components in the wave spectrum and describes how the response differs with frequency.

Superposition can be applied to determine the motion of the ship under the linearity assumption (Lewis 1988). RAOs are then used to predict forces acting on the ship based on wave behaviour as well as the expected motion of the ship once subjected to these forces. RAOs depend on the geometry of the hull, load conditions of the vessel as well as its speed and heading with respect to the waves. The first order of motion for the vessel is given by period and amplitude which are determined using potential theory.

RAOs transform signal linearly which means that the output signal (motion) are linear transformations to the input signal. In other words, a sinusoidal wave component is translated to another sinusoidal component with proportional amplitude, shifted phase and identical frequency. Transfer functions denoted RAO are usually expressed as the ratio of response amplitude per regular wave amplitude, which can be given in a phase form or a complex number. This is obtained by multiplication of the transfer functions with wave spectrum through equation (Bjornsson, 2013):

$$S_i(\omega, \theta) = RAO(\omega, \theta)^2 . S_j(\omega, \theta) \tag{21}$$

Where:
S_i: Response spectrum
S_j: Wave spectrum
RAO: Absolute value of the transfer function

RAO accuracy depends on the directional distribution of wave energy due to the wave direction being estimated visually and the measured spectrum contains all the wave energy from different directions. For a given wave spectrum and frequency the vessel motion response can be determined by:

$$S_i(\omega) = \int_{-\pi}^{\pi} S_j(\omega, \theta).RAO_i(\omega, \theta)^2 d\theta \quad (22)$$

The subscript i is for the Degree of Freedom (DOF) and S_i the response spectrum.

The equation for relationship between the RAO and ship motion energy spectrum can be written as:

$$RAO^2(\omega) = \frac{S_i(\omega)}{S_j(\omega)} \quad (23)$$

The RAO are very useful in understanding ship motion. By determining the RAO of the ship, which are able to predict ship motion and proactively take action based on the results. The actions can be in route planning, avoiding dangerous weather conditions and so on (Zwart, 2017).

The complex valued transfer functions are $RAO_i = (\omega_e, \mu)$ and $RAO_j = (\omega_e, \mu)$. i and j represent the relationship between the cross spectra and the directional wave spectrum. This was integrated by Bhattacharyya (1978) into the following equation:

$$S_{ij}(\omega_e) = \int_{-\pi}^{\pi} RAO_i(\omega_e, \mu) RAO_j^{\star}(\omega_e, \mu) S(\omega_e, \mu) d\mu \quad (24)$$

The * relates to the complex conjugate of a complex number. Taking the ship as a fixed axis, the $\mu = \theta$ rewriting the equation to:

$$S_{ij}(\omega_e) = \int_{-\pi}^{\pi} RAO_i(\omega_e, \theta) RAO_j^{\star}(\omega_e, \theta) S(\omega_e, \theta) d\theta \quad (25)$$

This equation derived from the ship motion is used to determine the wave energy spectrum through the motion energy spectrum (Iseki, 2000).

2.4 Encounter Frequency

Encounter Frequency is a seaway frequency adjusted based on the vessel speed and direction. For example, if a ship is moving toward the seaway at a constant velocity it will appear to meet the ship faster than the actual frequency of the wave. A vessel heading into the seaway encounters a greater frequency than the seaway frequency and moving in the same direction

the encounter frequency is lower. This frequency is observed and is used to calculate the actual wave frequency as seen in equation 28 below (Triantafyllou, 2003).

To drive the equation for encounter frequency ω_e, the incident angle of the ship μ and speed of the ship in direction of the wave $U_a = U\cos\theta$. The wave crest moves at different phases of speed $C_p = \omega/k$ and the relative speed between the ship and wave is written as:

$$U_r = U_a + C_p = U\cos\theta + \omega/k \tag{26}$$

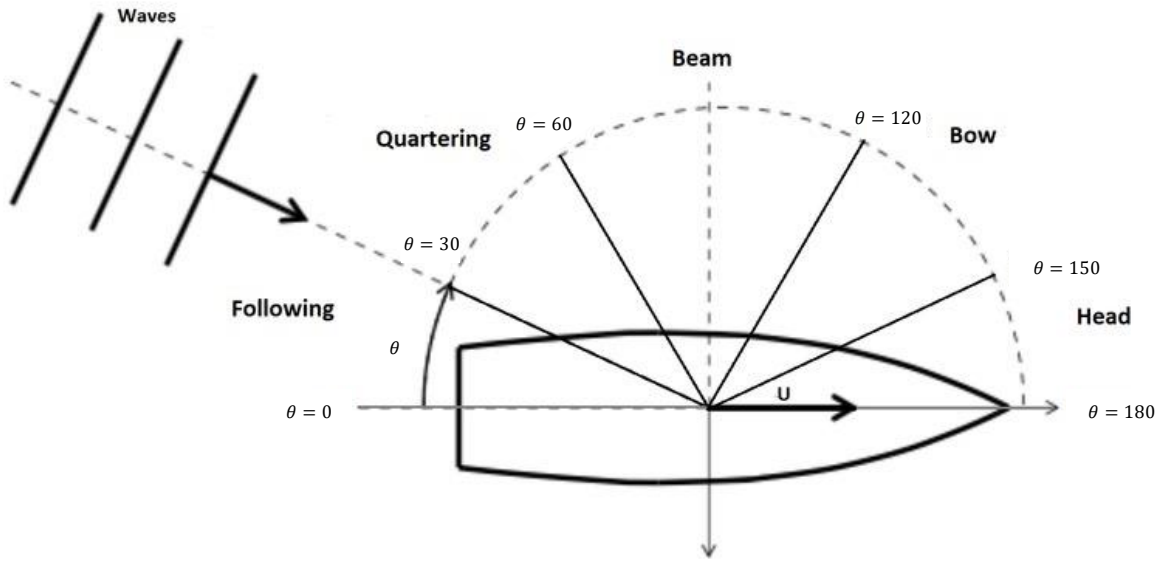

Figure 9: Relation of encounter angles (Selimovic, Lerga, Prpic-Orsic and Kenji, 2020)

Which means the U_r can be written as

$$U_r = \frac{\omega_e}{k} = U\cos\theta + \frac{\omega}{k} \tag{27}$$

Using this equation 9, the encounter frequency can be rewritten as:

$$\omega_e = \omega - \frac{\omega^2 U\cos\theta}{g} \tag{28}$$

The encounter frequency is observed, and the wave frequency will be derived through the encounter frequency equation, so taking the equation the actual frequency ω will be

$$\omega = \frac{g}{2U\cos\theta}\left\{-1 \pm \sqrt{1 + 4\omega_e \frac{U\cos\theta}{g}}\right\} \tag{29}$$

The heading angle determines the type of seas the ship experiences and are defined by the following:

Table 1: Types of Seas the ship experiences

Heading angle (θ)	Types of seas
0^0	Following seas
180^0	Head seas
90^0	Starboard beam seas
270^0	Following Seas
$0 \leq \theta \leq 90^0$	Quartering waves on the ship starboard side
$270^0 \leq \theta \leq 360^0$	Quartering waves on the ship port side
$90^0 \leq \theta \leq 180^0$	Bow waves on the starboard side
$180^0 \leq \theta \leq 270^0$	Bow waves on the port side

2.5 Seakeeping

Seakeeping is the ability of a vessel to withstand rough sea conditions. The seaworthiness must include all qualities in ship designs that allow the vessel to maintain safety while it continues with its duties. Predicting the ship's motions and wave loads with adequate engineering accuracy is crucial for ensuring the ship's strong seakeeping performance and safety. The assessment of seakeeping is extremely important, and two aspects are necessary (Kamal, 2007).

A ship response in waves containing the required frequency band comes after the wave conditions of the sea area, the assessment is related to how the total energy of the wave system is distributed with respect to frequency. The appropriate Response Amplitude Operator (RAO) will often describe these responses in terms of response per unit wave height. The evaluation of seakeeping of any ship design's performance depends on accurate theoretical hypotheses that have been verified by model tests and full-scale trials (Kamal, 2007).

Analysis of seakeeping of any ship’s design are usually obtained through theoretical predictions which are validated by model experiments and full-scale trials. Although numerous methods have been followed to estimate the ship's seakeeping. There are roughly three

approaches to investigate seakeeping which are: Numerical Approach, Experimental Approach and Full-Scale Measurement Approach (Kamal, 2007).

- Numerical Approach: This method is effective at predicting ship motion because it takes a variety of factors into account. It is separated into frequency domain and time domain, which are both frequently used for ship motion indicators. Hydrodynamic forces and ship RAO are mostly calculated using frequency domain analysis. The strip theory method is used in the frequency domain to determine all the force and motion coefficients as functions of frequency. The linear and non-linear methods are both time-domain methods. Though some excellent experimental findings have been obtained using linearized computations, nonlinearities have a greater impact on the outcomes, particularly when estimating the hull's immediate location in relation to the waves (Kamal, 2007).

- Experimental Approach: The most accurate way to assess a vessel's seakeeping is through experimentation. The main benefit of testing models is that ships don't need to be built to operate in the water. Model testing can be used to evaluate a ship's performance during the design phase. Appropriate measurements are typically simpler to make in model testing than at full scale. The experimental method is the best method for obtaining the RAO in regular waves since the wave may be controlled in the regular wave test. With this method, the model ship's actual behaviour can be discovered (Kamal, 2007).

- Full-Scale Measurement Approach: To verify a vessel's seakeeping performance, gather data for design purposes, and assess the reliability of numerical predictions and model testing, full-scale seakeeping trials are conducted. Full scale trials are not only utilized for seakeeping tests; they can also be used when the tasks of the vessel call for accurate estimation of ship motion and sea state. The full-scale approach pertains to motion analysis as a situation found in the real world (Kamal, 2007).

Seakeeping criteria can be defined into two characteristics: comfort standards that are met during working conditions and the capability of the vessel to carry out its mission. The governing criteria are the deck wetness, slamming, significant roll, pitch, and vertical acceleration. All of these address the effects of increasing motion on seaway-induced loads and dynamic stability (Bandyk, 2009).

To conclude, this chapter covers several important topics related to wave description, ship motion, strip theory, Response Amplitude Operators (RAO), encounter frequency, and seakeeping. The section begins by describing waves, specifically focusing on the directional wave spectrum (DWS). The DWS is discussed in detail, including various definitions that have been proposed in the literature. This provides a foundation for understanding the characteristics of waves in terms of their directionality and spectral content. Next, the review explores ship motion, which involves the movement of a vessel in response to wave forces. The concept of strip theory is introduced, highlighting both linear and non-linear strip theories. These theoretical frameworks are used to analyse and predict the behaviour of ships in waves, accounting for factors such as hull geometry and wave interactions.

The thesis also discusses the concept of Response Amplitude Operator (RAO), which represents the amplitude of ship motions in response to specific wave frequencies and directions. The RAO is an important parameter used in seakeeping analysis and design of ships and offshore structures.

Furthermore, the literature review touches upon the notion of encounter frequency, which refers to the frequency at which a ship encounters the most significant waves in a given sea state. Understanding encounter frequency is crucial for assessing the seakeeping performance and safety of vessels.

Finally, the section concludes with a discussion on seakeeping, which encompasses the ability of a ship to navigate and maintain its stability and safety in adverse weather conditions. Seakeeping analysis is essential in ship design, as it ensures that vessels can withstand and operate effectively in challenging sea states.

Overall, this literature review section provides an overview of key concepts related to wave description, ship motion, strip theory, RAO, encounter frequency, and seakeeping. It establishes a foundation of knowledge for the subsequent analysis and discussion in the research paper.

Full scale trails and a combination of other principles used to determine ship motion discussed in this chapter are used to obtain realistic results for the ship used in this thesis. The methods used are discussed in the next chapter.

CHAPTER 3

EXPERIMENTAL SETUP AND CALCULATION PROCEDURE

This research uses a comparison between measured ship motions obtained from a self-contained strap-on system which records the time series of roll, pitch and heave with motions computed from visually observed wave data and those obtained from the satellite (ECMWF). Experimental motion data were collected on the SA Agulhas II while the vessel was on a voyage in the Southern Ocean.

3.1 Measurement for Wave Spectrum

The wave data were obtained through visual observation from the recorded data in the vessel's logbook and available satellite data from European Centre for Medium Range Weather Forecasts (ECMWF).

3.1.1 Satellite Data

Satellite data are obtained from the ECMWF. This has over more than 50 years of development in numerical weather prediction and 100 years of development in synoptic and dynamic meteorology. ECMWF consists of five components: an ocean wave model, a general circulation model, data assimilation, ensemble forecast system and a monthly forecast system.

There are six equations that govern the ECMWF model, the first two are diagnostic and predict the static relation between different parameters.

- Gas Law – deals with the relationship between pressure, density, and temperature.
- Hydrostatic Equation – deals with the relationship between the air density and the decrease of pressure with height.
- Equation of Continuity – this determines the vertical wind speed and change in surface temperature through an expression for the conservation of mass.
- Equation of Motion – the acceleration and deceleration are described with respect to the pressure gradient force and the effects of Coriolis force contributes to the direction.
- Thermodynamic Equation – deals with the physical processes like evaporation, turbulent transport, radiative effects, condensation, and the changing temperature of air parcels by adiabatic cooling or warming during vertical displacements.

- Conservation of Moisture – deals with all expressions for the conservation of moisture content except for gains due to evaporation from clouds and rain, or from oceans and continents. Losses due to precipitation and condensation are not included.

The forecast will be based on the ECMWF Reanalysis 5th Generation (ERA5) which contains atmospheric parameters such as pressure and winds in different altitudes, surface parameters such as rainfall, air temperature, sea surface temperature, wave height and soil moisture content. ERA5 climate reanalysis gives a numerical description of recent climate combining models with observation. The ERA5 uses the 4DVar data assimilation in CY41R2 of ECMWF's integrated Forecast (IFS).

In this thesis, a 2D wave spectra for a specific time and grid points will be extracted from ECMWF using wave parameters such as significant wave height, mean period, and direction.

3.2.1.1 Procedures: The methods used to collect and process data.

All information was accessed through the ECMWF website. https://confluence.ecmwf.int/display/CKB/ERA5

1. ERA5 data was downloaded through the Climate Data Store (CDS) infrastructure. It can either be through the CDS web interface or programmatically using CDS API service.
2. The ERA5 data for this research was through the CDS API.
3. Firstly, CDS API needs to be installed and build a request.
4. To build a request for CDS API the system uses the Meteorological Archival and Retrieval System (MARS) catalogue.
5. Then the software called Python needs to be installed, it will be needed to access the results because it will be in web form.
6. For a step-by-step process on how to download ERA5 data visit the link: https://confluence.ecmwf.int/display/CKB/How+to+download+ERA5

Figure 10 shows a summarized overview of how the data was acquired from the ECMWF website.

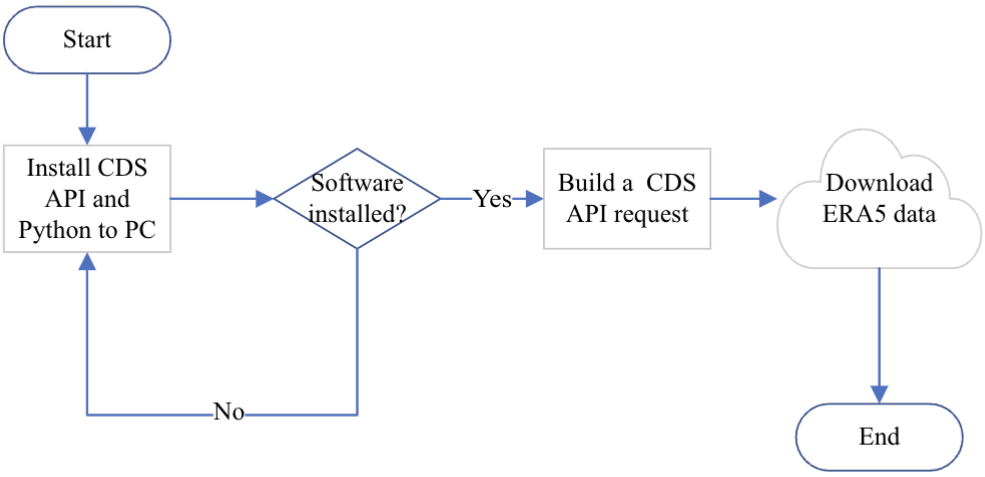

Figure 10: ERA5 Data Collection Process

3.1.2 Visual Observation

Wave data consists of significant wave height, peak period, and peak direction. Visual observation is used to collect data by taking records for several hours and neglecting the wind speed. Figure 12 shows an example of the logbook used for data collection. Only a trained Marine Officer is allowed to Log the observation hourly.

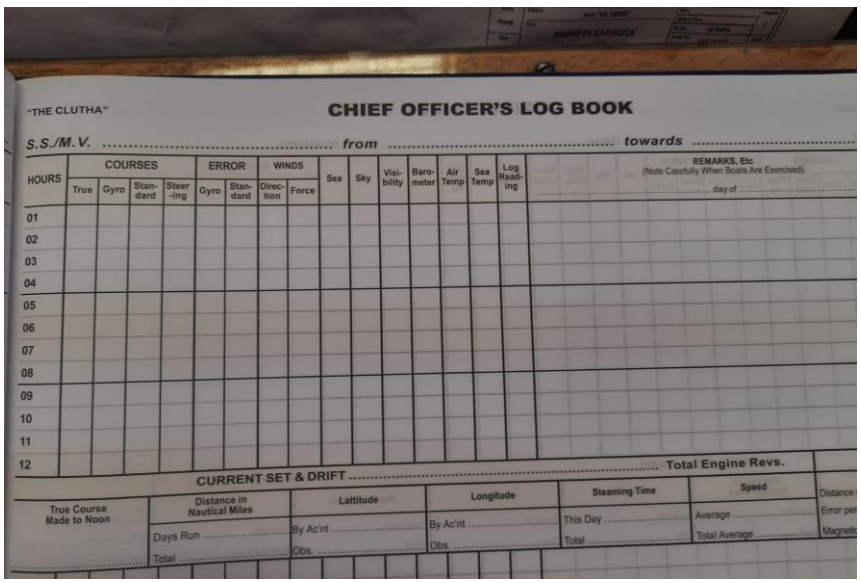

Figure 11: Officers Log Sheet

For the data analysis, the vessel was at various steady speeds for several hours. Table 2 shows the results of data collection at various speeds. The Bretschneider Wave Spectrum was used to

perform numerical calculation to obtain motion spectra based on the information gathered, and the results were graphically displayed using MATLAB (see Appendix G).

From equation 5, the significant wave height and peak frequency are used to determine paraments A and B. The results are displayed with respect to encounter frequency.

Table 2: Visual Observation Data Recorded

Speed(knots)	Significant Wave Height (m)	Peak Period (s)	Peak Direction
8.70	5.00	8.00	250
8.70	6.00	10.0	240
16.7	4.00	10.0	230
16.8	3.00	11.0	320
DP Mode	7.00	12.0	310
7.49	7.00	9.00	315
11.4	5.50	9.00	280
DP Mode	3.00	9.00	350
14.1	3.50	6.00	300
9.92	5.00	6.00	310
11.4	3.50	9.00	210
15.7	4.00	10.0	220
13.5	2.00	11.0	260
13.7	2.00	10.0	310
13.0	1.50	10.0	200

The significant wave height is defined as the parameter of sea state and the mean height of 1/3 of the highest wave or $H_s = 4.01\sqrt{m_0}$

m_0 is the zero spectral which is equal to the variance of surface wave displacement.

Using the methods mentioned in this chapter, the results are displayed through MATLAB (See Appendix G).

Chapter 4 will contain a discussion of the results obtained.

3.2 Response Amplitude Operator (RAO)

The oscillating motion of a ship appears in six degrees of freedom, as explained in Chapter two. However, only four of the six degrees of freedom are investigated in this work: roll; pitch (rotational mode) and surge; heave (translational mode) (Faltinsen, 1993; Perez and Fossen, 2006). The focus on this thesis will be on the DOF that have the most significant impact on ship performance and safety for their specific applications.

PDStrip (Public Domain Strip Method), an open-source program, was used to compute RAOs for this study. PDstrip is primarily confined to linear responses, but it takes nonlinear effects into account when determining the RAO such as the viscous damping. The ship's force and moments are calculated using the results of the hydrodynamic coefficients and the exciting wave load. The hull form description and hydromechanics parameters are required to determine the RAO.

While the vessel[3] was in dry dock, a 3D scan of the vessel's hull geometry was performed, which was used to obtain an exact hull form description of the SA Agulhas II. These data were obtained by the sound and vibration research group from Stellenbosch university. Strip theory can be used to obtain results from a two-dimensional hydrodynamic coefficient and exciting wave load by using forces and moments from a three-dimensional body. Each strip is modelled as a hydrodynamic segment of a cylinder that is infinitely long.

Required mass and stability parameters of the vessel are generated from the loading conditions, while the radius of inertial for roll k_{xx} resonance peak matches the resonance peak in the roll motion spectra. This does not apply to pitch, which makes the radius of inertia accessible by: k_{yy} 0.22 to 0.28 L (L is the ship length) and a proportionality factor of 0.24 (Molland, 2008).

Table 3: Input Data for RAO Computations

Stability and Mass data		
Draft	D	6.67m
Metacentric height(corr.)	GM	1.41m
Radius of inertia roll	k_{xx}	6.45m
Radius of inertia roll	k_{yy}	30.3m

[3] Note that the vessel scan was done by the Sound and Vibration Research Group from Stellenbosch University (Nickerson, & Bekker, 2017).

Table 4: PDstrip main characteristics to be aware of when using the software.

Maximum number of strips	100
Minimum recommended number of strips	30-40
Offsets/parameters per strip, max	100
Offsets/parameters per strip, min	10
Maximum number wavelength	200

Note that the code used in MATLAB is shown in Appendices E.

3.3 Full-Scale Measurement of Ship Motion

Ship motions were measured during a research voyage on the SA Agulhas II, a Polar Supply and Research Vessel (PSRV) built by STX Finland at the Rauma shipyard. The vessel is designed to carry about 50 crew and 100 scientists, bunker oil, laboratories, and cargo (Bekker, 2018). Measurements were taken from the vessel during her voyage from Cape Town – Antarctica – Cape Town from 28th June to 12th July 2017. Motions were recorded using two autonomous low-cost sensor boxes with gyroscopes and accelerometers, placed at different positions. Figure 13 shows a picture of the vessel and the vessel specifications in Table 3

Figure 12: SA Agulhas II

Table 5: SA Agulhas II spécifications (Bekker et al, 2018)

Lbp	122.25m
Beam	21.7m
Draught, design	7.65m

● Observation deck (Monkey deck)

■ Vicinity of centre of mass

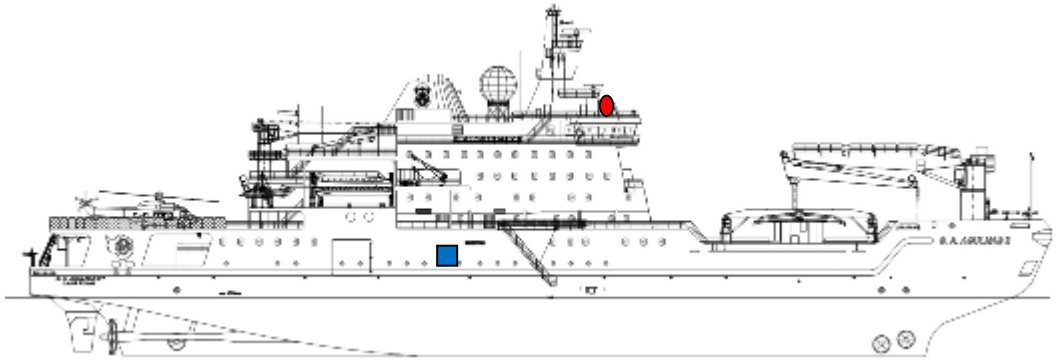

Figure 13: Location of the sensors on the SA Agulhas II (Adapted from Bekker and Omer, 2018)

Figure 14 illustrates how the sensor boxes were placed on the vessel. The first sensor box was placed at the longitudinal center of gravity 57m forward of the vessel in the engine control room which measures acceleration in three degrees of freedom and the rate of roll and pitch. The second sensor with the GPS reception that provides accurate time and position tags of the vessel is placed on the observation deck above the navigation bridge also known as the Monkey deck. This sensor gives 3D-information for both acceleration and angular rates. Synchronisation of the sensors using the respective angular rates provides a near-perfect agreement with the angular data (Chen et al. 2019).

3.3.1 Sensor Boxes

There are two types of sensors used in these boxes, a 3D acceleration sensor and two gyroscopes for the pitch and roll axes. The acceleration sensor is used to calculate the angle of roll and pitch based on the direction of gravity. If the box is accelerated with respect to an inertial system, pseudo forces[4] will cause an error in this measurement. Because gyroscopes provide angular velocity and are not affected by pseudo forces, the roll and pitch angle can be calculated by integrating the corresponding angular velocity. In practice, the gyroscope zero drift produces very unstable results. As a result, both acceleration and angular velocity data are saved for later processing.

Note that the two sensor boxes are similar in terms of their key functionality. However, the new sensor box has GPS data, something the old sensor box does not have. By using both sensor boxes, it allowed for the measurements of the precise time, date and location of the ship (i.e. for this research, the new sensor box provided the GPS data).

3.3.1.1 Original Sensor (No GPS)

The original sensor generates files with ten columns per sample, as shown in Table 6. Because the roll and pitch columns are calculated using the acceleration sensor, they are susceptible to pseudo forces. The roll and pitch columns, as well as the corresponding rates, use the same coordinate system. The accelerations are handled separately. Figure 14 depicts the coordinates.

[4] Pseudo force is also known as Inertial force, is an apparent force that affects an object in a non-inertial (accelerating) reference frame while no actual physical force is being to object (Molland, 2008).

The datasheet for the acceleration sensor states a sensitivity of a minimal 16.2 mg/bit, a typical 18 mg/bit and a maximal 19.8 mg/bit, here mg is “milli earth acceleration”. The calibration factor in the table is obtained from the measurement on the ship, it corresponds to 18.8 mg/bit.

The sample rate is 10 Hz.

In an old version of the software raw accelerations were written as integers into the file for debugging. In such files accelerations are not filtered properly and are not in sync (a bit ahead) of the roll, pitch, and rate data.

Lines starting with “#” are comments, explanations of the sensor, changes in settings or error conditions. These may appear anywhere in the file. Sensor files can be read into MATLAB.

Table 6: Columns for Original Sensor

Col	Name	Unit	Description	Calibration factor
1	t	s	Seconds since start	
2	Roll	deg	Roll angle calculated from accelerations	
3	Pitch	deg	Pitch angle calculated from accelerations	
4	Roll rate	mV	Gyro raw data	1/20 deg/s 1/mv
5	Pitch rate	mV	Gyro raw data	1/20 deg/s 1/mv
6	Uref	bit	debug information	
7	U	mV	Power supply voltage	
8	spix	bit	Acc. Raw data	9.81/53.1 m/s^2 1/bit
9	spiy	bit	Acc. Raw data	9.81/53.1 m/s^2 1/bit
10	spiz	bit	Acc. Raw data	9.81/53.1 m/s^2 1/bit
			Sample rate	10.0 Hz

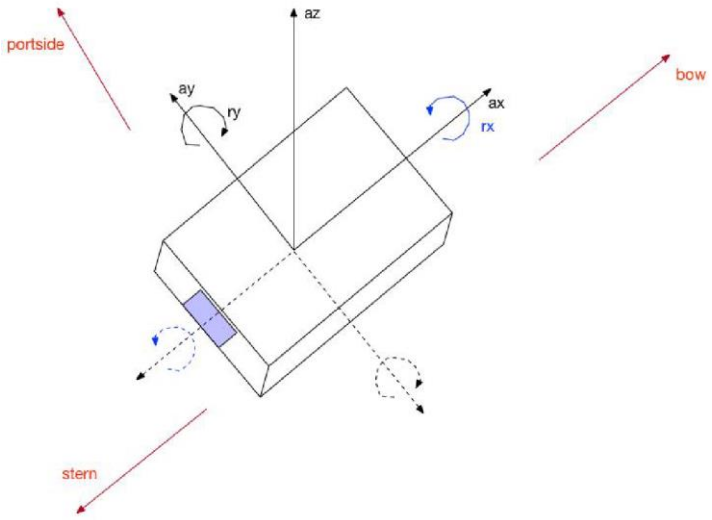

Figure 14: Coordinate System of the Old Sensor

3.3.1.2 New Sensor Box Set-up (with GPS)

The new sensor box starts recording to the SD card automatically if a card is inserted during bootup, it is recommended to remove the card during bootup. Power is supplied through the USB port; you may connect this to the power supply for autonomous operation or to a computer which will give a serial connection as well. The box requires a DC power between 8V and 12 V on the barrel jack on the rear. Positive voltage is on the inner pin, the negative pole is the ground potential and to be connected to the outer pole. A noisy power supply may degrade the function of the box, so it is recommended to use an AC power device. A FTDI driver is needed for the serial link.

After a successful boot, the display shows roll and pitch angle and symbols in the upper line, time and date are shown below. There are three symbols: the left one is for GPS (the icon should resemble a flying satellite). With an "x" show below, no GPS device is found. If there are three dots, a GPS is attached but has no fix. A check mark appears once a fix is achieved. Well, the GPS is in the small, black box (see Figure 15-16), the active area of the antenna is opposite to the receptacle. The device may be unplugged at any time.

Figure 15: Sensor Box Switched On.

The next symbol is for the SD-card. An "x" means no card; a check mark means that the card can be removed. Three dots mean the card is busy, while writing sensor data to the card a blinking arrow is shown. The moving symbol on the right is synchronized with data sampling, while it is moving data are sampled but depending on the settings perhaps not written.

Menu

The button on the very right unlocks the other keys and brings you into the menu. The left and right button below the display move to the previous or next menu point. The up and down buttons right to the display usually start actions. To step through the menu:

Display to bow or aft is just a reminder of the sensor orientation with respect to the ship. The value is logged in the output data, the output of the sensor data is not affected by this.

SD Logfile Logfiles are opened and closed. It is recommended to close a logfile before turning off the power or removing the card.

SD Dir After mounting the card, use the up- and down arrow keys to navigate through the card's directory. Again, a mounted card should be ejected before removing it or turning off the power. This can be done through the SD Logfile menu.

USART the serial port can be turned on and off here. A file header is included into the data each time the on-button is pressed.

Light it is about the display's backlight. Pressing a key keeps the backlight on for a while.

GPS Position, GPS (UTC) simply display the corresponding data.

The next menu point shows the number of satellites with a signal strength of more than 20dB (arbitrary unknown units) and the maximum signal strength. This is to help place the GPS antenna somewhere. Usually, a fix is achieved if there are more than 3 satellites > 20 dB. Since GPS reception depends on reflections as well, this is not a safe indicator.

RTC There is an internal clock with a battery backup. Sampling is synchronized with this clock. The down key will bring you into the settings menu, within this menu the left and right key move the cursor to the previous or next item. Finally, the option to set the clock or to cancel the process are offered. The new date-time is copied into the RTC now by pressing the ok button.

If a fix is available, the RTC can be synchronized with the GPS clock using the following menu options. UTC, UTC+1, and UTC+2 are possible time zones. The synchronization is not very accurate; a one-second difference is possible. The expert menu contains a collection of debugging information. As the name suggests, this is for experts.

Data

The sampling rate is 8 Hz in contrast to 10 Hz in the old device. It uses different sensors (with a three-axis gyro) with new calibration factors. The nominal calibration factors are given in the file header, namely gyroscope.

Datasheet Calibration: gx,gy,gz/131->deg/s, ax,ay,az /1024->9.81m/s^2

Data are filtered with a 6 dB-frequency of 3.5 Hz and a group delay of 242 ms which is not compensated in the output. On the SD-card there is a file "readSensor.m" which reads data files into MATLAB.

Both sensors use the same right-handed coordinate system with the x-axis pointing through the display and the z axis upwards (see figure 14). The columns in the data are date, time as given by the internal RTC. Please refer to Table 7.


Figure 16: Sensor Box Back and Front View.

Data being filtered by a 6 dB frequency of 3.5Hz and on the SD-card a file called 'readsensor.m' reads the data into MATLAB. The sensor uses the right-handed coordinate system with the x-axis pointing through the display and the z-axis upwards.

Table 7: Columns on the New Sensor Box

Col	Example	Explanation	Calibration factor
1	2021-01-20	year-month day of the internal clock	
2	21:46:46.500	hour:minute:second of the internal clock	
3	1	gpsFlag: gps data invalid if zero	
4	2021-01-20	gpsDate (UTC)	
5	21:46:47.000	gpsTime: always rounded to integer seconds (UTC)	
6	53.1	lat	
7	8.19	lon	
8	321	gx: roll	1/131 deg/s 1/bit
9	-343	gy: pitch	1/131 deg/s 1/bit
10	-268	gz: yaw	1/131 deg/s 1/bit
11	57.6	ax: surge	9.81/1024 m/s^2 1/bit
12	7.92	ay: sway	9.81/1024 m/s^2 1/bit
13	989	az: heave	9.81/1024 m/s^2 1/bit

This chapter discusses how the experiments were set up to measure the wave spectrum, the Response Amplitude Operator (RAO), and full-scale measurements of the ship motion using two gyroscopic sensors.

In the wave measurement section, the discussion was centered around how data was acquired from satellite data (ECMWF), where the key steps required were highlighted. It also showed

the results obtained from visual observations. (i.e., data being logged hourly by trained marine officers).

This chapter further went on to discuss how the RAO was computed with PDStrip, highlighting the key input data that was used.

To summarize this chapter, the full-scale measurement of the ship was measured. Two sensors were combined, one with specialized GPS functionality while the other captured information such as the roll, pitch, and time.

The next chapter discusses the results in more detail.

CHAPTER 4

RESULTS

Ships respond to different motions at different periods, within the same wave spectrum, a ship can have its rolling period while also having a different average pitching period and heaving period. Motion records usually have the same appearance as wave records (Kwak et al. 2012).

The wave description offers in-depth information about the sea which is usually a superposition of different wave systems for instance sea swells, region, and location dependence. The sea state is measured using mathematical, statistical, probabilistic, and empirical models. The assumption is that for a limited period of time and in a specific geographical location, wave conditions frequently vary in a steady way known as the sea state.

Wave conditions are described as mathematical models based on several specified sea state features. The change in sea state parameters, for instance, significant wave height, zero-crossing period and mean wave direction vary at a lesser speed compared to the wave surface elevation that causes sea motions, are modelled through means of probabilities (Bitner-Gregersen et al., 2016). Wave conditions for design and operations can be obtained using the long-term and short-term statistical models for sea state. The data obtained from the phase-average wave models are used in this process. Furthermore, in addition to the standardized global parameters, the description of a sea state consists of a wave spectrum and wave directional spreading of the total sea and swell.

For computing ship motions, can use the probable resulting motions for each wave spectrum. This is possible using an electronic filter analogy.

Figure 17: Electronic filter analogy

In this analogy, waves are the input parameters, ship motions are the output of the system, and the filter is the ship “black box” represented by the transfer function (RAOs). In other words, the ship receives the wave as input and generates ship motions as output. This analogy works as long as the filter is linear which means that the output amplitude must be proportional to the input amplitude.

In this chapter, the three different components of the electronic filter are presented. The ship "black box" is the SA Agulhas II, her transfer function is developed. Wave data from visual observations recorded during the voyage are presented using a Bretschneider spectrum and data from re-analysis of remote sensing data by ECMWF and finally, measured ship motions from the sensors.

4.1 INPUT – Wave Spectrum Results

In the analogy of an electronic filter, the challenge is always determining how to combine the input and the filter to produce the output. Two different sources of wave data were used in this work to obtain wave energy spectrums. The two sources are:

1. Remote sensing with satellite data (ECMWF)
2. Visual observation wave data

4.1.1 Satellite Data Results (ECMWF)

This is a reanalysis of remote sensing data for prediction of waves in real time and in the future. It is also referred to as wave nowcast and forecast. For this work, reanalysis of remote sensing data used was obtained from the European Centre for Medium Weather Forecast (ECMWF). Figure 18 below shows a wave spectrum from satellite data obtained from the ECMWF. Wave data extracted from the 5th of July 2017 at 09:00 am.

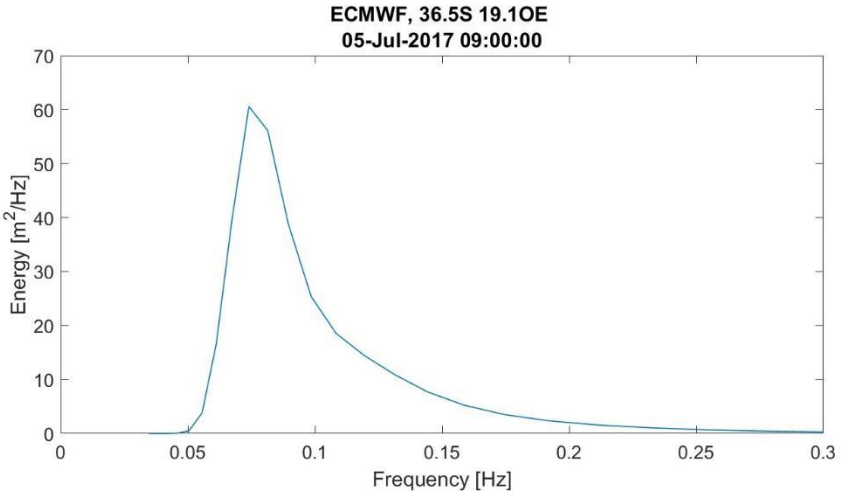

Figure 18: Wave Spectrum for ECMWF (5th of July 2017)

4.1.2 Visual Observation

Estimation of the long-term value of wave-induced load in marine structures depends on the statistics of waves in different ocean areas. The first type of wave statistics made available was from visual observations. Even though many other sources of wave data are now available, visual observations are still one of the major sources that cover most of the ocean areas. These

recorded data need to be calibrated to some extent with measurements (Soares, 1986). During the voyage, on the SA Agulhas II, wave data were recorded in the chief officer's logbook. It consists of the significant wave height, peak period as well as direction. The recording is done every three hours by a trained officer onboard according to the World Meteorological Organization guidelines. It is important to mention that in most cases databases offer bias toward the lower wave height (Michel, 1968).

There are several possible techniques for visual observation. The first and most common technique is a simple visual estimate of the wave motions that occur when a ship moves past a fixed point. The technique is adequate and is frequently used to obtain a reliable range of values, especially if the spectrum does not omit low-frequency wave values. Theodolites, range, and other devices that can magnify the sea surface are also used in visual observation. Until the point of observation is obtained, the device can provide a scale in the ship's distance. Improvements are made in these other techniques when the data is required and more precisely when the data is used to determine sea motions (Rossi, Crenna, and Scamardella, 2010).

The figure below depicts the wave spectrum generated from data collected on June 30, 2017 at 8:00 a.m. The parameters were collected by the watch officer on the date recorded. The wave parameters are as follows:

- Significant height, $H_S = 5$
- Peak period, $T_1 = 10$
- Direction, $D = 250$

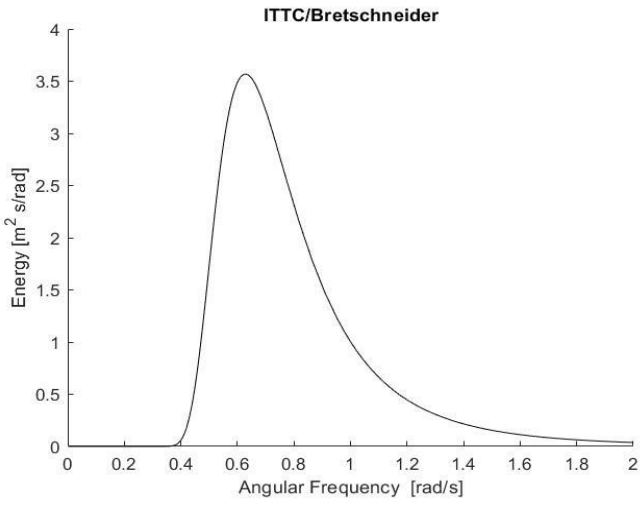

Figure 19: Wave energy spectrum from visual observation (30th of June 2017)

4.2 Response Amplitude Operator's Computations

The reaction of a ship to a particular harmonic wave can be calculated numerically depending on speed and angle of incidence in the form of Response amplitude Operator (RAO). For a particular ship speed and incident wave angle, the Response Amplitude Operators give amplitude and phase for each mode of the ship motion in relation to wave weight and wave frequency.

4.2.1 Hull Modelling

PDstrip requires a hull form description as well as the hydrodynamics input data. For the vessel used in this work, which leveraged the hull measurements taken from the S.A. Agulhas II by the Sound and Vibration Research Group from Stellenbosch University (Nickerson & Bekker, 2017). They performed a 3D laser scan was performed while she was in dry dock. The scan allowed them to extract the hull form of the vessel. The required hull was generated and consists of 27 stations placed more densely at bow and aft compared to the midship section. The stations are equally spaced between the aft and forward submerged extremities, and equally spaced waterlines from the keel to the calm waterline. Where the hull does not extend across all waterlines, offsets are modified to ensure an even number of intervals for each waterline spacing (Journee, 2001). Figure 20 shows different angle of the hull sectional offsets of the SA Agulhas II used in PDStrip.

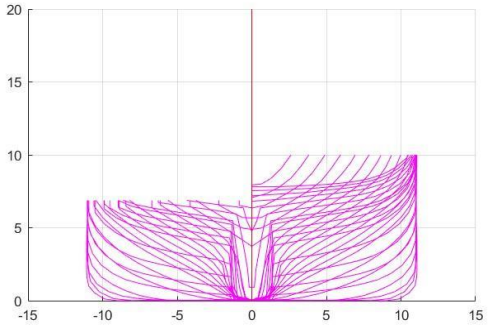

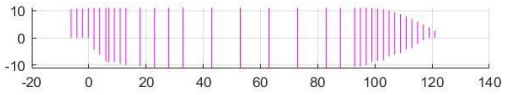

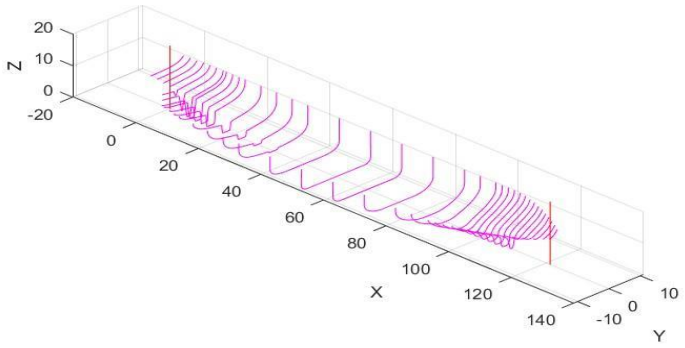

Figure 20: Sectional offsets for the SA Agulhas II[5]

The required mass and stability parameters used to compute the RAOs were provided by the loading computer. The radius of gyration for roll, k_{xx}, were estimated in such way that the resonance peak in the RAOs matches the resonance peak in the roll motion spectra. This technique was not used to determine the radius of gyration for pitch because there is no pronounced resonance here. The radius of gyration for the pitch was therefore estimated from the empirical rules given in (Journee and Adegeest, 2003)

$$k_{yy} \approx 0.22 \,.\, L \text{ to } 0.28 \,.\, L$$

where L is the length of the ship, the proportionality factor was turned to be 0.24. The mass and stability parameters data used can be find in the table 4.

The metacentric height (GM) was corrected iteratively such that the roll resonance in the RAOs matches the clearly visible peak in the motion spectra.

Basically, the hull is divided into sections along the longitudinal axis. In each of these sections, two-dimensional potential theory is applied to determine hydrodynamic, and wave loads as if the section were infinitely long. In this approximation, all diffracted and radiated waves propagate perpendicular to the longitudinal axis of the ship, which is experimentally observed in the midship sections only. Emphasis needs to be made on the fact that this approach is well fitted for long and slender ships. The ratio of length to breadth should be greater than three. PDstrip used a strip-wise Rankine source method with a symmetry condition on the seabed. No flow separation was specified along the hull. The linear seakeeping method was used, and

[5] Note that this is unpublished work from another researcher and there was authorisation given to be used.

transom was set up as wet at zero forward speed and dry at non-zero forward speeds. Potential theory does not handle viscous damping, it was therefore modelled using the semi-empirical Ikeda method.

RAOs amplitudes for a constant speed of 7.5 knots and angles of wave incidence from 0° to 180° with an increment of 30^0 are given in the following sections.

4.2.2 RAOs Calculations

The Response Amplitude Operator relationships are calculated through the monitoring of the ship hull. Response Amplitude describes the amount of movement that a passing hydrodynamic wave causes in a floating object.

A ship's longitudinal axis is oriented with respect to a reference direction by a fundamental parameter known as the heading angle, which is frequently expressed in degrees or radians. To establish how the ship is directed or aligned, the hull of the ship is directly related to its heading angle. In essence, the direction in which the hull is orientated is changed when the ship's heading angle changes. This orientation has an impact on the ship's ability to navigate, steer, and react to outside influences including wind, currents, and waves. As a result, the heading angle is an important factor in ship management, course maintenance, and manoeuvring. As such, it should be considered while designing ship control systems and by ship operators (Sullivan et al, 2019).

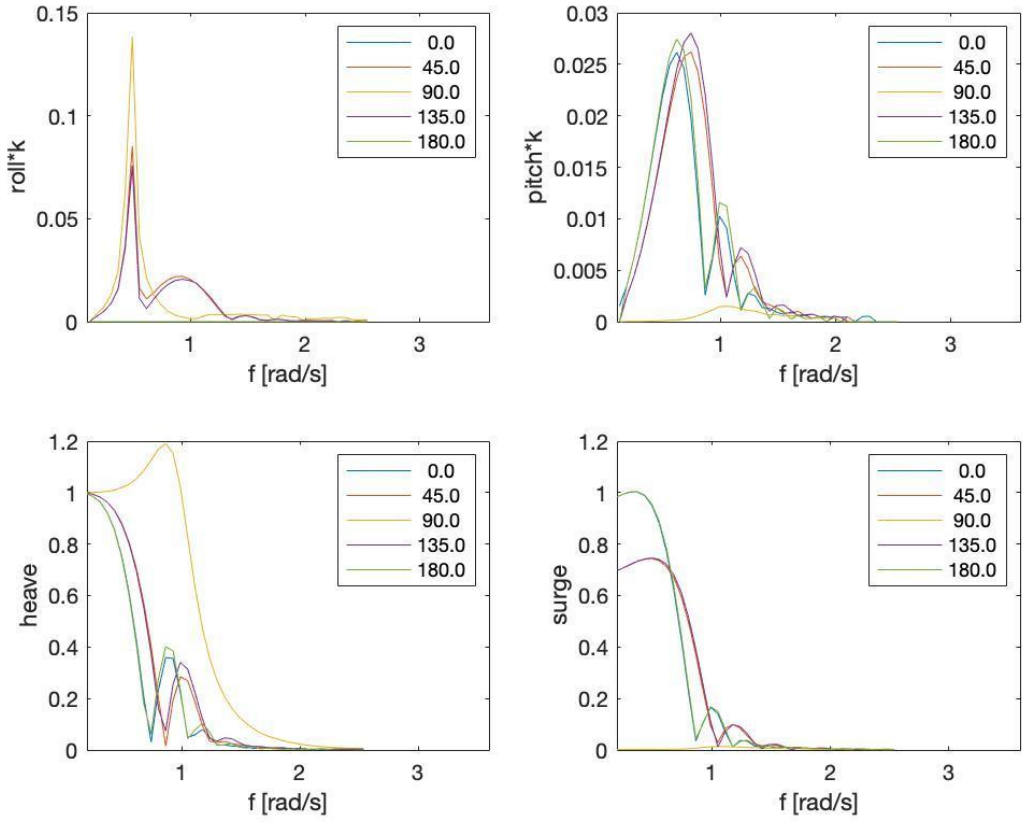

Figure 21: RAO obtained from PDstrip

Rolling is caused by the waves moving in a perpendicular direction to the motion of the ship. According to the results the roll motions are vital in re-scheduling the route of the ship and guarantee effective and quick actions. In other, reasonable approaches to prevent routes modifications, the exploit involves a discount in speed, therefore, tolerating go-slow due to adversative conditions in weather (windy, speed).

The results shown in figure 21 shows at difference incident angle, the roll motion curves similarly. The graph shows that the max peak period is at 0.14. This shows that regular roll motions of the ship result in regular frequency rates. However, at an angle of 180 degree the ship does not experience roll motion, while its highest peak is at 90 degrees. The regular scenario of the roll versus frequency depicts a little perturbation to develop a parametric timbre with arithmetical models. The results of roll versus frequency show a gradual reduction in roll at 0.02 causes the increase in frequency. Small variances are observed to primary operation conditions as they show to be sufficient in reacting to synchronous tone causing multiple peaks in the graph.

Pitch motion is when bow is lifted to the crest of the wave then the stern descends into the following trough. The results show the amplitude for Pitch seems to be constant at all angles except at 90^0 which only shows slight increase in amplitude to about 0.001 between 0.6 – 2 frequencies. A sinusoidal form with a maximum amplitude of 0.028 at various incident angles.

Heave are the action of the motion of the sea that causes the vessel to steadily move out of the sink or water underneath the waterline. It is the aspect that causes the buoyant and displacement forces that create subsequent forces that attempt to reinstate ships to the creative waterline (Bell & Kirtman, 2018). The ship responds distinctly in heave when waves approached hull from the side. The graph (figure 21) shows that there is a peak in heave reaching 1.19 at an incident angle of 90 degrees. The graph shows a slope of the sine function which constantly fluctuates in all angles. Heave decreases if the wave frequency increases. Heave response is similar in head and following waves.

Looking at the graph, the incident angle is divided into two groups: higher surging between 0 and 45 degrees and lower surging from 90 degrees upwards. This is a typical event that can happen when a ship is exposed to wavelengths and ocean currents. The ship appears to be steady and constant at the zero line for surge and frequency at 90. As a result, the higher the frequency of the water waves, the less surging effect on the watercraft.

4.3 Ship Motions

As mentioned by St Denis and Pierson, a ship can be treated as a black box is in an electronic filter. If the filter is linear, the analogy will remain true. The black box receives the waves as input and generates ship motions as output. This can be represented by equation 19.

The motion energy spectrum is computed from ship motions measured during the voyage and calculated using response amplitude operators (RAOs) given in section 4.2 combined with the wave spectrum generated from visual observation data and the wave energy spectrum generated through a reanalysis of remote sensing data provided by the ECMWF.

4.3.1 Calculated Motion Energy Spectrum from Visual Observation Data

Visual observations collected from the ships are applied in the design and operations on the ship. The average wave climate of the sea areas with correction presented due to zero-crossing wave period inaccuracy is recommended in ship design. Visual data presents a satisfactorily long observation history that offers reliable global climatic statistics in the sea waves. The observations of the wave height, direction, and period are collected from ships according to the

World Meteorological Organization guidelines. The data collected by the ships include bad weather avoidance from the ships trying to avoid storms on sea and weather forecasts from meteorological offices (Michel, 1968). Thus, it is important to note that the databases offer bias towards the lower wave heights. The Bretschneider spectrum is the numerical method used to determine the ship motion.

The estimation procedure of the Bretschneider spectrum is presented using fundamental concepts and equations. While evaluating the procedure, the computations are done in controlled settings following the terms of the computational simulations. The identification of practical aspects of the estimation procedure ensures that the appropriateness of the degree of freedom estimates when using the motion spectra is understood. The practical aspects include the computational procedure's limitations, spectral calculations, and transfer functions of motion. All these factors contribute to the contextualization of the appropriate sea-state estimation.

The Bretschneider spectrum is a standardized method and is applied to the ship's response. Wave spectra are developed and used, which are presented in different forms where the transformation of spectra on frequency domains is used in the determination of the ship motion. The parameters used in the quantification of waves and their relationship to the motion of the ship are analysed (See Appendix G). The response of the ship to waves is oftentimes considered linear in Response Amplitude Operators.

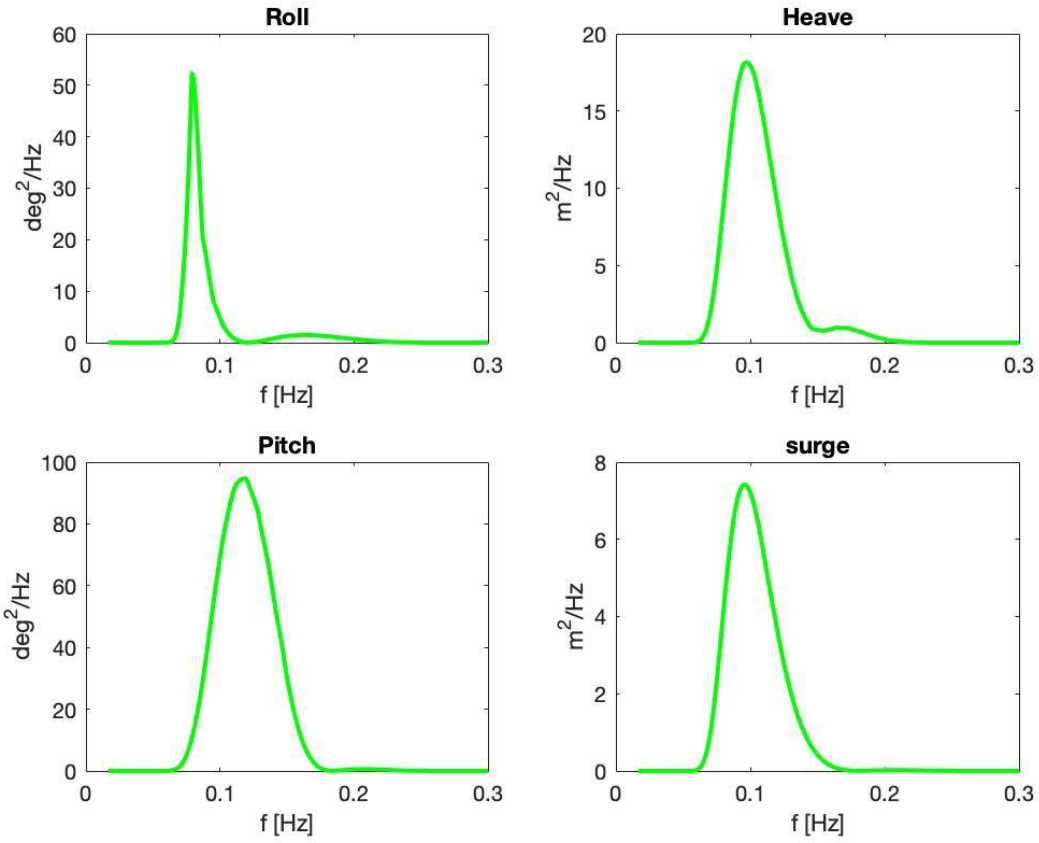

Figure 22: Ship Motion Calculated from Visual Observation

The ship motion calculated from the Bretschneider spectrum using the recorded data obtained through visual observations for one set of data in table 3 is shown in figure 22. The set of data used was at 7.49 knots significant wave height of 7 m, peak period of 9s and peak direction of 315. All motion seems to be influenced by a single dominant wave component with slight deviation for roll and heave. The highest peak for roll is at 52 deg^2/Hz with a frequency of 0.08Hz and the second peak form at 2 deg^2/Hz at a frequency of 0.15Hz. Heave maximum peak was at 18m^2/Hz with a frequency of 0.1Hz. There seems to be a slight increase in heave after graph decreasing to it minimum creating an additional peak. Pitch has a maximum peak of 94 deg^2/Hz at a frequency of 0.12Hz, while surge maximum peak was at 7.6 m^2/Hz at 0.1Hz. The slight deviation may have occurred due to wind or other environmental factors that might have not been considered.

4.3.2 Ship Motion Calculated Results from ECMWF Data

The results shown below at Figure 23 was extracted from 5th of July 2017 at exactly 8 am. The software code using the python programming language was used to extract the data and computed in MATLAB to provide the graphic presentation (See Appendix F). The encounter

frequency shows how wave energy is distributed in frequency by integrating overall direction with respect to the power spectral densities (PSD). From the figure there is a consistency with the form of the graph and the highest encounter frequency is at 0.3Hz.

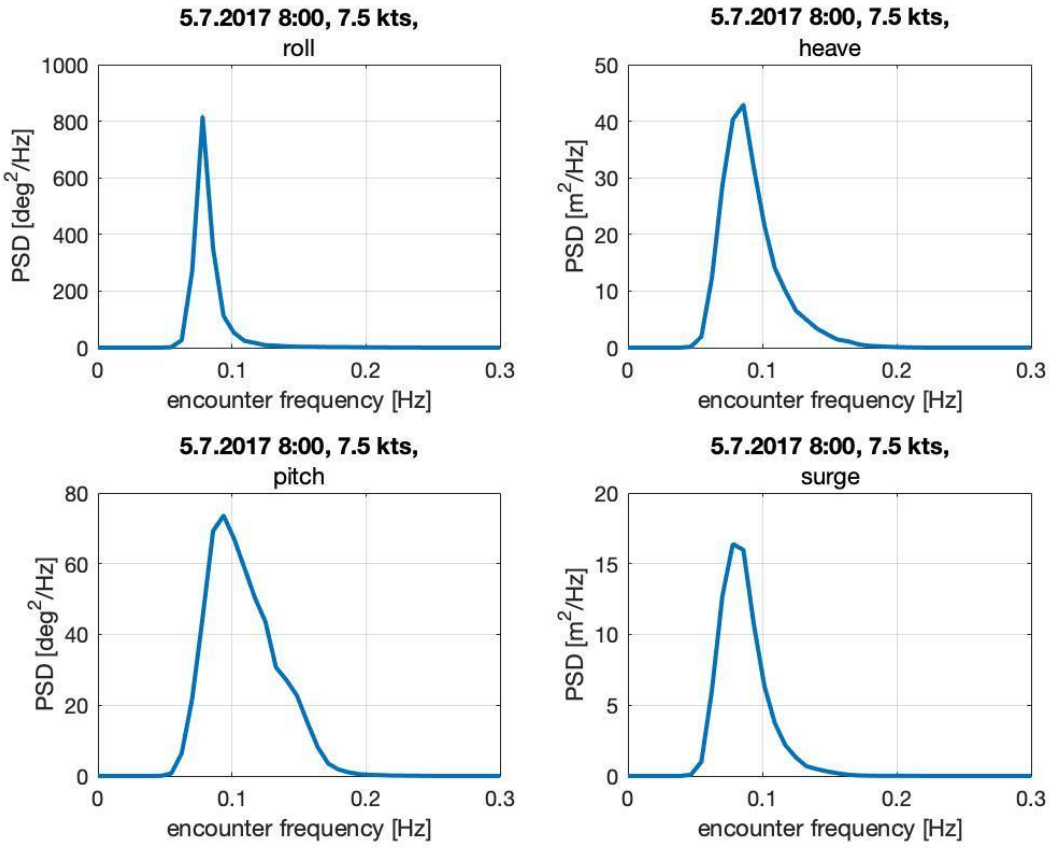

Figure 23: Ship Motion Measured through ECMWF

Remote sensing is applied the most in climate studies and ocean weather, evaluating primary efficiency, water quality evaluation, and detecting the zones that could have marine life (fish zones) (Nieslen, Brodtkorb & Soronsen, 2019). It helps in sensing waves and ocean currents, without affecting the marine environment. Figure 23 shows the results obtained for ship motion; roll reached a maximum peak of 810 deg^2/Hz at an encounter frequency of 0.08Hz. The area underneath the graph is less than the others. While pitch has the largest area underneath the graph and a maximum peak of 87 deg^2/Hz at 0.08Hz. All the four motions seem to reach their maximum peak at the same encounter frequency.

4.3.3 Measured Motion Energy Spectrum

The results of the measured ship motion obtained from the sensor box the voyage hs presented in this section. This data was taken on the 5th of July 2017 at exactly 8am, the file name was saved as ship motion (SM) 28.

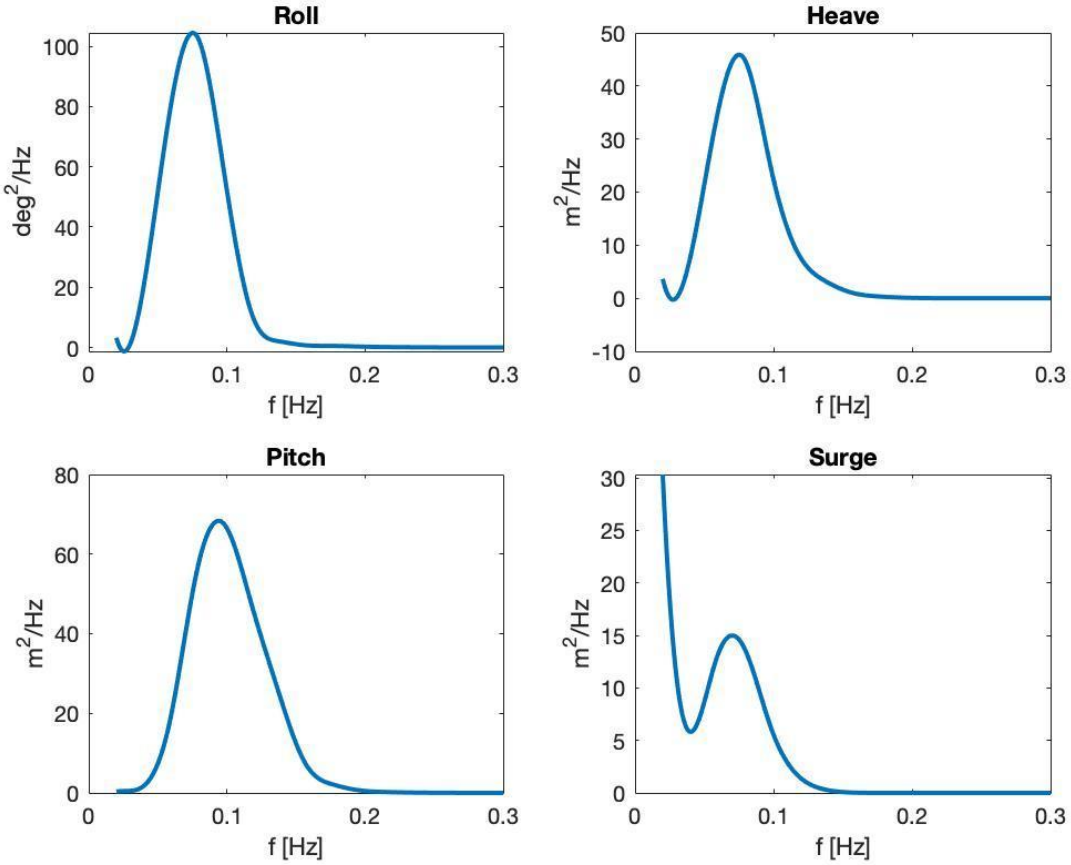

Figure 24: Measured Ship Motion from sensor box

The roll and pitch motion energy spectrum, the encounter wave slope energy spectrum needed to be determined. For the encounter wave slope energy spectrum, see equation 24.

Figure 24 shows that pitch, roll, and heave all peaked at similar encounter frequencies, whereas surge appears to have a much lower encounter frequency. The motion spectrum for surge is defective at low frequencies. The Surge has a flaw that could have been influenced by the inherent limitations from the RAO calculated in 4.2.2. In the following chapter, a comparison will be made to determine which results are more accurate.

This chapter speaks to the results obtained from the experimental setup discussed in the previous chapter. It discusses results obtained from wave spectrum via remote sensing with satellite data and from visual observation.

It also discussed how the RAO was computed using PDStrip. The RAO required using hull modelling as inputs so for this thesis, the hull measurements used was from the work done on the S.A. Agulhas II by the Sound and Vibration Research Group from Stellenbosch University (Nickerson & Bekker, 2017)

Data acquired was then used to estimate the ship motions. The chapter shows the results observed from visual data used, measured results from satellite data and results obtained from the gyroscopic sensors.

In the next chapter, a comparative analysis is done between the ship motion results obtained in this chapter.

CHAPTER 5

DISCUSSION AND COMPARISON

A comparison between the calculated motion spectrum using wave data obtained from visual observations. ECMWF and measured motion are presented. The ECMWF is first compared with the measured motion, and then the visual observation is also compared with the measured motion.

5.1 Ship Motion Results Comparison

5.1.1 ECMWF and Measured Motion Comparison

The Copernicus Climate Change Service Information wave models were used to collect data. The climate reanalysis is called ERA5 based on the ECMWF fifth major global reanalysis earth system model IFS. Figure 25 shows the comparison between the measured ship motion and the computed motions with wave data obtained from ECMWF. The predicted motion will represent ECMWF results and motion measured will represent the ship sensors using just one file recorded on the 5th of July 2017 at exactly 8AM. The results are displayed in PSD with respect to the same encounter frequency.

The chosen frequency resolution has a major impact on the amplitude of the power spectral density (PSD), so it must be considered before beginning any investigation. The accuracy with which the spectrum is separated into distinct frequency intervals which is referred to as frequency resolution. Although a finer frequency resolution enables the detection of narrower frequency components in the signal, it could also lead to lower intervals amplitudes because more intervals are used to divide the energy. In contrast, a coarser resolution integrates energy from nearby frequency components, resulting in greater amplitudes in the corresponding bins. Because of this, selecting a frequency resolution directly affects the sensitivity and granularity of the PSD analysis, thus it is imperative to find a balance that aligns with the specific goals (Oppenheim, 1997).

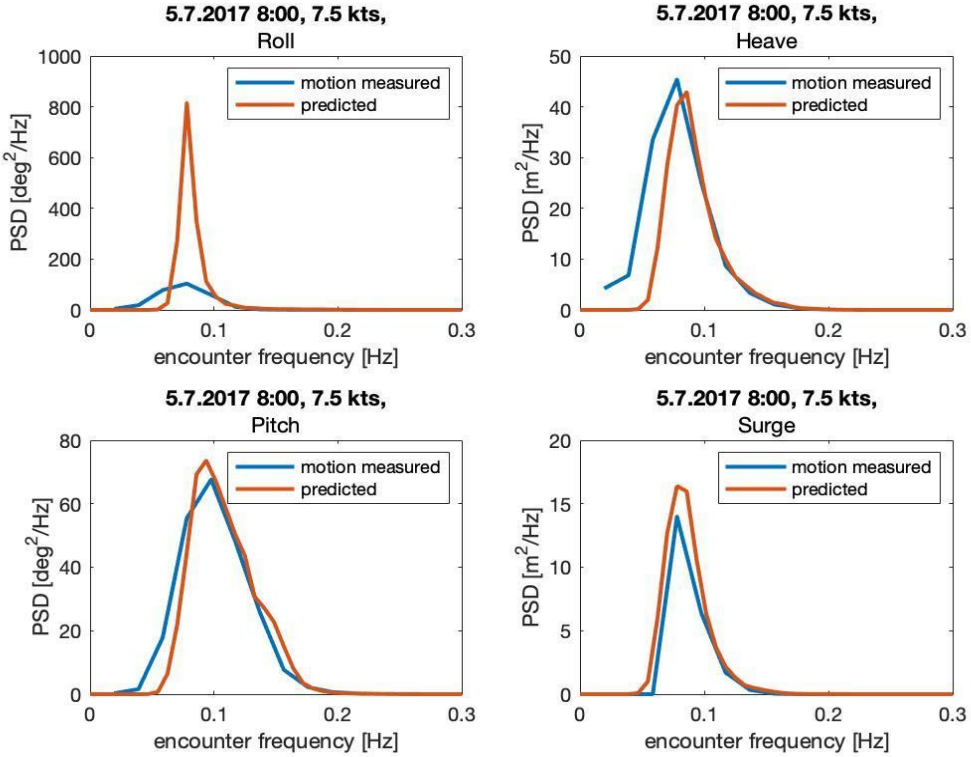

Figure 25: ECMWF Comparison to measured motion from 5.7.2017 at 8am

Table 8: Peak results of ECMWF Comparison to measured motion from 5.7.2017 at 8am

5th July 2017	Roll		Heave		Pitch		Surge	
	PSD (deg^2/Hz)	Hz	PSD (m^2/Hz)	Hz	PSD (deg^2/Hz)	Hz	PSD (m^2/Hz)	Hz
Motion Measured	103	0.08	45.4	0.08	67.1	0.10	14.0	0.07
Predicted	816	0.08	42.9	0.09	73.6	0.09	16.4	0.08

Table 9: Area Underneath the graph between Measured and Predicted Motion

	Roll	Heave	Pitch	Surge
Area Motion Measure	5.82	2.48	4.63	0.43
Area Predicted	13.8	1.67	4.43	0.6

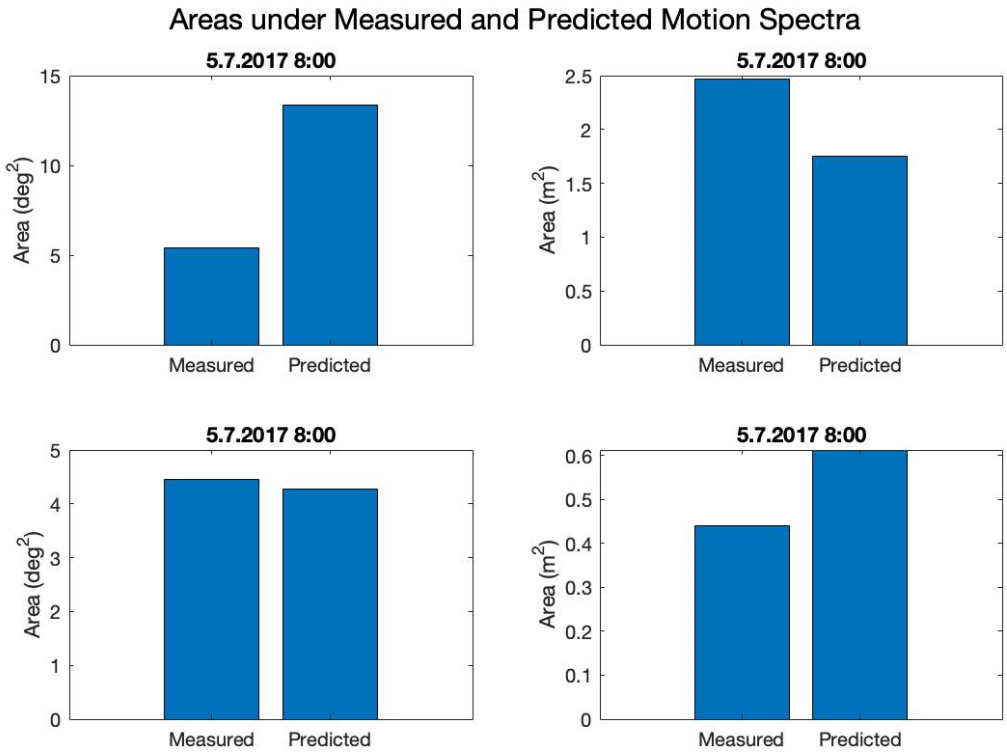

Figure 26: Area graph between Motion Measured vs Predicted

The area underneath the graph for all motion represents the total energy. The results are in good agreement with not much difference for the area underneath the graph and the encounter frequency except for roll. The encounter frequency is with the waves rather than the absolute wave frequency is used when ship dynamics are taken into consideration. This is since the ship is moving relative to the waves and depending on whether it is advancing into the waves or going in their direction, then ship will encounter subsequent peaks and troughs in a shorter or longer time interval (Cheirdaris, 2021).

From the results shown in figure 25, the predicted motion all seems to have equivalent surface areas except for roll. The difference between the measured and prediction motion for roll is quite large. The maximum peak predicted is at 816 deg^2/Hz at an encounter frequency of 0.08 Hz. While the maximum peak for the measured motion is at 103 deg^2/Hz at same encounter frequency as the predicted 0.08Hz. Many environmental uncertainties could have caused the discrepancies in the results. This could be due to the delicacy of the damping of the roll in RAO as this is a delicate component.

The results presented in figure 25, when comparing heave demonstrates that EMCWF prediction yield similarity to the measured. The lowest point of the heave starts at 0 all the way

to a frequency of 0.3Hz, while the highest point with a critical peak heave of about 45.4 m^2/Hz at a frequency of 0.09 Hz in the predicted motion. The acceleration measurement at 0Hz would be dependent on the capabilities of the acceleration sensor. The measured results show the starting heave at 5m^2/Hz with a frequency of the 0.02 Hz rising to a critical heave peak of 45.4m^2/Hz with a frequency of 0.08 Hz. The error that occurred can be caused by oscillation at a lower frequencies than what is predicted from wave spectrum and RAO calculations.. All in all, the result for heave shows good agreement and heaving causes an imbalance force in buoyancy and weight forces, therefore it is crucial ensuring the vertical motion when wave strikes the ship along its path.

Looking at the graphic diagram presented in figure 25 the measured and predicted motion spectrum of pitch are in good agreement. According to theoretical studies pitch motion is not directly influenced by the beam sea unless there is a shift in the centre of buoyancy due to the exciting heave motion (Zakki, 2021). The highest pitch reached according to the predicted results is 73.6 deg^2/Hz at an encounter frequency of 0.09 Hz. While the highest pitch motion measured is 67.1 deg^2/Hz at about 0.1 Hz. The result for pitch corresponds with each other, this motion is usually created by waves moving in the same direction as the ship and can occur naturally. This is crucially monitored during poor weather conditions at sea (Zakki, 2021).

The surge results show the predicted and measured have similar tends which means they are in good agreement. The highest peak for the measured motion is 14 m^2/Hz with a frequency of 0.08Hz. While the predicted motion is 16.4 m^2/Hz with the same frequency the difference in the peak of the surge is about 2m^2/Hz. Surging is the longitudinal motion of the ship and is affected by the rapid acceleration and deceleration which rocks the ship back and forth. The low surge results were due to the fact the ship was at constant speed.

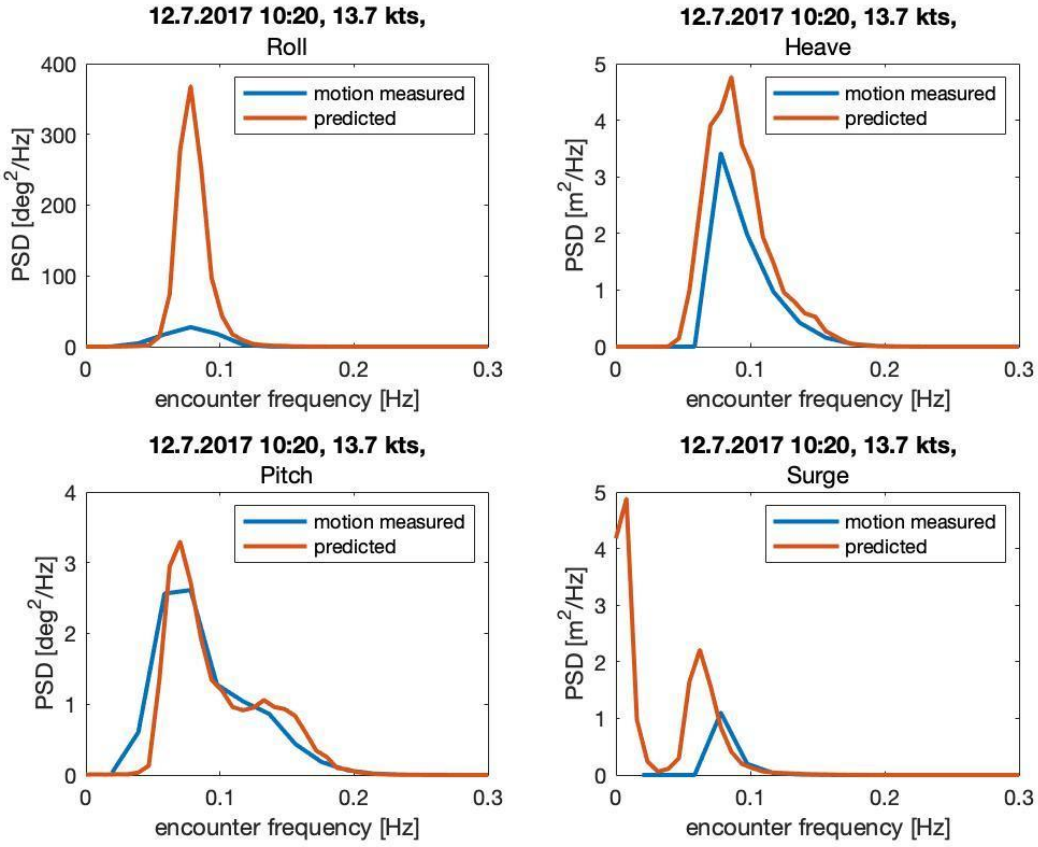

Figure 27: ECMWF Comparison to Measured Motion from 12.7.2017 at 10:20am

Table 10: ECMWF Comparison to Measured Motion from 12.7.2017 at 10:20am

12th July 2017	Roll		Heave		Pitch		Surge	
	PSD (deg^2/Hz)	Hz	PSD (m^2/Hz)	Hz	PSD (deg^2/Hz)	Hz	PSD (m^2/Hz)	Hz
Motion Measured	30.4	0.08	3.41	0.08	2.72	0.08	1.1	0.06
Predicted	368	0.08	5.49	0.09	3.3	0.07	2.2	0.08

Table 11: Area Underneath the Graph between Measured and Predicted Motion

	Roll	Heave	Pitch	Surge
Area Motion Measure	1.84	0.14	0.18	0.043
Area Predicted	9.2	0.24	0.21	0.13

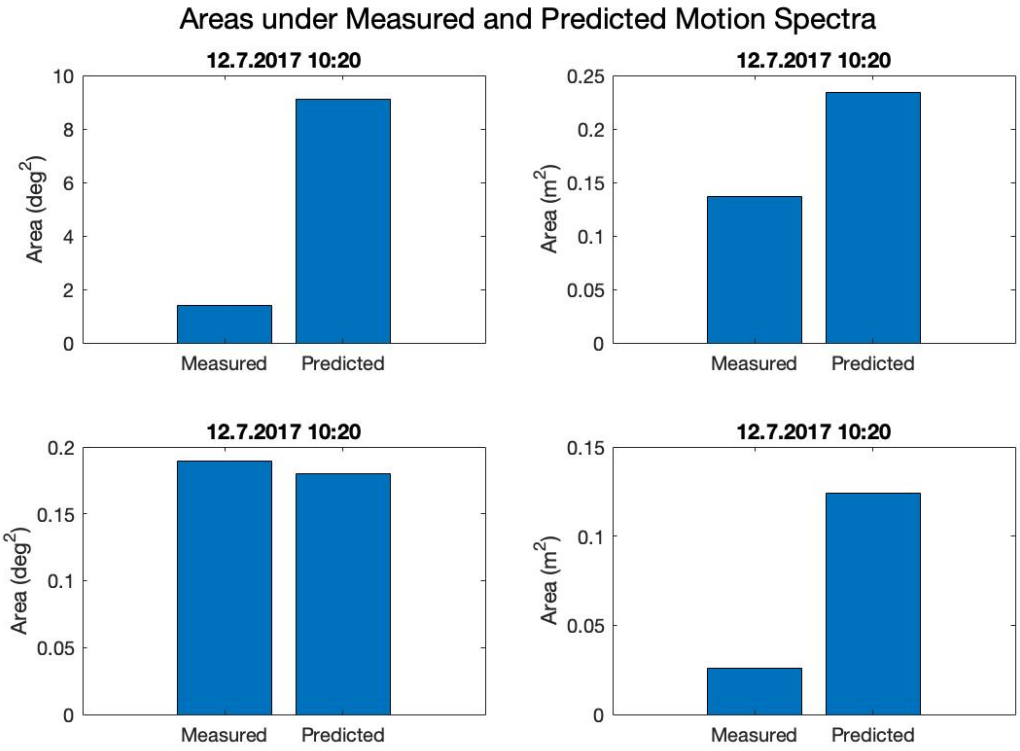

Figure 28: Area under Measured and Predicted Motion Spectra

Figure 27 shows another set of data for ECMWF comparison to measured motion. This data was collected on the 12th of July 2017 at 10.20 am at 13.7 knots. The results show similarities and differences to Figure 25. Looking at surging results from ECMWF it is clear to say the results for predicted shows major errors. This is because surging is cause by the acceleration and deceleration of the ship in the wave. It is difficult for remote sensing to determine this from the satellite data without having any connection to the vessel. The measured motion for surge shows slight surging and this is caused by the vessel having a constant vessel speed of 13.7 knots. Looking at the overall results the measured motion seems to have accurate displayed measurement compared to ECMWF for this set of data. More results are shown in the appendices.

5.1.2 Visual Observation and Measured Motion Comparison

Visual observation data is recorded and entered by monitoring the wave height, speed, direction, and vessel heading. Slight modifications are made to the calculated data and are computed through the Bretschneider spectrum to determine the motion spectrum. This data is compared with the measured motion obtained from the sensors.

The Bretschneider spectrum is an open water spectrum designed to monitor and present both falling and rising seas and developing seas (Yılmaz, 2007). If a point spectrum individually

placed in a vessel does not match the Bretschneider spectrum, the differences are found to disappear using statistical averaging. Hence the spectra are considered as approximate, which does not permit wave height and period to be measured separately. The spectrum and sea observations are used in the determination of wave height and period. The characteristic period, recorded as T is taken as the zero-crossing period. A wave height and period visually observed are computed and results reported in equation 5. The calculated results are used in finding significant wave height before the complete spectrum calculation according to specific equations. The Bretschneider spectrum is used for finding the average sea conditions in terms of motion when their wave height is the only information available (Yılmaz, 2007).

The estimation procedure of the Bretschneider spectrum is presented using fundamental concepts and equations. While evaluating the procedure, the computations are done in controlled settings following the outcome of the computational simulations. Identification of practical aspects of the estimation procedure ensures that the appropriateness of the degree of freedom estimates when using the motion spectra. The practical aspects include the limitations to this computational procedure, spectral calculations, and transfer functions of motion. All these factors contribute to the contextualization of the appropriate sea-state estimation.

Modifying ship motion parameters offers a mechanism to verify models, gauge how sensitive calculations are to various variables, examine various scenarios, and improve ship designs. Researchers can increase the precision of ship motion predictions and take well-informed judgments about ship operations and construction by comparing the adjusted parameters with observed or recorded values (Lewis,1988).

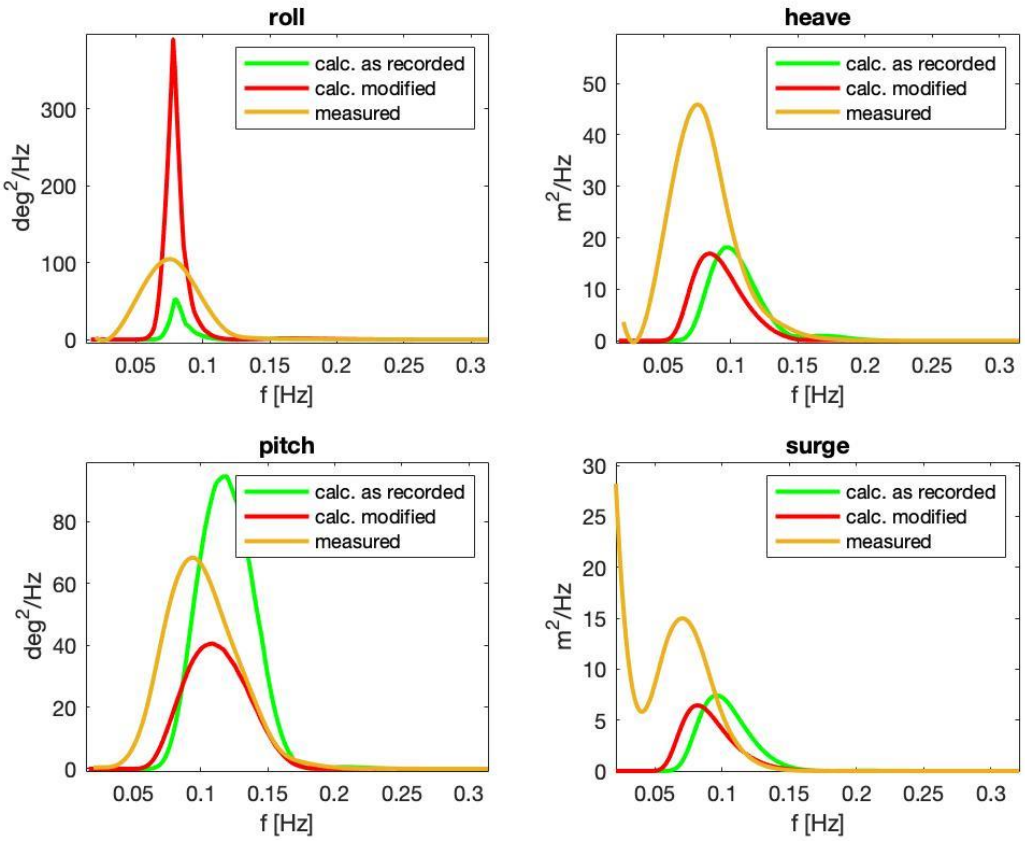

Figure 29: Visual Observation Compared with Measured Motion 5.7.2017 at 8:00am

Table 12: Visual Observation Compared with Measured Motion 5.7.2017 at 8:00am

5th July 2017	Roll		Heave		Pitch		Surge	
	PSD (deg^2/Hz)	Hz	PSD (m^2/Hz)	Hz	PSD (deg^2/Hz)	Hz	PSD (m^2/Hz)	Hz
Calculated as Recorded	48.4	0.08	16.5	0.1	85.7	0.12	6.79	0.10
Calculated Modified	363	0.08	15.6	0.09	37.0	0.1	5.93	0.08
Measured	104	0.08	45.8	0.08	68.3	0.09	15.0	0.07

Table 13: Area Underneath the Graph in Figure 29

	Roll	Heave	Pitch	Surge
Calc. as recorded	0.08	0.78	4.82	0.34
Calc. Modified	5.24	0.782	2.65	0.940
Measured	5.42	2.41	4.46	0.30

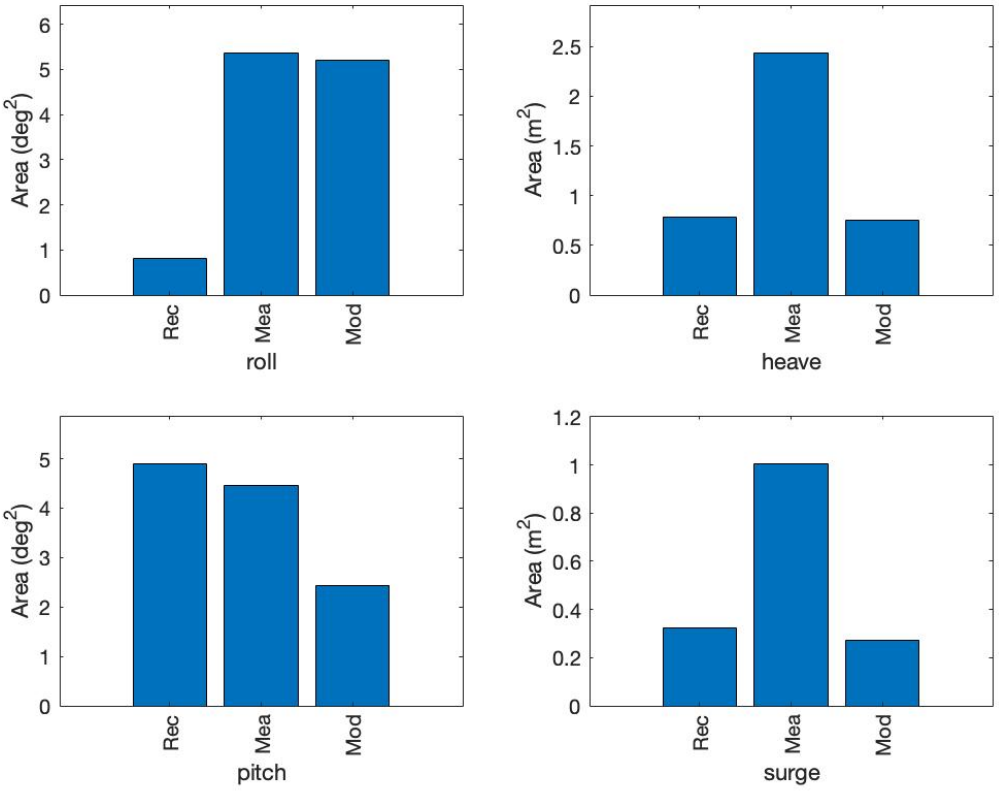

Figure 30: Area graph for Visual observation comparison 5.17.2017

Models of ship motion are frequently based on a variety of presumptions and experimental evidence. By changing the parameters, scientists can evaluate the model's accuracy by contrasting the projected ship motions with the measured or recorded values. If the output of the model and the actual measurements match better as a result of the updated parameters, the model may be more accurate (Lewis, 1988).

Figure 29 shows the results obtained for visual observations using the Bretschneider spectrum. Looking at heave, the area underneath the graph is very similar between the modified and recorded. The measured seems to have a higher amplitude with corruption at low frequencies which might have been caused by external factors. Overall, the heave results between the modified and recorded agree but can be improved.

The roll graphs show large discrepancies between the modified and the recorded. The amplitude of the modified was over 363 deg^2/Hz, while the lowest amplitude peak was the recorded 48.4 deg^2/Hz. However, measured, and recorded amplitude are not much different, the frequency in the measured line starts off very strongly producing more area underneath the graph. The difference between the recorded and modified data can be caused by over modification of the recorded values making it unjustifiable to modify the values.

Pitch computed spectra results look better than the other results. There are small discrepancies, but the overall results agree. The frequency appears to be higher than for the other methods. The highest amplitude obtained was about 85.7 deg^2/Hz. Though, there is a big difference in amplitude between the modified and recorded, the results look satisfactory and justifies the improvement in the modified values. The measured results fall in-between with the peak being slightly off and this is due to the frequency picking up earlier than the others.

Surge, on the other hand, had a major corruption effect at low frequency on the measured spectrum. The calculation of motion spectra is done using the observed angle of linear motion to the horizontal given by the sensor system. When there is a small error in the angles the gravitational acceleration is affected which is then present in the linear degree of freedom. However, overlooking the error, the areas underneath the graphs are not far off from each other. The highest peak was at 15 m^2/Hz and the highest frequency is at 0.1Hz. the modified and recorded values are in satisfactory agreement with each other.

There is room for improvement in the overall comparison. The measured spectrum is wider compared to the other 2 methods, which could indicate an angular spread in the exciting wave spectrum. All the data sets collected show similar trends, and no further attempt was made to use a correction method to ensure that the parameters of the recorded values are a better fit to the measured data. All results show that more wave parameters are needed to provide enough information about the detectable ship motion. The reader may refer to the appendix for an Excel sheet for data used with different modifications.

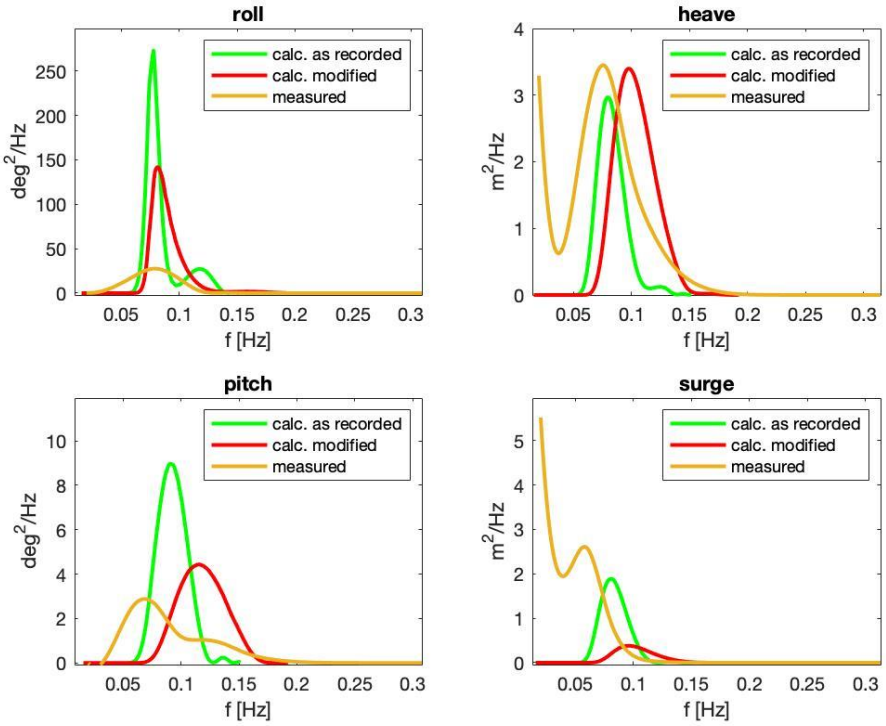

Figure 31: Visual Observation Compared with Measured Motion 12.7.2017 at 10:20am

Table 14: Visual Observation compared with Measured Motion 12.7.2017 at 10:20am

12th July 2017	Roll		Heave		Pitch		Surge	
	PSD (deg^2/Hz)	Hz	PSD (m^2/Hz)	Hz	PSD (deg^2/Hz)	Hz	PSD (m^2/Hz)	Hz
Calculated as Recorded	273	0.08	2.95	0.08	8.96	0.09	1.88	0.08
Calculated Modified	142	0.08	3.40	0.06	4.23	0.1	0.38	0.09
Measured	27.5	0.08	3.45	0.08	2.88	0.07	2.61	0.06

Table 15: Area Underneath the graph in Figure 31

	Roll	Heave	Pitch	Surge
Calc. as recorded	4.50	0.081	0.28	0.06
Calc. Modified	3.62	0.232	0.241	0.02
Measured	1.42	0.154	0.158	0.150

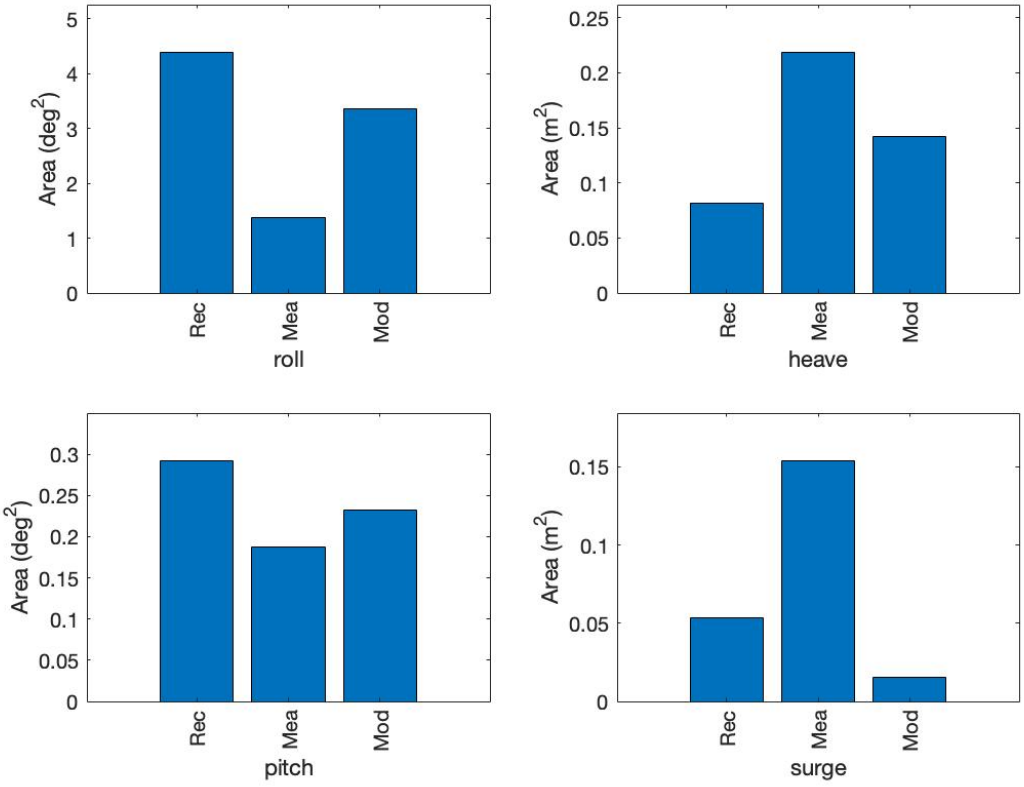

Figure 32: Area graph for Visual Observation 12.7.2017

The figure 31 was collected on the 12th of July 2017 at exactly 10:20am. The results show major similarities with slight differences to figure 29. The measured data for surge shows it started off at very high speed and decreased quickly to a constant speed. The data does not correspond to the data calculated and this might be due to errors that might have occurred during data collection.

In Figure 31 the recorded roll seems to have a very high peak compared to the modified and measured data. This might have occurred due to an over modification of the values. Heave and pitch show agreement between the modified and measured. However, for heave the measured motion and modified show good agreement compared to the recorded. Apart from surge, the modified measurement falls between the calculated and measured values when looking at figure 31. In terms of the overall results the measured motion good agreement with calculated motion from visual observations.

In the results, it was noticed that some discrepancies between the measured and calculated modified data. Figure 25 for example the noticeable differences between the calculated results

compared with measured results. Note that these variations, do not necessarily imply that the employed numerical method requires improvement. Rather, they underscore the complexity of accurately predicting ship motions in real-world conditions. Below are some of the factors that may have contributed to these differences:

1) Transfer Function and Numerical Model: It is important to note that the transfer function used for calculating the Response Amplitude Operator (RAO) is based on the PDSTrip method, which may have its limitations. While the PDSTrip method provides valuable insights, it is not a direct representation of the ship's behaviour. This choice may be a factor that contributed to some of the disparities observed.

2) Sensitivity to Draft and Gyration: The RAO is highly sensitive to the ship's draft and gyration characteristics. Even minor variations in these parameters can lead to significant differences in the predicted ship motions. As such, variations in draft and gyration, crucial for accurate motion prediction, may not have been fully captured. This is the distance between the waterline and bottom of the hull.

3) Stability and Visual Observation: Visual observations of wave characteristics are limited in capturing the complete dynamics of the ship-wave interaction. Stability effects, which can have a substantial impact on ship motions, may not be fully accounted for during visual observation. These effects may have influenced the actual measurements, causing the disparities.

4) Point vs. Distributed Observations: In visual observation, waves are characterized as a single point, whereas sensors provide data for multiple points along the ship's hull. This fundamental difference in observation methodologies can lead to variations in results. The sensors identify the entire range of wave interactions with the hull, providing a more comprehensive but possibly more complex dataset.

This chapter performs a comparative analysis of the results obtained from the previous chapter. In chapter 4, the results obtained for ship motion were measured data from satellite data, measured data from visual observation and measured data from gyroscopic sensors.

The results from the sensors were compared with data obtained from the satellite results and visual observation results in this chapter.

When the sensor results were compared with satellite data, it was observed that the measured ship motions were in alignment except for the roll.

When the sensor data was compared with visual observation results, a similar pattern was observed where the data was in alignment with the sensors except for roll. Note that both results were captured twice at different dates and time.

The roll misalignment could have been due to several factors which includes, damping coefficient being misconstrued. It could also be the placement of the sensor not capturing the roll. These are factors that can be further investigated in future work.

CHAPTER 6

CONCLUSION AND RECOMMENDATIONS

6.1 Conclusion

In the field of sea keeping, there is a need for data analysis for the assessment of performance. Some studies have emphasized the need for simulating the operation of vessels in realistic waves. This research aims to use the electronic filter method approach to determine the ship motion in predicted wave spectra.

- The estimation of measuring the ship motion through its wave spectrum using remote sensing and visual observations. From the data collected it is safe to conclude that similar results were obtained from ECMWF and the computed motion. The difference between visual observation and computed motion is noticeable. This might have been small errors which might have occurred during the data collection. There can be errors up to 100 percent in the magnitude of motion that occurs when one obtains insufficient wave data. The data on the occurrence of wave heights and period probability is needed (Soares, 1991).

- Determine ship motion using electronic filter analogy. This approach involved determining the transfer function of the ship which is known as a Response Amplitude Operator (RAO) using specialized computer software. The RAO is dependent on the frequency function, which presents the response spectrum's ratio to the input spectrum over a frequency range. In this case, the actual frequency was used not the encounter frequency (as used for computing ECMWF) for the calculation in PDstrip. The results obtained in chapter shows that objective was achieved.

- Will the sensors installed on the ship be able to provide accurate data for ship motion? The low-cost gyro and accelerometer-based sensor recorded ship motions in different files. The files were extracted, and ship motion was derived. The development of an affordable sensor that enhances the operational safety of ships while offering valuable tools for vessel tests is imperative to the shipping industry. The sensors' results are satisfactory when compared to the others in Chapter 5 and can conclude that the goal was met.

- Will the ship motion measured from the sensor agree with the computed motion using wave data from ECMWF (satellite/remote sensing) and visual observations? From the data collected, it is safe to conclude that similar results were obtained from ECMWF and the computed motion. The difference between visual observation and computed motion is noticeable, especially with the roll. The roll not being aligned could be due to several factors. Sensor limitations could be one. It is possible that the sensors may be limited in accuracy and precision due to factors such as sensor drift, noise, calibration issues, and environmental conditions. Inaccuracies or errors in the sensor readings could contribute to the misalignment with the satellite data. It could also be due to the way the data is measured. Gyroscopic sensors for example measure the roll motion directly from the ship, while the ECMWF satellite data might estimate roll motion indirectly based on other parameters such as the atmospheric conditions, wind direction or wave height. These differences in how the data is measured could be a factor in the discrepancies observed. Roll motion can vary spatially and temporally due to the local sea state, wave conditions, and perhaps vessel dynamics. The satellite data obtained may have provided a broader view of the ocean or a different temporal resolution, thus leading to differences in the observed roll motion compared to the localized measurements from the sensors (Soares, 1991). The data is recorded in the logbook.

However, there are challenges in obtaining accurate wave condition data, because of visual observations. Hence, the vessel must rely on the probability of occurrence of wave period and heights. Another characteristic of the data required for the vessel is the sea spectrum which can be reconstructed from visual observation. Sea spectrum is a data recording showing the dispersal of wave energy based on frequency. The sensitivity of the prediction according to spectral models shows that the instant response of the ship increases sensitivity to the spectral model.

Simulating sea vessel operations to respond to realistic waves is also required. Previous studies, like this one, have shown that errors in the magnitude of motion can reach 100% due to insufficient wave data for a sea vessel. (Soares, 1991) investigated the sensitivity of motion prediction to spectral models and discovered that the vessel's short-term responses are sensitive to a specific spectral model while other models cannot be used like the JONSWAP spectrum. Since the research was conducted in two different locations, the measured data was retrieved

from amalgamated sea waves and low-frequency swell, as there is no standard spectrum used in local wave conditions. The Bretschneider spectrum closely matches the estimation, but the spectrum height and peak frequency are frequently overestimated. The Bretschneider spectrum, according to some researchers, bears no resemblance to local sea wave conditions (Soares, 1991).

Consequently, the estimates of the motion spectrum were applied to a range with similar encounter frequencies. Determining the motion spectrum, a fine frequency resolution was worked with due to its enhanced efficient computational estimation algorithm. However, as this was a real-case practice of ship, the resolution was significantly lower so that the computational speed of analysis is fully optimized. At a certain point in the study, the wave estimates were affected by the characteristics of wave obtained by the watch officer through visual observation.

6.2 Recommendations

The following could be recommended for this thesis. The wave data are obtained from the remote sensing and visual observation, where ship motion is computed from the records.

Visual observation is not a reliable source for predicting wave due to the watch officer not always being accurate with his/her reading. Human error is likely to occur and the probability of the readings not being accurate is extremely high. Each officer will have a different reading for similar encounters.

In addition, the records with multiple spectral peaks and the percent occurrences of multi-modal spectra were computed without further analysis. Because sea states have such a large impact on the operation of sea vessels and other engineering applications, it is important to further investigate the characteristics of spectra on the sea (Soares, 1991).

In Bretschneider spectrum, spectra height and the peak frequency are overestimated in most cases. The evaluation of these method suggests that there is a need for the development of visual observation entries in the detection of motion in the sea. The spectra obtained in the date recorded peak frequencies are observed on considerably calm days. The measurement of vessel motions using the visual approach is expensive, not easily installed, and unreliable when compared to the use of remote-sensing data(Yılmaz, 2007).

The observed discrepancies can be addressed, and the accuracy of ship motion predictions can be increased, by looking at several potential study avenues. The first focus of future study can

be on improving the numerical models that are used to predict ship motion. It may be necessary to investigate alternative strategies or enhance the PDSTrip method to reflect the precision of ship-wave interactions more effectively (Smith et al, 2020). In addition, further research should be done to understand how stability affects ship motions. To do this, study how stability features affect RAO and incorporate those findings into numerical models (Dimitrov & Wang, 2017). There are steps that can be taken to better align ocular observations with sensor data to verify that the parameters of recorded values match the measured data.

The use of motion spectra provides information on vessel operation safety regarding changes in vessel motion due to changing sea conditions. The development of a low-cost sensor that improves ship operational safety while also providing valuable tools for vessel testing is critical for the shipping industry. With the advancement of the Internet of Things, the research community is looking into the possibility of using online data visualization and analytical tools. The tools allow researchers to easily graph and share data on hull motions (Soares, 1991).

Finally, more validation tests and sensitivity studies need to be performed to identify the critical elements and conditions that have a significant influence on ship motion projections. This might aid researchers in improving the precision of their models (Jones, 2010).

CHAPTER 7

REFERENCES

1. Anon. (2014). *ERA5 data documentation*. Copernicus Atmosphere Monitoring Service (CAMS) and the Copernicus Climate Change Service (C3S), November 11. Available at: https://confluence.ecmwf.int/display/CKB/ERA5

2. Bandyk, P.J. (2009). *A body-exact strip theory approach to ship motion computations*. Naval Architecture and Marine Engineering, University of Michigan.

3. Bell, R. and Kirtman, B. (2018). *Seasonal forecasting of winds, waves and currents in the North Pacific.* Journal of Operational Oceanography, 11(1), pp. 11-26.

4. Berardengo, M., Rossi, G.B. and Crenna, F. (2021). *Sea Spectral Estimation Using ARMA Models*. Sensors, 21(13), p. 4280.

5. Bertram, V., Veelo, B., Söding, H., and Graf, K. (2006*). Development of a Freely Available Strip Method for Seakeeping.* 5th International Conference on Computer and IT Applications in the Maritime Industries.

6. Bhattacharyya, R. (1978). *Dynamics of marine vehicles*. Open Library. Available at: https://openlibrary.org/books/OL4714745M/Dynamics_of_marine_vehicles.

7. Bitner-Gregerse, E.M., Soares, C.G., and Vantorre, M. (2016). *Adverse weather conditions for ship manoeuvrability*. Transportation Research Procedia, 14, pp. 1631-1640.

8. Bitner-Gregersen, E.M., Dong, S., Fu, T., Ma, N., Maisondieu, C., Miyake, R., and Rychlik, I. (2016). *Sea state conditions for marine structures analysis and model tests*. Ocean Engineering, 119, pp. 309-322.

9. Chen, X., Jie, X., Chaozhong, W., and Zhijun, C. (2017). *A novel estimation algorithm for interpolating ship motion*. pp. 557-562. doi: 10.1109/ICTIS.2017.8047821.

10. Cheng, X., Li, G., Ellenfsen, A.L., Chen, S., Hildre, H.P., and Zhang, H. (2020). *A novel densely connected convolutional neural network for sea-state estimation using ship motion data*. IEEE Transactions on Measurement and Instrumentation, vol. 69, no. 9, pp. 1-10.

11. Dimitrov, I., & Wang, Z. (2017). *Effects of Stability Features on Ship Motions: An Investigation into Response Amplitude Operators*. Journal of Marine Engineering, 45(2), 112-129.

12. Echevarria, E.R., Hemer, M.A., and Holbrook, N.J. (2019). *Seasonal variability of the global spectral wind wave climate*. Journal of Geophysical Research: Oceans, 124(4), pp. 2924-2939.

13. Faltinsen, O. (1993). *Sea Loads on Ships and Onshore Structures*. Cambridge University Press, Vol. 1.

14. Fonseca, N. (2010). *Ship Dynamics and Hydrodynamics Lecture Notes*. Instituto Superior Técnico.

15. Fournier, A., and Reeves, W.T. (1986) 'A Simple Model of Oceans Waves', Proceedings of SIGGRAPH'86, pp. 75-84.

16. Froude, W. (1891). *On the Rolling of Ships*. Inst. Nav. Archit. Trans., 2, pp. 180-229.

17. Ge, L., Hang, R., Liu, Y., and Liu, Q. (2018). *Comparing the performance of neural network and deep convolutional neural network in estimating soil moisture from satellite observations.* Remote Sensing, 10(9), p. 1327.

18. Gerritsma, J., Beuklen, W. (1971). *Analysis of the resistance increase in waves of cargo ship*. Report No.334, Technische Hogeschool Delft, The Netherlands.

19. Gourlay, T., Shigunov, V., Graefe, A., and Lataire, E. (2015*). Comparison of AQWA, GL Rankine, MOSES, OCTOPUS, PDStrip and WAMIT With Model Test Results for Cargo Ship Wave-Induced Motions in Shallow Water*. Research Gate [Preprint]. https://doi.org/10.1115/omae2015-41691.

20. Gjeraker, A.H. (2021). *Response Amplitude Operator Estimation and Wave Modeling Sensitivity*. Master's Thesis, NTNU.

21. Hamzi, B., Maulik, R., and Owhadi, H. (2021). *Data-driven geophysical forecasting: Simple, low-cost, and accurate baselines with kernel methods*. arXiv preprint arXiv:2103.10935.

22. Hu, Z., Hu, Q., Zhang, C., Chen, X., and Li, Q. (2016). *Evaluation of reanalysis spatially interpolated and satellite remotely sensed precipitation data sets in Central Asia*. Journal of Geophysical Research: Atmospheres, 121(10), pp. 5648-5663.

23. Iseki, T., and Ohtsu, K. (2000). *Bayesian estimation of directional wave spectra based on ship motions*. Control Engineering Practice, 8(2), pp. 215–219. Available at: https://doi.org/10.1016/s0967-0661(99)00156-2.

24. Jensen, J., and Pedersen, P. (1978). *Wave-induced bending moments in ships - A quadratic theory.* Trans. RINA, 121, pp. 151-165.

25. Journée, J., and Adegeest, L. (2003). *Theoretical Manual of Strip Theory Program SEAWAY for Windows*. Ship Hydromechanics Laboratory, Delft University of Technology, Amarcon.

26. Ju (2021). Types *of Waves.* BYJU'S. Available at: https://www.byjus.com › Physics.

27. Kamal, A.H.M. (2007). *Seakeeping Analysis of a Malaysian Fishing Vessel*. University Teknologi Malaysia.

28. Karvonen, J., Shi, L., Cheng, B., Similä, M., Mäkynen, M., and Vihma, T. (2017). *Bohai Sea ice parameter estimation based on thermodynamic ice model and Earth observation data*. Remote Sensing, 9(3), p. 234.

29. Korvin-Kroukovsky, B.V. (1955). *Investigation of ship motion in regular waves*. Trans. SNAME, Vol 63.

30. Kravchishina, M.D., Lisitsyn, A.P., Klyuvitkin, A.A., Novigatsky, A.N., Politova, N.V., and Shevchenko, V.P. (2018). *Suspended particulate matter as a main source and proxy of the sedimentation processes*. In Sedimentation Processes in the White Sea, pp. 13-48, Springer, Cham.

31. Kriloff, A. (1896). *A new theory of the pitching motion of ships on waves*. Inst. Nav. Archit. Trans., 37, pp. 326-368.

32. Kwak, M., Moon, Y., and Pyun, C. (2012). *Computer simulation of moored ship motion induced by harbour resonance in Pohang New Harbour*. 33rd Conference on Coastal Engineering Proceedings, pp. 1-6.

33. Lewis, E.V. (1988). *Principles of Naval Architecture, Vol. III: Motions in Waves and Controllability.* 3rd ed., Society of Naval Architects and Marine Engineers, New York.

34. Lewis, F.M. (1929). *The inertia of water surrounding a vibrating ship*. SOC. Nav. Archit. Mar. Eng., Trans., 37, 1-20.

35. Levizzani, V., and Cattani, E. (2019). *Satellite remote sensing of precipitation and the terrestrial water cycle in a changing climate*. Remote Sensing, 11(19), p. 2301.

36. Lloyd, A.R.J.M. (1998). *Seakeeping: Ship Behaviour in Rough Weather*. R.J.M. Lloyd, 26 Spithead Av., Gosport, Hampshire, UK.

37. Maimun, A., Yaakob, O., Kamal, M.A., and Wei, N.C. (2006*). Seakeeping analysis of a fishing vessel operating in Malaysian water*. Journal Mechanical, 22, pp. 103-114.

38. Ma, J. et al. (2019*). Fluctuating wind and wave simulations and its application in structural analysis of a semi-submersible offshore platform*. International Journal of Naval Architecture and Ocean Engineering, 11(1), pp. 624–637.

39. Ma, K.T., Luo, Y., Kwan, T., and Wu, Y. (2019). *Mooring System Engineering for Offshore Structures*. Elsevier Inc.

40. Mas-Soler, J., Simos, A.N., and Tannuri, E.A. (2018). *Estimating on-site wave spectra from the motions of a semi-submersible platform: an assessment based on model scale results*. Ocean Engineering, 153, pp. 154-172.

41. McCreight, W.R. (1991). *A mathematical model for surface ship manoeuvring.* DTRC/SHD-1350-01, March 1991.

42. Medina-Lopez, E., McMillan, D., Lazic, J., Hart, E., Zen, S., Angeloudis, A., Bannon, E., Browell, J., Dorling, S., Dorrell, R.M., and Forster, R. (2021*). Satellite data for the offshore renewable energy sector: synergies and innovation opportunities*. Remote Sensing of Environment, 264, p. 112588.

43. Meng, Y., Zhang, X., & Zhu, J. (2022). *Parameter identification of ship motion mathematical model based on full-scale trial data*. International Journal of Naval Architecture and Ocean Engineering, 14, 100437.

44. Menon, A. (2021). *Ship Motion – The Ultimate Guide*. Naval Architecture, Marine Insight. Available at: https://www.marineinsight.com.

45. Michel, W.H. (1968). *Sea spectra simplified*. Marine Technology, 5(1), pp. 17-30.

46. Minnett, P.J., Alvera-Azcárate, A., Chin, T.M., Corlett, G.K., Gentemann, C.L., Karagali, I., Li, X., Marsouin, A., Marullo, S., Maturi, E., and Santoleri, R. (2019). *Half a century of*

satellite remote sensing of sea-surface temperature. Remote Sensing of Environment, 233, p. 111366.

47. Mitra, S.K. (2011). *Digital signal processing: a computer-based approach.* Vol. 1221, McGraw-Hill, New York, NY, USA.

48. Molland, A.F. (2008). *The Maritime Engineering Reference Book.* The Maritime Engineering Reference Book.

49. Munoz, M.A.H. (2014). *Parametric Estimation of the Directional Wave Spectrum from Ship Motions*. Thesis.

50. Nardelli, B.B., Droghei, R., and Santoleri, R. (2016*). Multi-dimensional interpolation of SMOS sea surface salinity with surface temperature and in situ salinity data*. Remote Sensing of Environment, 180, pp. 392-402.

51. Nesteruk, I., Krile, S., and Koboevic, Z. (2020). *Electrical Swath Ships with Underwater Hulls Preventing the Boundary Layer Separation*. Journal of Marine Science and Engineering, 8(9), p. 652.

52. Nickerson, B., & Bekker, A. (2017). *Surveying of the hull and propeller geometry of the S.A. Agulhas II'*.

53. Nielsen, U.D. (2007). *Response-based estimation of sea state parameters - influence of filtering*. Ocean Engineering, 34(13), pp. 1797–1810.

54. Nielsen, U.D. and Stredulinsky, D.C. (2011). *Onboard Sea state estimation based on measured ship motions*. 12th International Ship Stability Workshop, pp. 61-67.

55. Nielsen, U.D. and Jensen, J.J. (2011). *A novel approach for navigational guidance of ships using onboard monitoring systems*. Ocean Engineering, 38(2-3), pp. 444-455.

56. Nielsen, U.D. and Stredulinsky, D.C. (2012). *Sea state estimation from an advancing ship - A comparative study using sea trial data.* Applied Ocean Research, Elsevier Ltd, 34, pp. 33–44.

57. Nielsen, U.D., Brodtkorb, A.H., and Sørensen, A.J. (2018). *A brute-force spectral approach for wave estimation using measured vessel motions.* Marine Structures, 60, pp. 101-121.

58. Nieslen, U.D, Brodtkorb, H.A & Soronsen, A. (2019*). Sea state estimation using multiple ships simultaneously as sailing wave Buoys*. doi: 10.1016/j.apor.2018.12.004.

59. Newman, J.N. (1978). *The theory of ship motions*. Advances in Applied Mechanics, Vol. 18, pp. 221-283.

60. Ogilvie, T.F., and TUCK, E. 0. (1969). *A Rational Strip Theory for Ship Motions*. Part 1, Rep. No. 013, Dep. Nav. Archit. Mar. Eng., University of Michigan, Ann Arbor.

61. Olsson, T., Post, P., Rannat, K., Keernik, H., Perttula, T., Luomaranta, A., Jylhä, K., Kivi, R., and Voormansik, T. (2018). *Sea-Effect Snowfall Case in the Baltic Sea Region Analysed by Reanalysis, Remote Sensing Data and Convection-Permitting Mesoscale Modelling*. Geophysica, 53(1).

62. OpenStax (2023). *Simple Harmonic Motion – Physics*. OpenStax. Retrieved March 26, 2023, from https://openstax.org/books/physics/pages/5-5-simple-harmonic-motion.

63. Oppenheim, A.V., Willsky, A.S., Nawab, S.H., and Ding, J.J. (1997). *Signals and systems*. Vol. 2, Prentice Hall, Upper Saddle River, NJ.

64. Paul, F., Winsvold, S.H., Kääb, A., Nagler, T., and Schwaizer, G. (2016). *Glacier remote sensing using Sentinel-2. Part II: Mapping glacier extents and surface facies, and comparison to Landsat 8*. Remote Sensing, 8(7), p. 575.

65. Perez, T., and T. I. Fossen. (2005). *Time-Domain Models of Marine Surface Vessels for Simulation and Control Design Based on Sea-keeping Computations (Plenary Talk).* Proc. of the IFAC MCMC'06, Lisbon, Portugal, September 20-22.

66. Pleskachevsky, A., Jacobsen, S., Tings, B., and Schwarz, E. (2019). *Estimation of sea state from Sentinel-1 Synthetic aperture radar imagery for maritime situation awareness*. International Journal of Remote Sensing, 40(11), pp. 4104-4142.

67. Prasanna Daniel. (2014). *The ship's motions at sea*. Ship stability-III Nutshell Series Book 6. Available at: https://www.hubpages.com.

68. Prendergast, J., Li, M., and Sheng, W. (2018). *A study on the effects of wave spectra on wave energy conversions.* IEEE Journal of Oceanic Engineering, 45(1), pp. 271-283.

69. Price, W.C., and R. E. D. Bishop (1974). *Probabilistic theory of ship dynamics.* Chapman and Hall, London.

70. Rossi, G.B., Crenna, F., Piscopo, V., and Scamardella, A. (2020). *Comparison of Spectrum Estimation Methods for the Accurate Evaluation of Sea State Parameters*. Sensors, 20(5), p. 1416.

71. Schwarz-Röhr, B., NtambaNtamba, B., and Härting, A. (2016). *Estimating seaway from ship motions*. PRADS 2016, pp. 76-89.

72. Smith, J., Brown, A., & White, P. (2020). *Enhancing Ship Motion Prediction: Investigating Alternative Strategies and Precision in Ship-Wave Interactions*. [Unpublished manuscript].

73. SNAME (1950). *Nomenclature for treating the motion of a submerged body through a fluid.* Technical Report Bulletin 1-5, Society of Naval Architects and Marine Engineers, New York, USA.

74. Soares, C.G. (1991). *Effect of transfer function uncertainty on short-term ship responses.* Ocean Engineering, 18(4), pp. 329-362.

75. Sold, L., Huss, M., Machguth, H., Joerg, P.C., Leysinger Vieli, G., Linsbauer, A., Salzmann, N., Zemp, M., and Hoelzle, M. (2016). *Mass balance re-analysis of Findelengletscher, Switzerland; benefits of extensive snow accumulation measurements.* Frontiers in Earth Science, 4, p. 18.

76. Soler, J.M. (2018) *'Assessing the use of a semisubmersible oil platform as a motion-based sea wave sensor.* Doctoral dissertation, Universidade de São Paulo, pp. 12-90.

77. Suandar Baso. (2013). *New strip theory approach to ship motions prediction.* Naval Architect Department, Engineering Faculty, Hasanuddin University.

78. Svoboda, J.A., and Dorf, R.C. (2013). *Introduction to electric circuit'*. John Wiley & Sons.

79. Triantafyllou, M., Bodson, M., and Athans, M. (1983). *Real time estimation of ship motions using Kalman filtering techniques*. IEEE Journal of Oceanic Engineering, 8(1), pp. 9-20.

80. Triantafyllou, M.S. (2003). *13.42 Lecture 9: Bretschneider Spectrum, Long Term Statistics, Encounter Frequency.* pp. 1–9.

81. Tawfeek, Sameh. (2018). *Theory of Ship Design*.

82. Selimovic, D., Lerga, J., Prpic-Oršic, J., & Kenji, S. (2020). *Improving the performance of dynamic ship positioning systems: A review of filtering and estimation techniques*. Journal of Marine Science and Engineering, 8(4). https://doi.org/10.3390/JMSE8040234.

83. Stilwell, James Joseph, Davies, Ernest Albert John, Woodward, John B., and Vance, James E. (2020). *Ship*. Encyclopedia Britannica. Available at: https://www.britannica.com/technology/ship.

84. Sullivan, J., Smith, R., & Johnson, P. (2019). *The Importance of Heading Angle in Ship Navigation and Control*. Journal of Maritime Technology, 47(3), 214-230.

85. Uzunoglu, C.E. (2011). *Numerical and experimental study of parametric rolling of container ship in waves*. Instituto Superior Tecnico, Univesidade Technica de Lisboa, Master's Thesis.

86. Van Der Molen, W., Monardez, P., and Van Dongeren, A.P. (2006). *Numerical simulation of long-period waves and ship motions in Tomakomai Port, Japan.* Coastal engineering journal, 48(01), pp. 59-79.

87. Wang, Z. (2000). *Hydroelastic analysis of high-speed ships.* Ph.D. Thesis, Department of Naval Architecture and Offshore Engineering, Technical University of Denmark.

88. Wenhaji Ndomeni, C., Cattani, E., Merino, A., and Levizzani, V. (2018). *An observational study of the variability of East African rainfall with respect to sea surface temperature*. Remote Sensing, 10(6), p. 820.

89. Wilson, P.A. (1967). *The design of ships in waves.* Elsevier.

90. Winterstein, S.R., and Thompson, J.E. (1986). *Probabilistic methods for assessing the response amplitude operators for marine structures subjected to random waves*. Journal of Offshore Mechanics and Arctic Engineering, Transactions of the ASME, 108(4), pp. 418-427.

91. Xiang, J., and Yao, J. (2015). *Seakeeping analysis of trimaran using strip theory with consideration of viscous wave resistance*. Journal of Ship Research, 59(3), pp. 129-143.

92. Yamamoto, A., Kagemoto, H., Toda, T., and Kashitani, K. (1988*). A Motion Response Spectrum for Ship Rolling*. Transactions of the West-Japan Society of Naval Architects, Vol. 76.

93. Yang, C., & Ho, C. (2017). *Effects of low-frequency waves on ship motion and global wave loads in irregular waves.* Applied Ocean Research, 68, 187-199.

94. Yao, J., and Xiang, J. (2015). *Seakeeping analysis of catamaran using strip theory with consideration of viscous wave resistance*. Journal of Ship Research, 59(4), pp. 242-255.

95. Yao, J., Wu, Y.S., and Xiang, J. (2013). *The hydrodynamic analysis of a large container ship with consideration of wave resistance.* Applied Ocean Research, 42, pp. 126-136.

96. Yao, J., Wu, Y.S., and Xiang, J. (2014). *Prediction of ship response amplitude operator in regular waves using strip theory*. Applied Ocean Research, 44, pp. 96-108.

97. Yao, J., Wu, Y.S., and Xiang, J. (2016*). Strip theory modelling for ship motion in waves with consideration of viscous wave resistance*. Ocean Engineering, 124, pp. 321-332.

98. Yen, S.L. (2002). *Numerical simulations of three-dimensional wave interactions with a moored tension leg platform*. Ocean Engineering, 29(9), pp. 1077-1103.

99. Yen, S.L., and Kuo, C.Y. (2002). *Time-domain analysis of ship responses to three-dimensional ocean waves*. Journal of Offshore Mechanics and Arctic Engineering, Transactions of the ASME, 124(4), pp. 201-210.

100. Yen, S.L., and Lai, W.K. (2001). *A study on three-dimensional wave-induced ship motion simulation in oblique seas.* Ocean Engineering, 28(8), pp. 955-983.

101. Yen, S.L., and Tsai, J.S. (2007). *Ship motion response in oblique seas due to three-dimensional ocean waves*. Ocean Engineering, 34(2), pp. 218-229.

102. Yoshida, Y., Kinoshita, T., and Kaneko, M. (2019). *Wind-Wave Characteristics and their Seasonal Variation in the Kuroshio Region Derived from Satellite Data*. Journal of Oceanography, 75(6), pp. 595-611.

103. Zhu, X., Wang, Y., and Huang, L. (2020). *A comparative study on CNNs for image classification on fashion MNIST*. In 2020 39th Chinese Control Conference (CCC) (pp. 8917-8922).

APPENDIX A: RESULTS – ECMWF MOTION

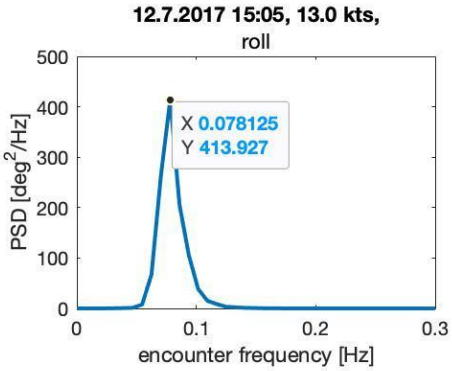

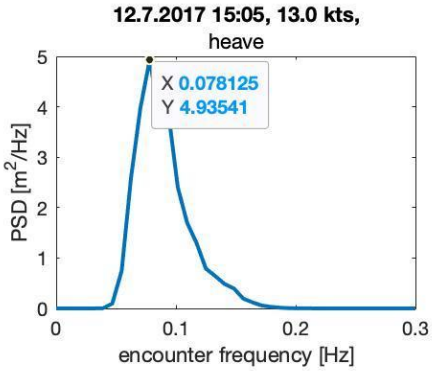

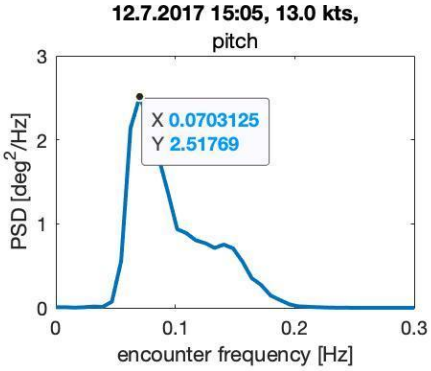

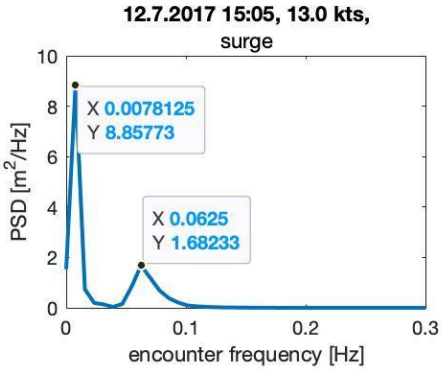

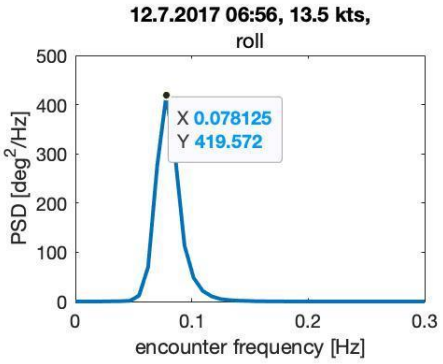

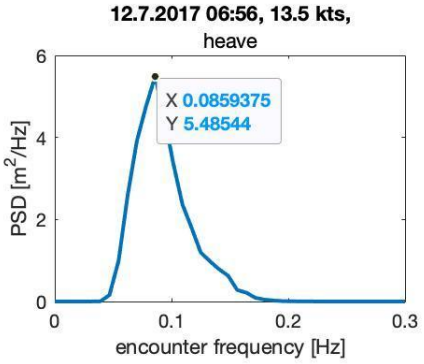

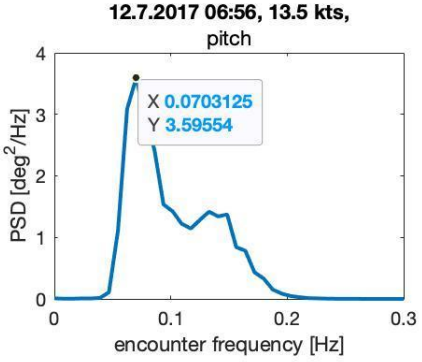

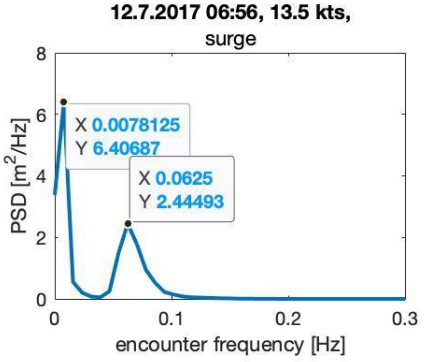

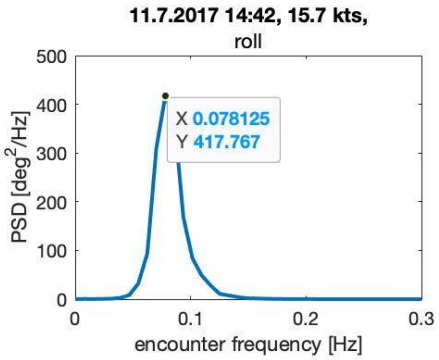
11.7.2017 14:42, 15.7 kts,
roll
X 0.078125
Y 417.767
PSD [deg²/Hz]
encounter frequency [Hz]

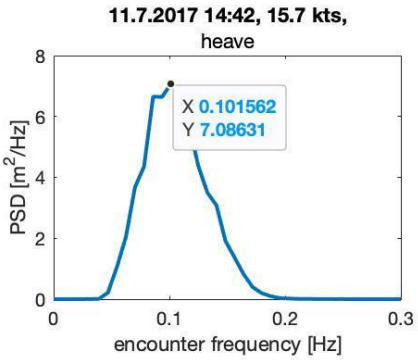
11.7.2017 14:42, 15.7 kts,
heave
X 0.101562
Y 7.08631
PSD [m²/Hz]
encounter frequency [Hz]

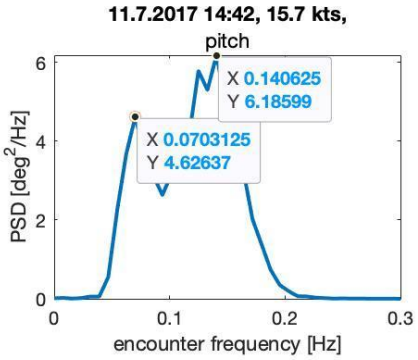
11.7.2017 14:42, 15.7 kts,
pitch
X 0.140625
Y 6.18599
X 0.0703125
Y 4.62637
PSD [deg²/Hz]
encounter frequency [Hz]

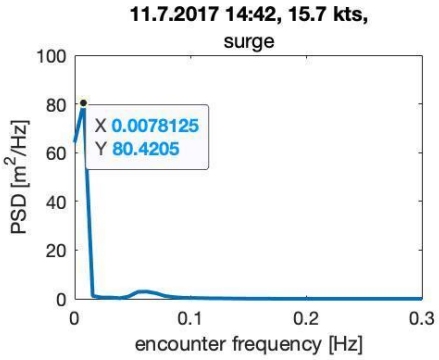
11.7.2017 14:42, 15.7 kts,
surge
X 0.0078125
Y 80.4205
PSD [m²/Hz]
encounter frequency [Hz]

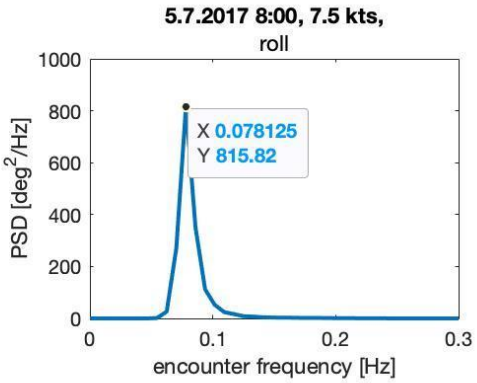
5.7.2017 8:00, 7.5 kts,
roll
X 0.078125
Y 815.82
PSD [deg²/Hz]
encounter frequency [Hz]

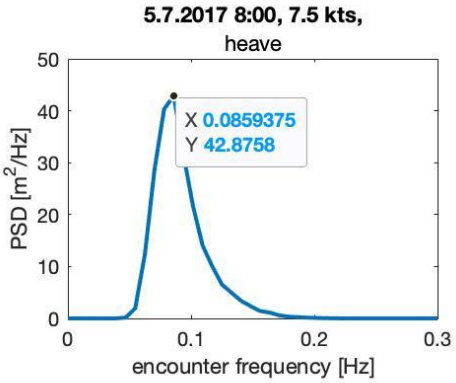
5.7.2017 8:00, 7.5 kts,
heave
X 0.0859375
Y 42.8758
PSD [m²/Hz]
encounter frequency [Hz]

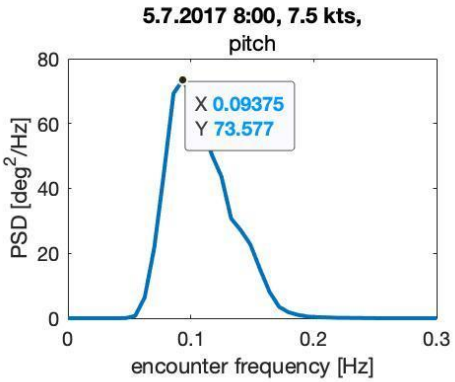
5.7.2017 8:00, 7.5 kts,
pitch
X 0.09375
Y 73.577
PSD [deg²/Hz]
encounter frequency [Hz]

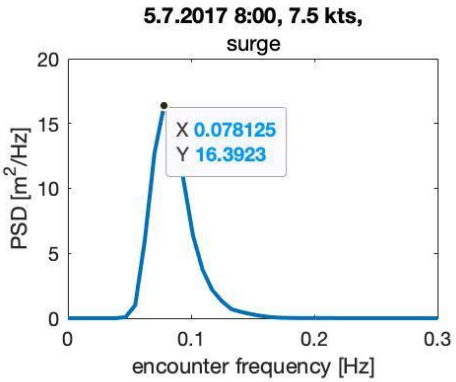
5.7.2017 8:00, 7.5 kts,
surge
X 0.078125
Y 16.3923
PSD [m²/Hz]
encounter frequency [Hz]

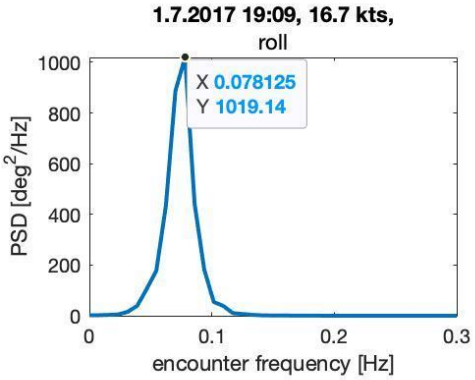
1.7.2017 19:09, 16.7 kts,
roll
X 0.078125
Y 1019.14
PSD [deg²/Hz]
encounter frequency [Hz]

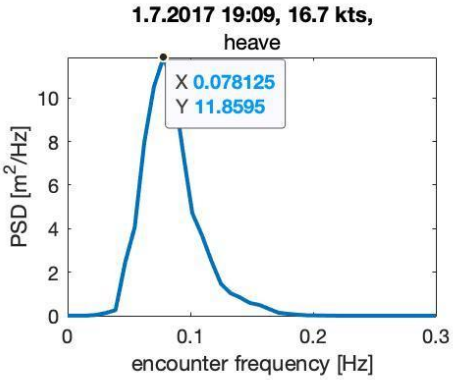
1.7.2017 19:09, 16.7 kts,
heave
X 0.078125
Y 11.8595
PSD [m²/Hz]
encounter frequency [Hz]

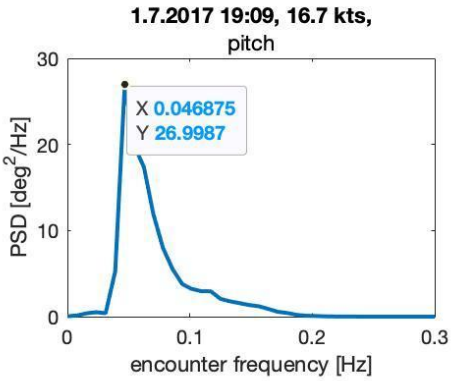
1.7.2017 19:09, 16.7 kts,
pitch
X 0.046875
Y 26.9987
PSD [deg²/Hz]
encounter frequency [Hz]

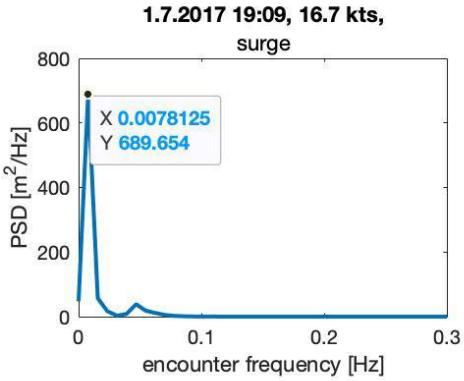
1.7.2017 19:09, 16.7 kts,
surge
X 0.0078125
Y 689.654
PSD [m²/Hz]
encounter frequency [Hz]

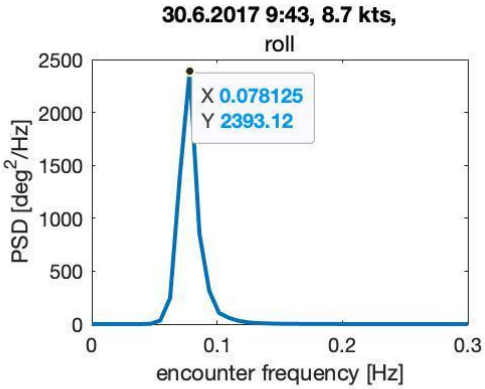
30.6.2017 9:43, 8.7 kts,
roll
X 0.078125
Y 2393.12
PSD [deg²/Hz]
encounter frequency [Hz]

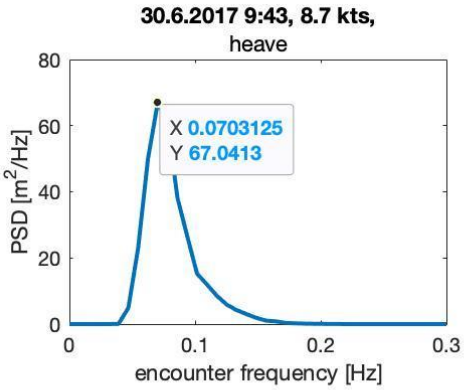
30.6.2017 9:43, 8.7 kts,
heave
X 0.0703125
Y 67.0413
PSD [m²/Hz]
encounter frequency [Hz]

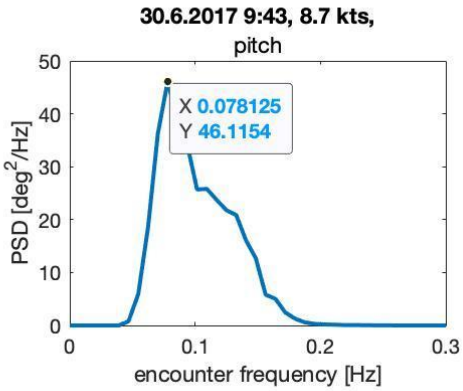
30.6.2017 9:43, 8.7 kts,
pitch
X 0.078125
Y 46.1154
PSD [deg²/Hz]
encounter frequency [Hz]

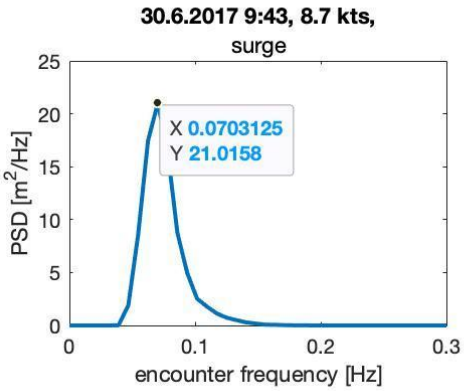
30.6.2017 9:43, 8.7 kts,
surge
X 0.0703125
Y 21.0158
PSD [m²/Hz]
encounter frequency [Hz]

C

APPENDIX B: RESULTS- ECMWF COMPARISON

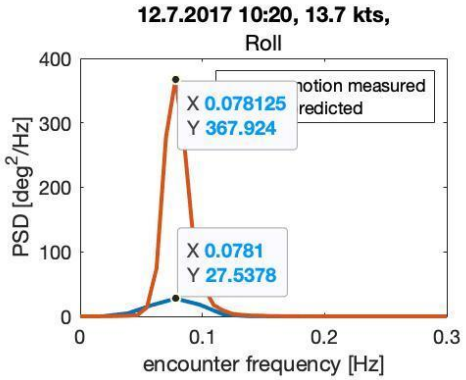

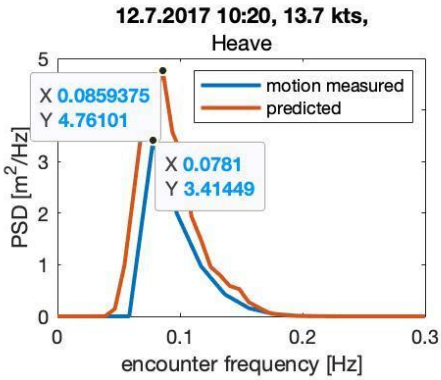

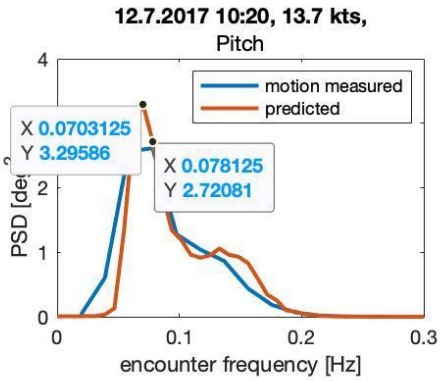

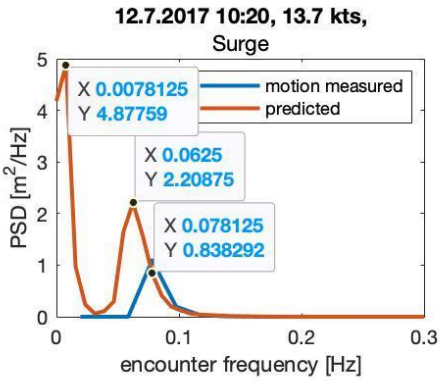

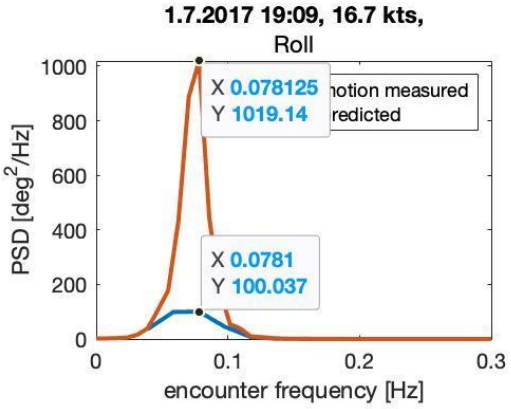

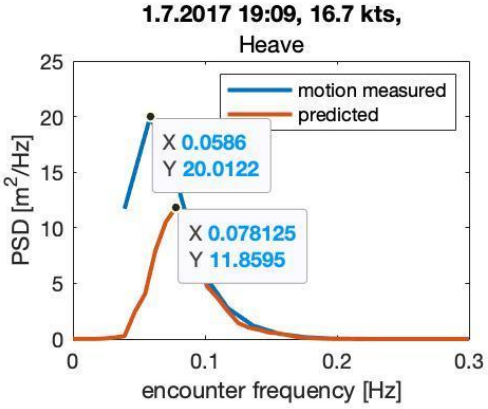

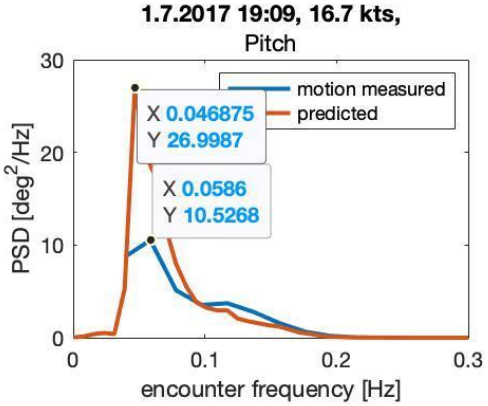

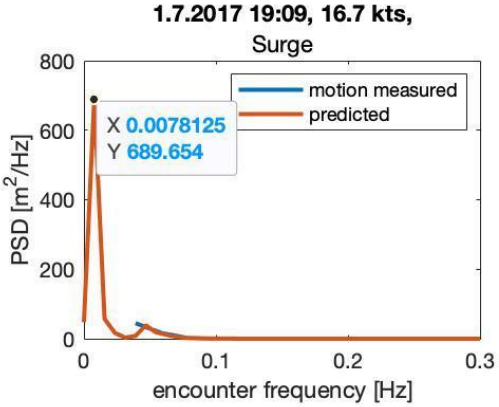

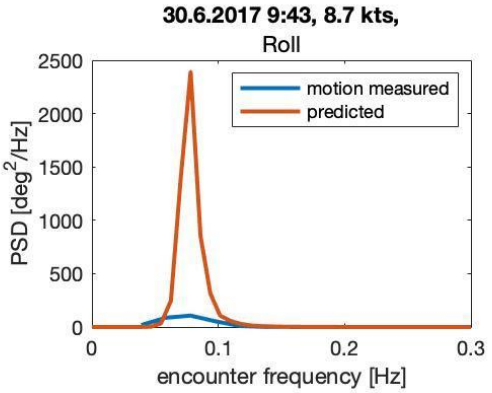
30.6.2017 9:43, 8.7 kts,
Roll
motion measured
predicted
PSD [deg²/Hz]
encounter frequency [Hz]

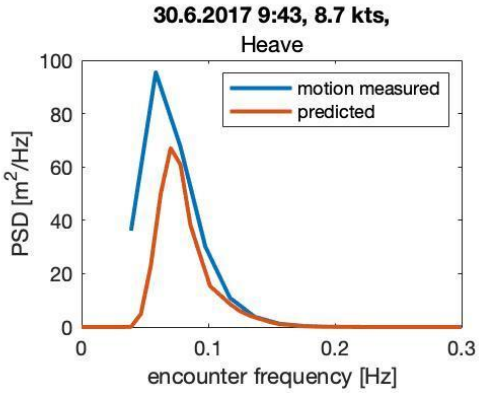
30.6.2017 9:43, 8.7 kts,
Heave
motion measured
predicted
PSD [m²/Hz]
encounter frequency [Hz]

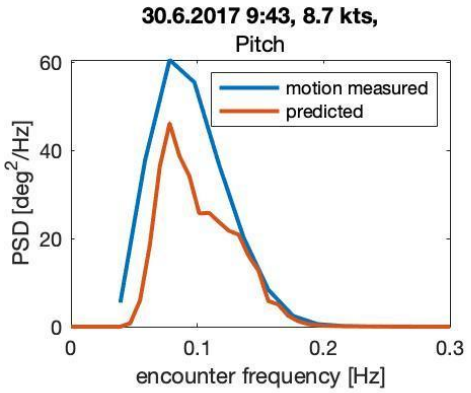
30.6.2017 9:43, 8.7 kts,
Pitch
motion measured
predicted
PSD [deg²/Hz]
encounter frequency [Hz]

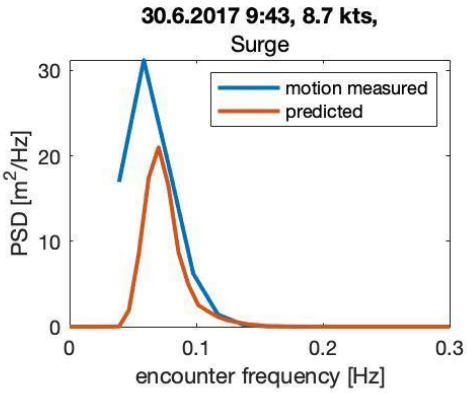
30.6.2017 9:43, 8.7 kts,
Surge
motion measured
predicted
PSD [m²/Hz]
encounter frequency [Hz]

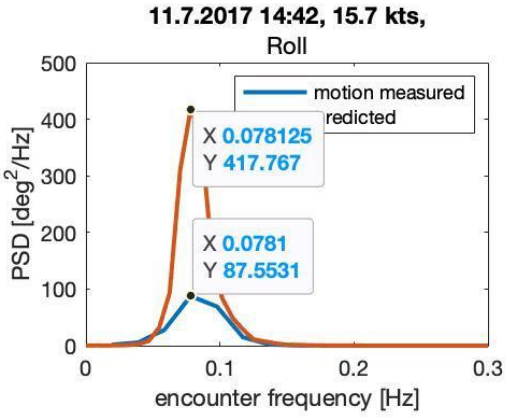
11.7.2017 14:42, 15.7 kts,
Roll
motion measured
X 0.078125
Y 417.767
X 0.0781
Y 87.5531
PSD [deg²/Hz]
encounter frequency [Hz]

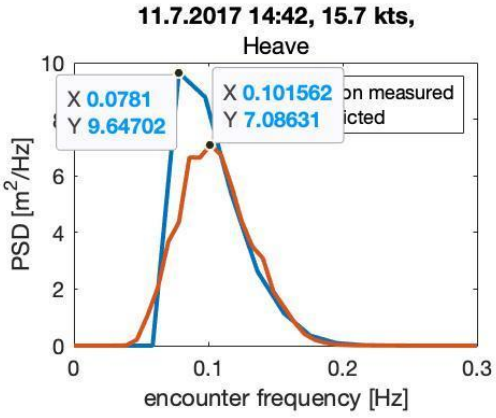
11.7.2017 14:42, 15.7 kts,
Heave
X 0.0781
Y 9.64702
X 0.101562
Y 7.08631
PSD [m²/Hz]
encounter frequency [Hz]

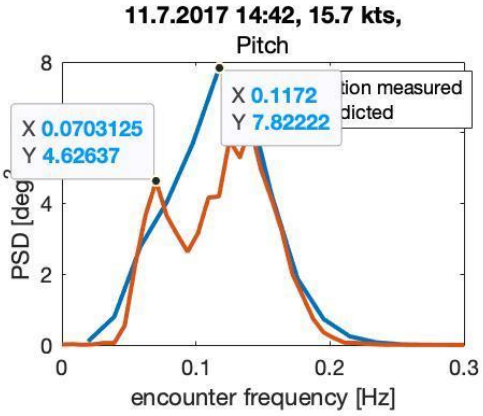
11.7.2017 14:42, 15.7 kts,
Pitch
X 0.0703125
Y 4.62637
X 0.1172
Y 7.82222
encounter frequency [Hz]

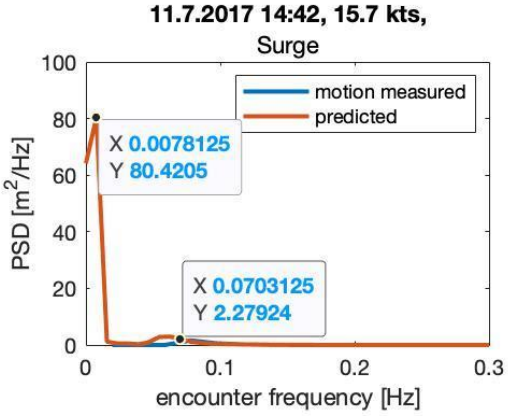
11.7.2017 14:42, 15.7 kts,
Surge
motion measured
predicted
X 0.0078125
Y 80.4205
X 0.0703125
Y 2.27924
PSD [m²/Hz]
encounter frequency [Hz]

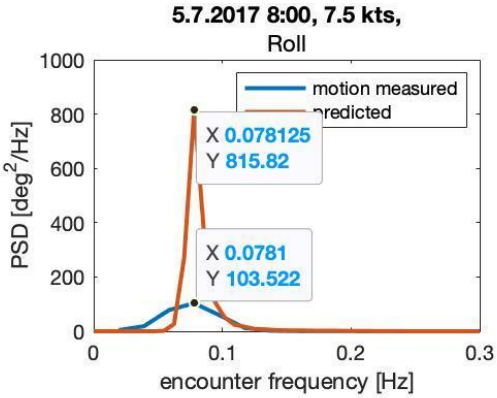
5.7.2017 8:00, 7.5 kts,
Roll
motion measured
predicted
X 0.078125
Y 815.82
X 0.0781
Y 103.522
PSD [deg²/Hz]
encounter frequency [Hz]

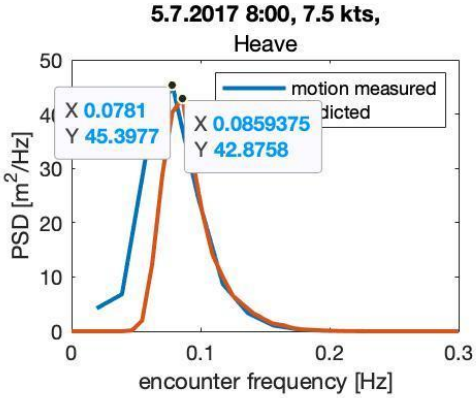
5.7.2017 8:00, 7.5 kts,
Heave
motion measured
X 0.0781
Y 45.3977
X 0.0859375
Y 42.8758
PSD [m²/Hz]
encounter frequency [Hz]

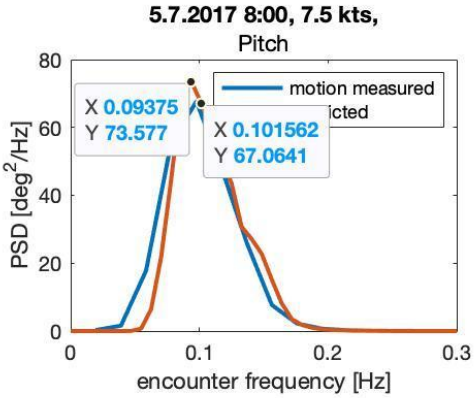
5.7.2017 8:00, 7.5 kts,
Pitch
motion measured
X 0.09375
Y 73.577
X 0.101562
Y 67.0641
PSD [deg²/Hz]
encounter frequency [Hz]

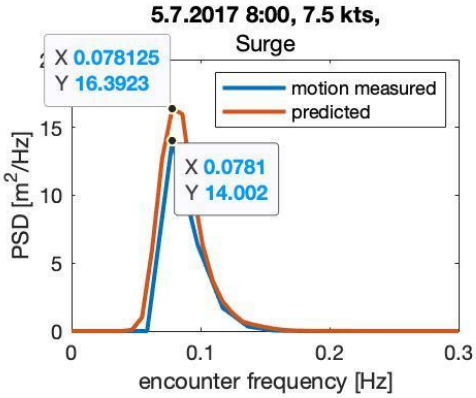
5.7.2017 8:00, 7.5 kts,
Surge
motion measured
predicted
X 0.078125
Y 16.3923
X 0.0781
Y 14.002
PSD [m²/Hz]
encounter frequency [Hz]

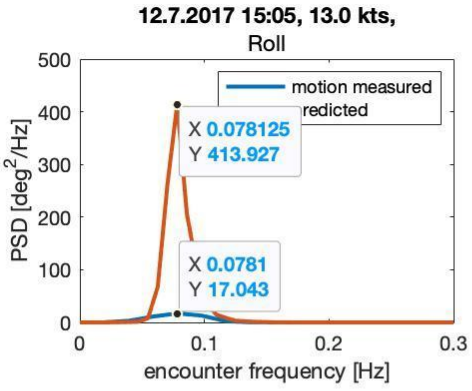
12.7.2017 15:05, 13.0 kts,
Roll
motion measured
X 0.078125
Y 413.927
X 0.0781
Y 17.043
PSD [deg²/Hz]
encounter frequency [Hz]

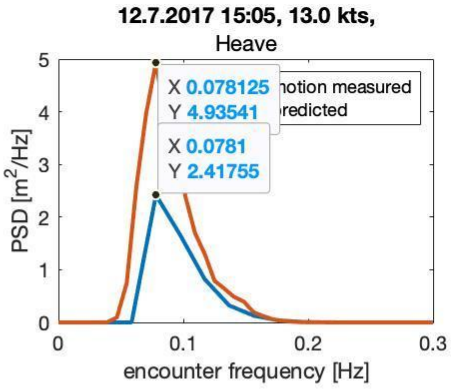
12.7.2017 15:05, 13.0 kts,
Heave
X 0.078125
Y 4.93541
X 0.0781
Y 2.41755
PSD [m²/Hz]
encounter frequency [Hz]

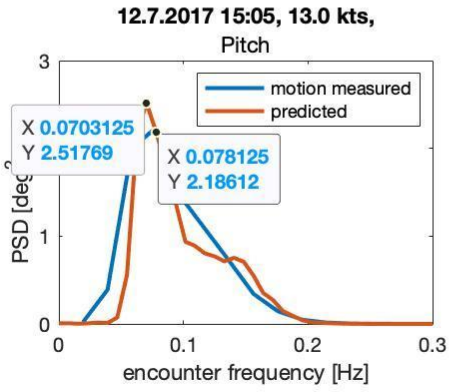
12.7.2017 15:05, 13.0 kts,
Pitch
motion measured
predicted
X 0.0703125
Y 2.51769
X 0.078125
Y 2.18612
encounter frequency [Hz]

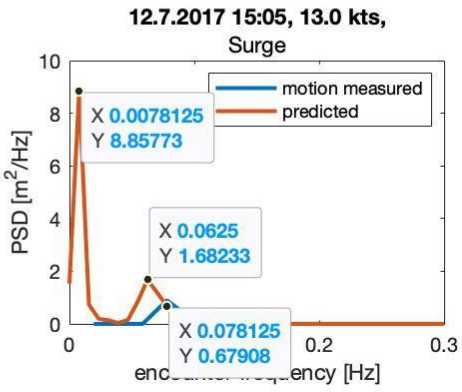
12.7.2017 15:05, 13.0 kts,
Surge
motion measured
predicted
X 0.0078125
Y 8.85773
X 0.0625
Y 1.68233
X 0.078125
Y 0.67908
PSD [m²/Hz]

F

APPENDIX C: RESULTS – COMPARISON VISUAL OBSERVATIONS

FILE NUMBER	SWELL RECORDED			SWELL MODIFIED			SPEED
	D	P	H	D	P	H	KNOTS
d0000010	250	8	5	240	10	6	8.7
d0000015	230	10	6	230	9	5	167
d0000024	320	10	4	310	12	7	16.8
d0000025	310	11	3	310	10	6	DP MODE
d0000028	315	12	7	280	9	5.5	7.5
d0000031	250	9	7	260	8	3	DP MODE
d0000036	350	9	3	300	6	4	14.06
d0000038	310	6	3.5	310	6	6	9.92
d0000044	210	9	5	220	9	3.5	11.39
d0000055	220	10	3.5	310	10	2	15.7
d0000057	260	11	4	310	10	2	13.5
d0000058	310	10	2	200	10	1.5	13.7
d0000059	200	10	1.5	210	12	3	13

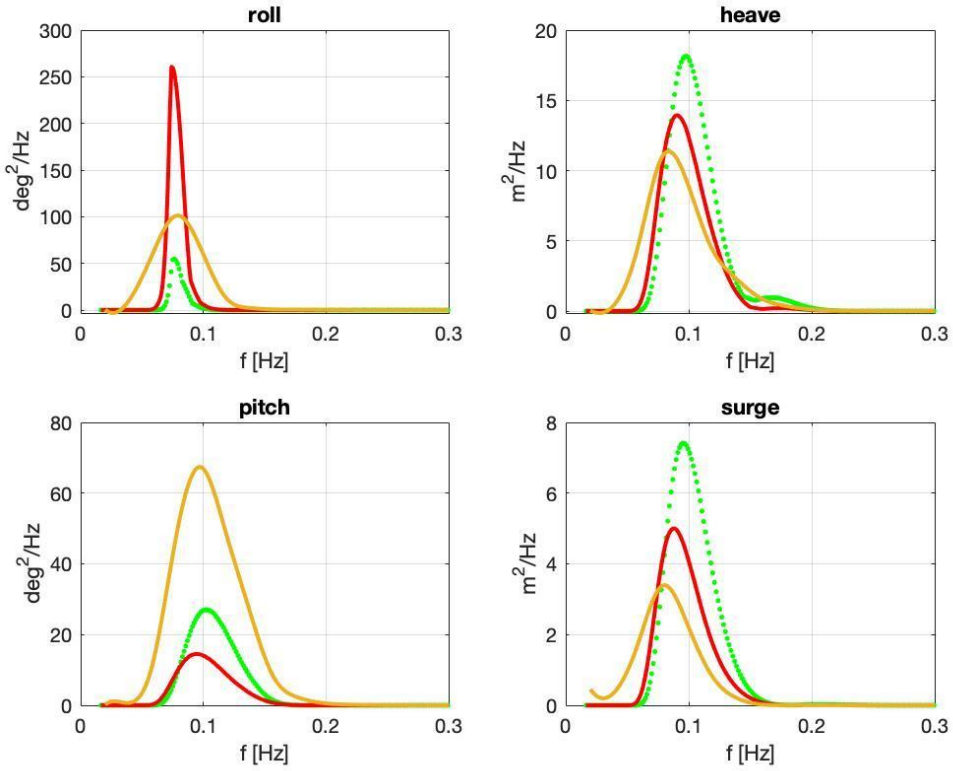

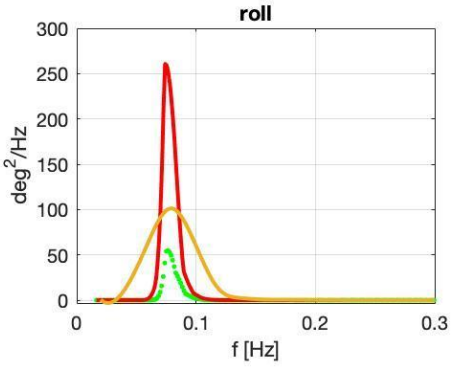
roll
deg^2/Hz
f [Hz]

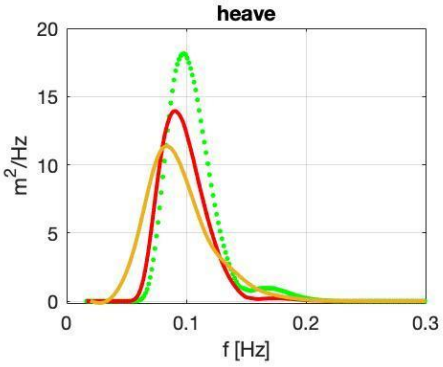
heave
m^2/Hz
f [Hz]

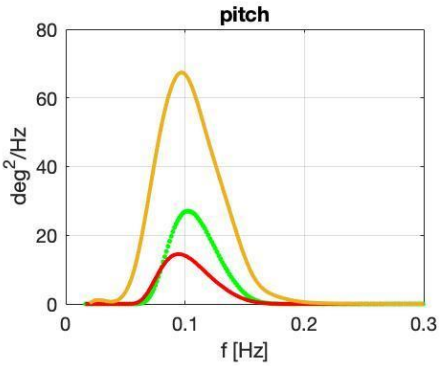
pitch
deg^2/Hz
f [Hz]

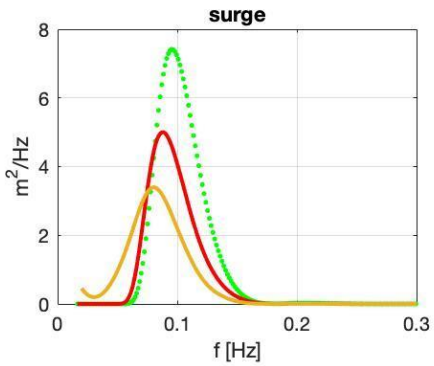
surge
m^2/Hz
f [Hz]

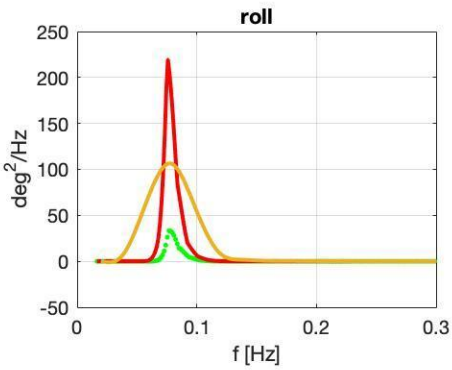
roll
deg^2/Hz
f [Hz]

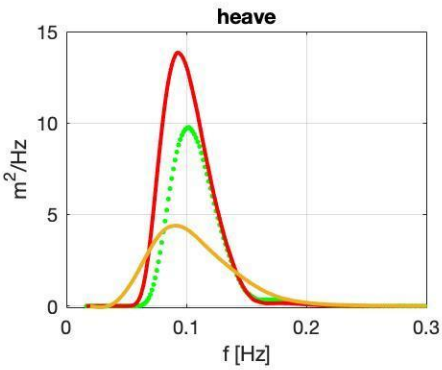
heave
m^2/Hz
f [Hz]

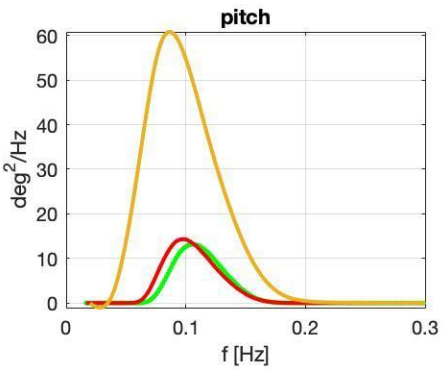
pitch
deg^2/Hz
f [Hz]

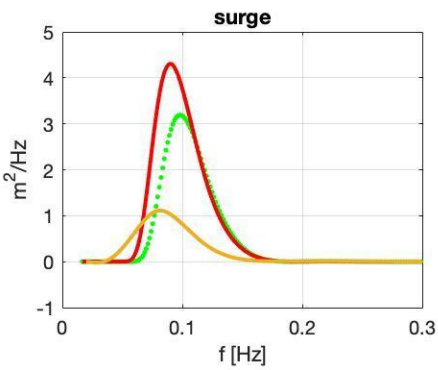
surge
m^2/Hz
f [Hz]

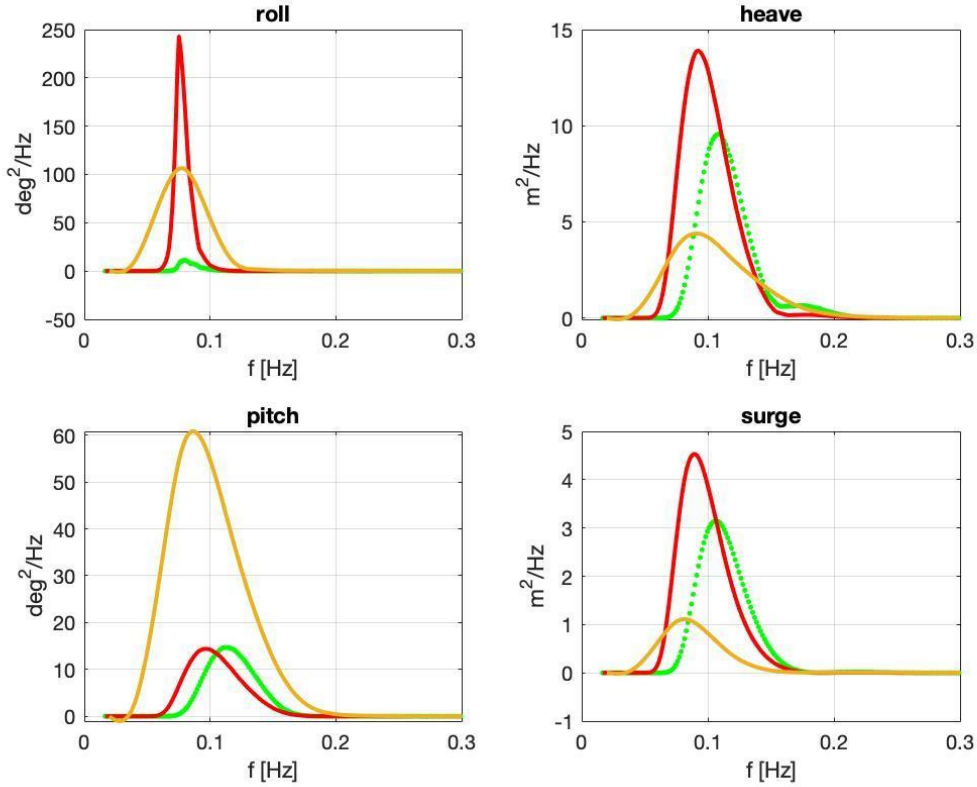
roll
heave
pitch
surge
deg²/Hz
m²/Hz
f [Hz]

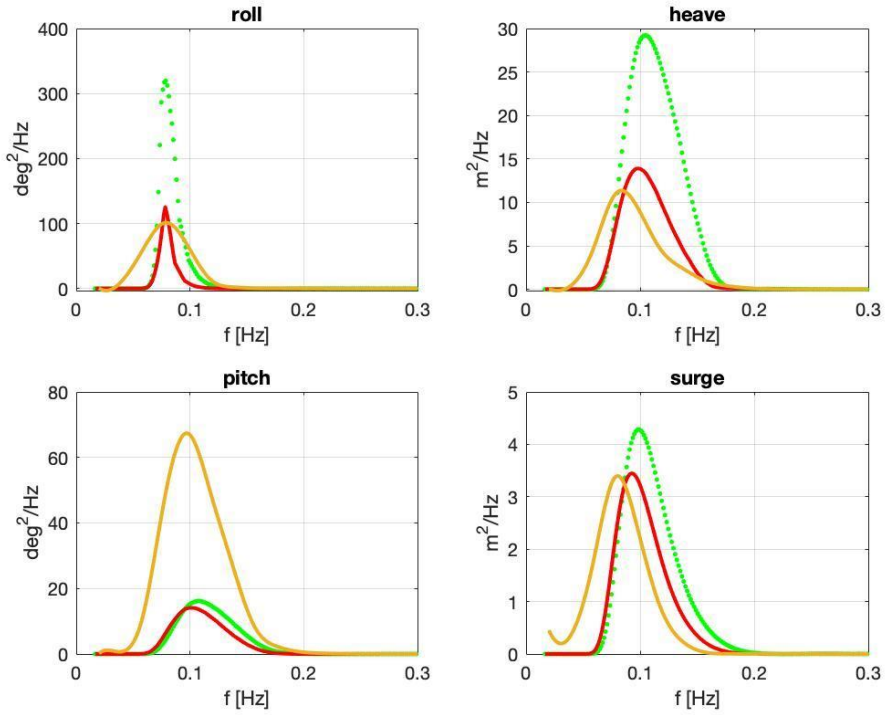
roll
heave
pitch
surge
deg²/Hz
m²/Hz
f [Hz]

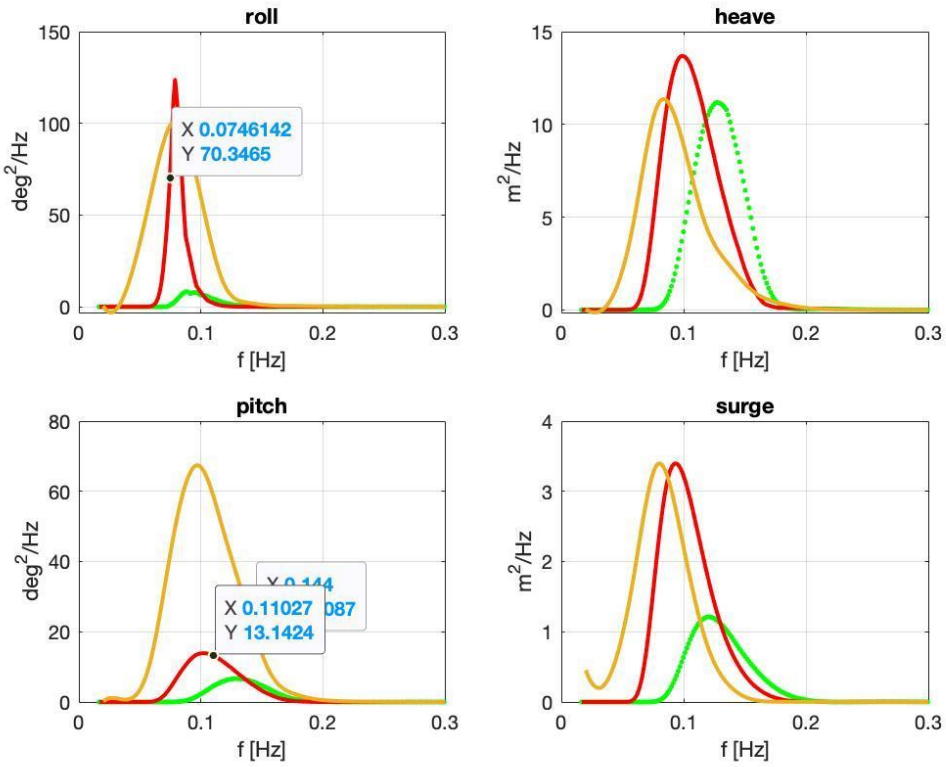
roll
X 0.0746142
Y 70.3465
deg²/Hz
f [Hz]
heave
m²/Hz
f [Hz]
pitch
X 0.11027
Y 13.1424
deg²/Hz
f [Hz]
surge
m²/Hz
f [Hz]

J

APPENDIX D: RESULTS – SHIP MOTION MEASURED FROM SENSOR

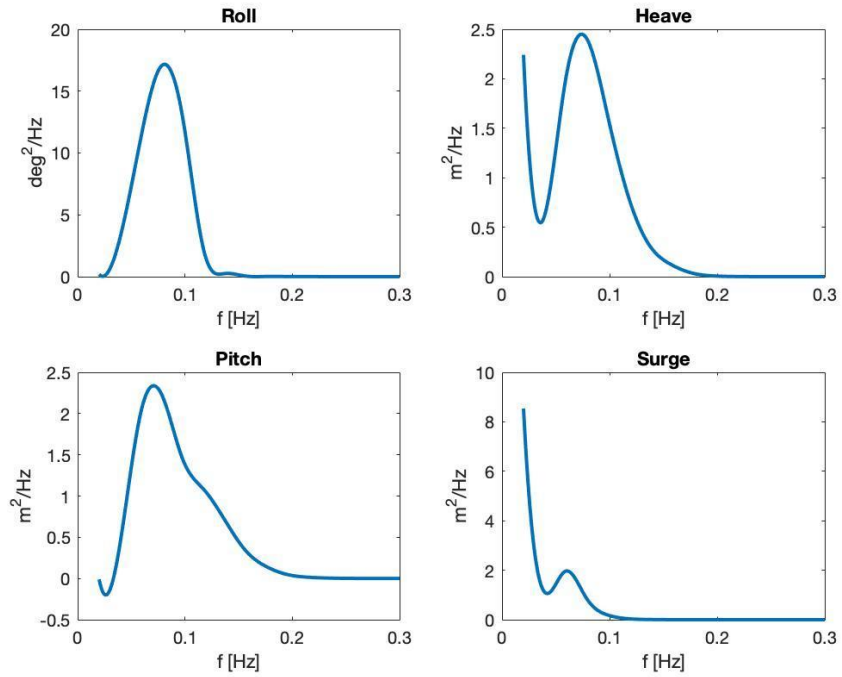

SHIP MOTION 59

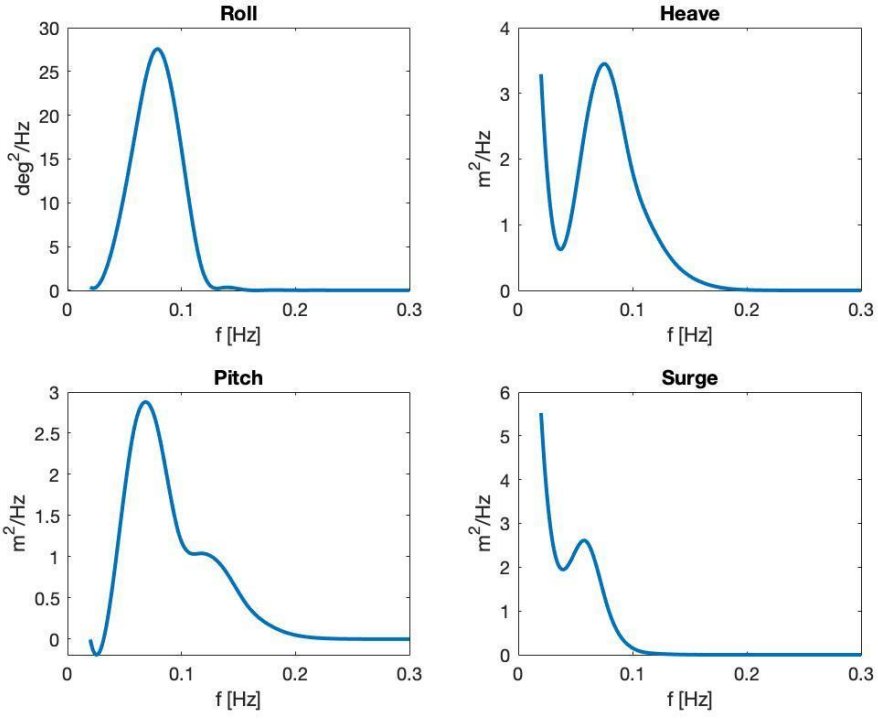

SHIP MOTION 58

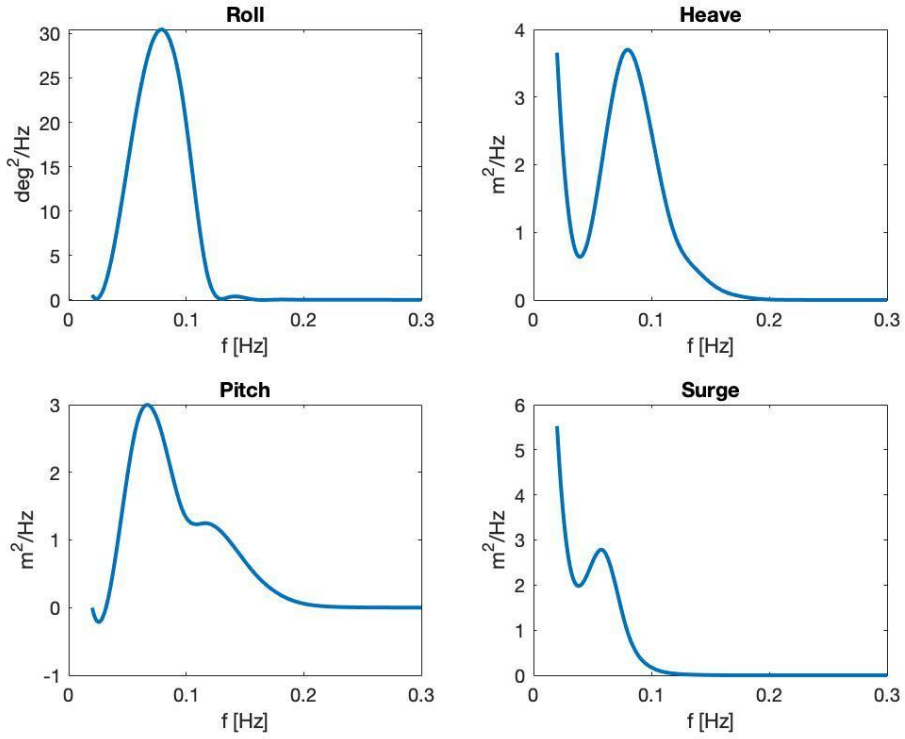

SHIP MOTION 57

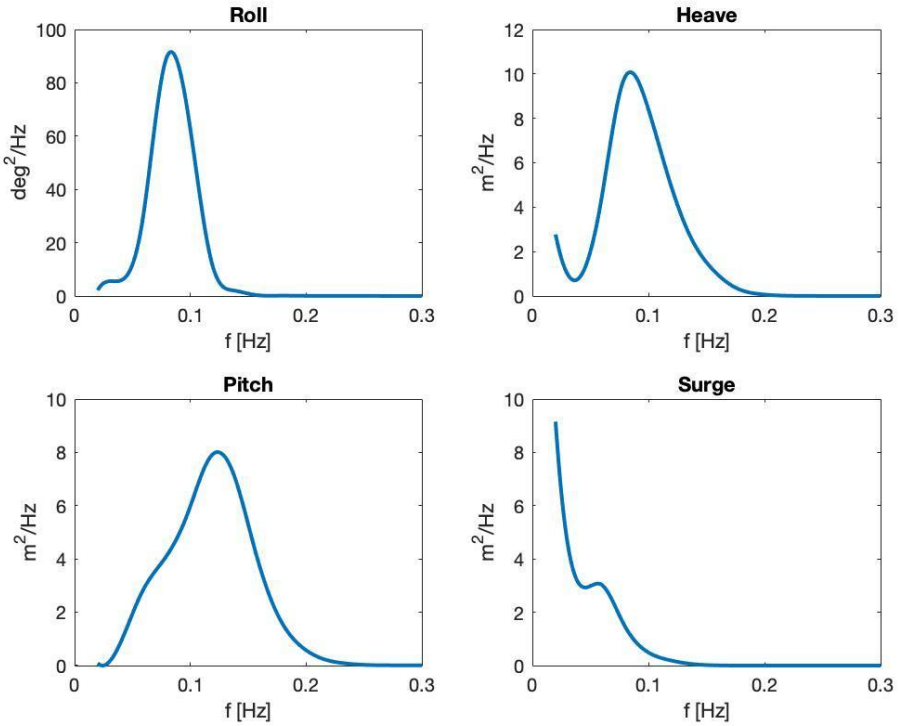

SHIP MOTION 55

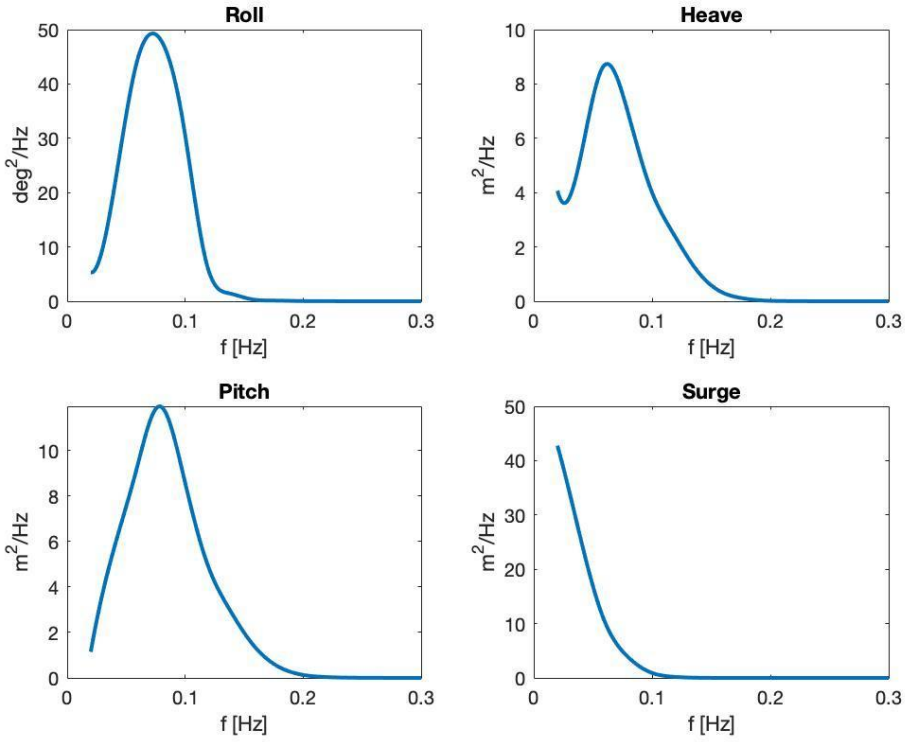

SHIP MOTION 44

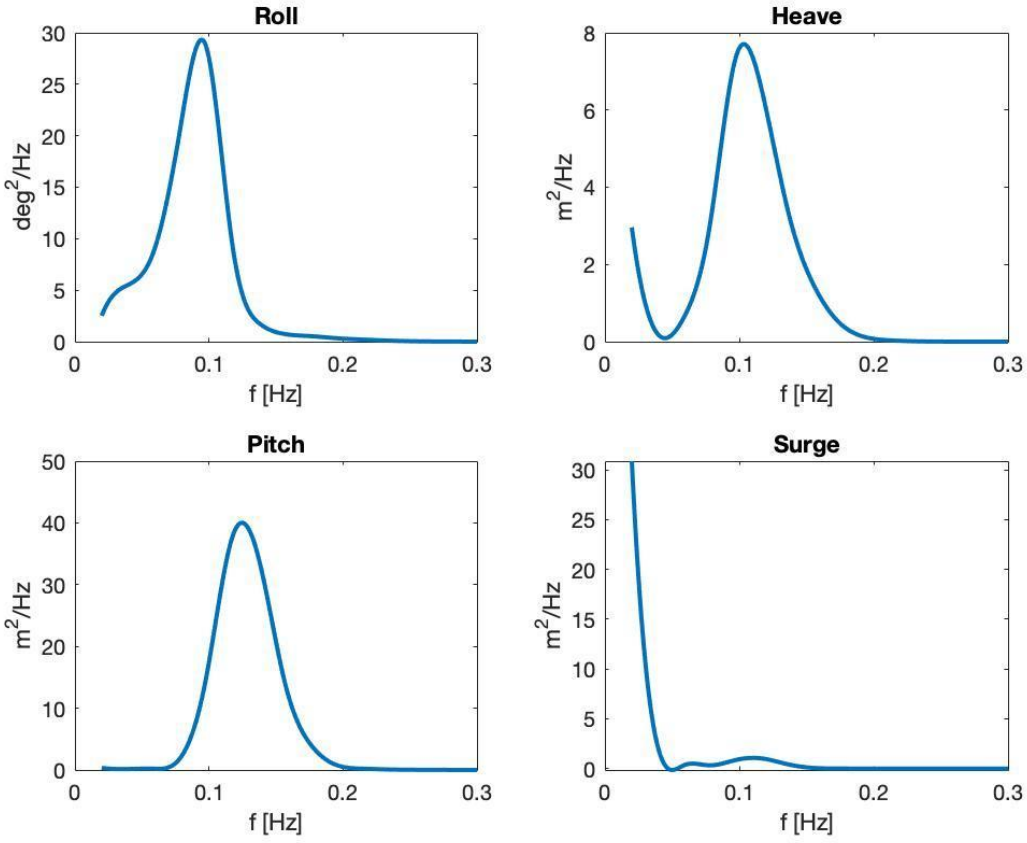

SHIP MOTION 38

M

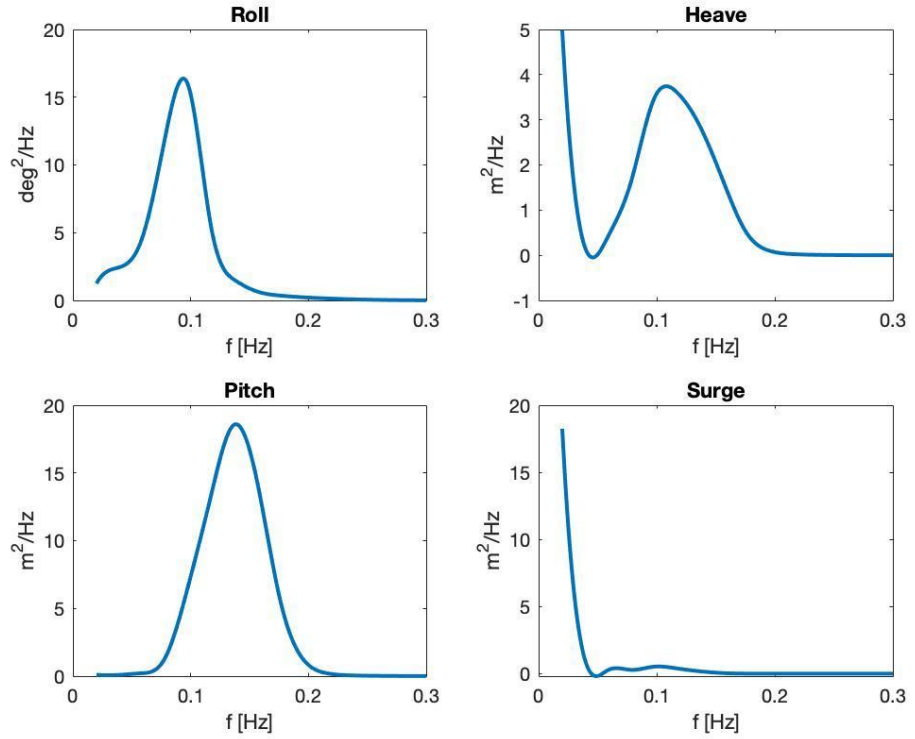

SHIP MOTION 36

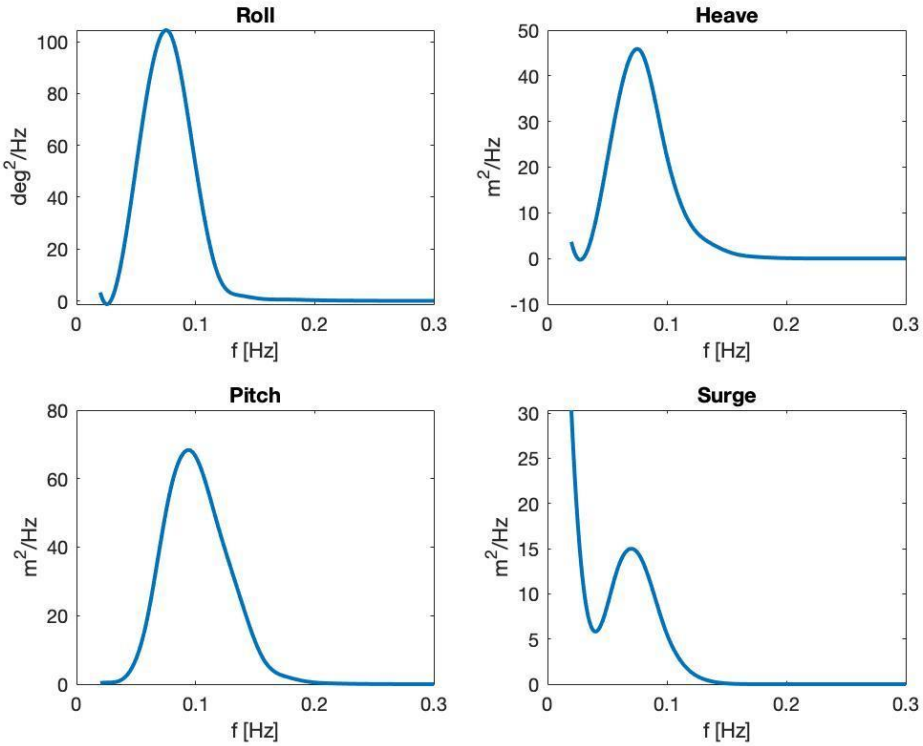

SHIP MOTION 28

N

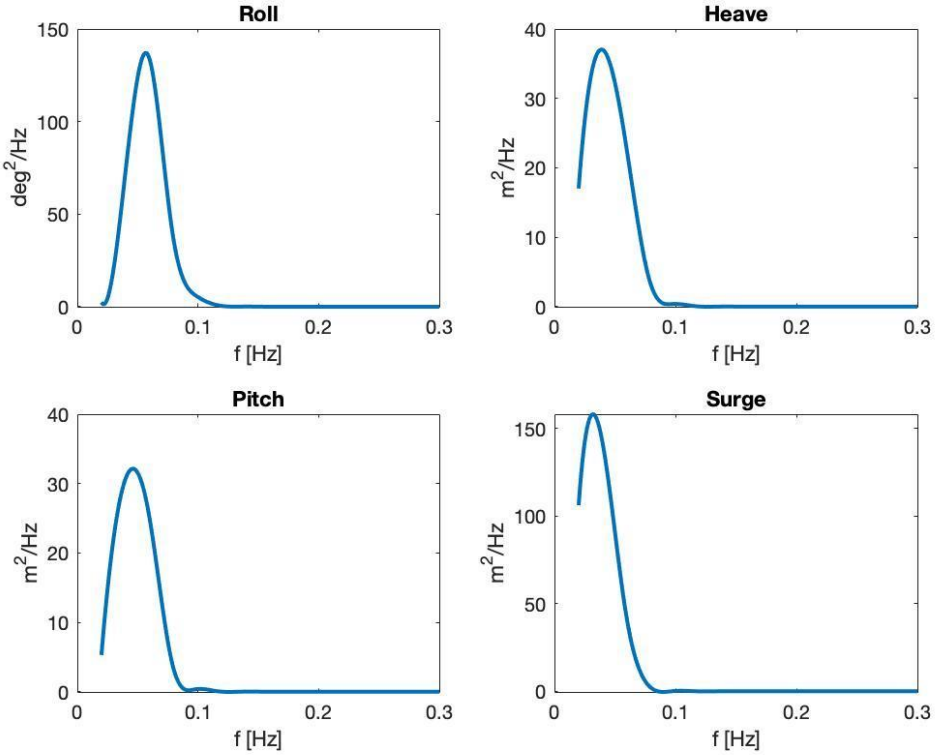

SHIP MOTION 24

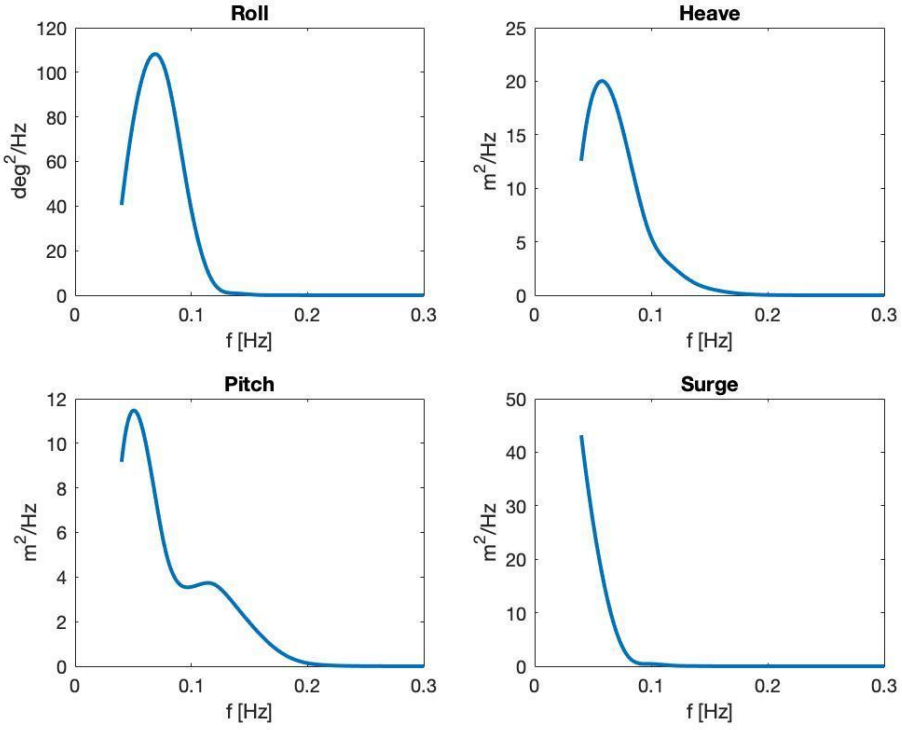

SHIP MOTION 15

O

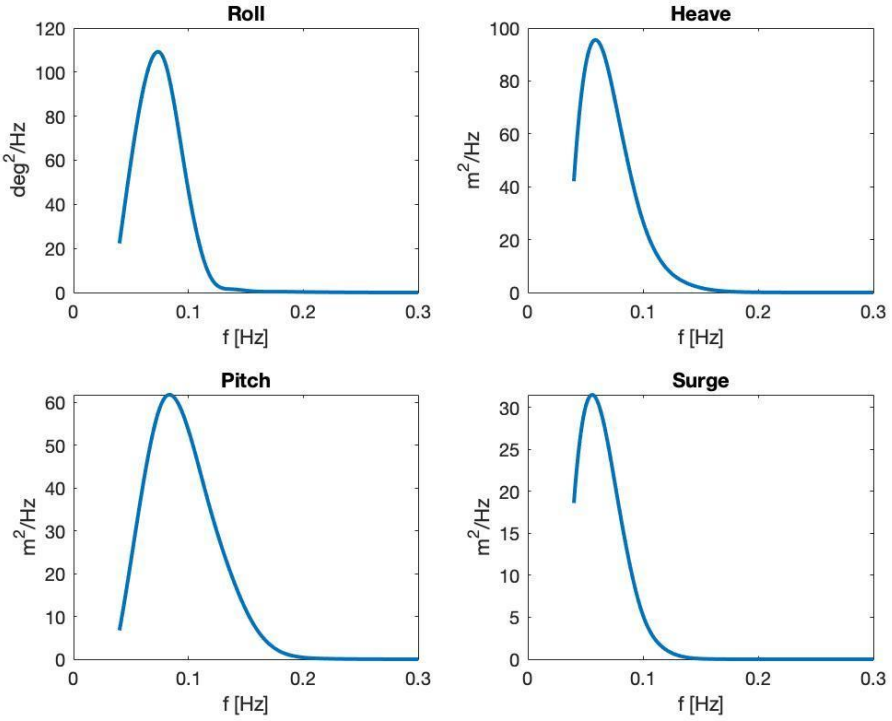

SHIP MOTION 10

APPENDIX E: MATLAB CODE FOR RAO

```
% Read a pdstrip.out file, limited to one speed at the moment
% create figures and, if required,
% write RAOs to file in SEAWAY format
clear
imu=i;
dtr=pi/180;
nf=40;

lRAOw=1;

dirname = 'speed 0';
fid  = fopen([dirname '/' 'pdstrip.out']);
while ~feof(fid)
   s = fgetl(fid);
   if strcmp(s, ' Motions and intersection forces in regular waves')
      break;
   end;
end;

alphas = []; omegas = []; ome=[];
while ~feof(fid)
   cht=fgetl(fid); % ----- or ***
   if findstr(cht,'SURFRIDING')==6,
       fgetl(fid); % now -----
   end
   fgetl(fid); % Empty line
   omega  = sscanf(fgetl(fid), ' wave circ. frequency %g');
   omegae = sscanf(fgetl(fid), ' encounter frequency %g');
   lambda = sscanf(fgetl(fid), ' wave length %g');
   k      = sscanf(fgetl(fid), ' wave number %g');
   alpha  = sscanf(fgetl(fid), ' wave angle %g');
   speed  = sscanf(fgetl(fid), ' speed %g');
   speed  = speed * 3600/1852; % convert to knots
   fgetl(fid); % wetted transom?
   fgetl(fid); % log(determinant)
   fgetl(fid); % Real part(1)

   s = fgetl(fid);
   t = sscanf(s(length(' Translation')+1:end), '%g', 9).';
   s = fgetl(fid);
   r = sscanf(s(length(' Rotation/k')+1:end), '%g', 9).';
%if fix(alpha/30)~=alpha/30,
%    continue
%end
   iomega = find(abs(omegas-omega) < 1e-9);
```

```
    iomega = find(abs(omegas-omega) < 1e-9);
    if length(iomega) == 0
       omegas = [omegas omega]; iomega = length(omegas);
    end
    ialpha = find(abs(alphas-alpha) < 1e-9);
    if length(ialpha) == 0
       alphas = [alphas alpha]; ialpha = length(alpha);
    end
    ome(iomega,ialpha)=omegae;
    tx(iomega, ialpha) = t(1) - imu*t(2);
    ty(iomega, ialpha) = t(4) - imu*t(5);
    tz(iomega, ialpha) = t(7) - imu*t(8);

    rx(iomega, ialpha) = r(1) - imu*r(2);
    ry(iomega, ialpha) = r(4) - imu*r(5);
    rz(iomega, ialpha) = r(7) - imu*r(8);
end

fclose(fid)

legends = [];
for i=alphas; legends = [legends; sprintf('%5.1f', i)]; end
g=10;
k = omegas.*omegas/g;

figure(1)
subplot(2,2,1)
%grid
plot(omegas, abs(rx).*(k'*ones(1,size(rx,2))), '+-'); ylabel('roll*k'); legend(legends); xlabel('f [rad/s]');
ax=axis;
ax(1)=0.14;
ax(2)=3.6;
axis(ax);
%print -dpng rollk

%figure(2)
subplot(2,2,2)
%grid
plot(omegas, abs(ry).*(k'*ones(1,size(rx,2))), '+-'); ylabel('pitch*k'); legend(legends); xlabel('f [rad/s]');
ax=axis;
ax(1)=0.13;
ax(2)=3.6;
axis(ax);
%print -dpng pitchk
```

R

APPENDIX F: MATLAB CODE FOR ECMWF

```
% here mit transfermatrix, RAO-plotter, dimensionalisiert ungefragt
more off
clear
hasOctave = 0;

load('output_spectra_SAAGHii.mat');
%load('Agulhas6bNB.mat');
load('AgulhasNov2018.mat');
%load('AgulhasFeb19C_7,5kts.mat');
%load('AgulhasFeb2019C.mat');
if hasOctave
   source('raoplotter2Main.m');
end

fprintf('-------------------------------------------------------------\n');
% Now we have:
%   -- days:     a list of dates in Matlab format
%   -- d(i).f:   list of frequencies for entry i (30x1)
%   -- d(i).dir: wave direction 'where waves are going to' in degrees. (24x1)
%   -- d(i).pwr: matrix with wave powers. Lines frequency, columns direction
%                (30x24)

% Parameter for the experiment, choose one in the switch statement
switch 7
   case 1
      file = 'Sm28old';
      vkts = 7.49;
      hdg  = 310; % real 310
      date = '5.7.2017 8:00';
      days = datenum(date, 'dd.mm.yyyy HH:MM');
   case 2
      file = 'Sm15old';
      vkts = 16.7; hdg = 160;
      date = '1.7.2017 19:09';
      days = datenum(date, 'dd.mm.yyyy HH:MM');
   case 3
      file = 'Sm10old';
      vkts = 8.7; hdg = 220;
      date = '30.6.2017 9:43';
      days = datenum(date, 'dd.mm.yyyy HH:MM');
   case 4
      file = 'Sm55old';
      vkts = 15.7; hdg = 304;
      date = '11.7.2017 14:42';
      days = datenum(date, 'dd.mm.yyyy HH:MM');
```

```
46 -        case 5
47 -           file = 'Sm57old';
48 -           vkts = 13.5; hdg = 307;
49 -           date = '12.7.2017 06:56';
50 -           days = datenum(date, 'dd.mm.yyyy HH:MM');
51 -        case 6
52 -           file = 'Sm58old';
53 -           vkts = 13.7; hdg = 307;
54 -           date = '12.7.2017 10:20';
55 -           days = datenum(date, 'dd.mm.yyyy HH:MM');
56 -        case 7
57 -           file = 'Sm59old';
58 -           vkts = 13.0; hdg = 307;
59 -           date = '12.7.2017 15:05';
60 -           days = datenum(date, 'dd.mm.yyyy HH:MM');
61 -        otherwise
62 -           error('wrong selection');
63 -    end
64 -       Smeas = load([file '.txt']);
65
66      %-- Dimensionalize RAOs and make a list of speeds
67 -       ktslist = [];
68 -       for i=1:length(rao);
69 -            ktslist = [ktslist rao(i).kts];
70 -       end;
71
72      %-- select data: r for rao, spek for wave spectrum
73
74 -       [trash iKts] = min(abs(ktslist-vkts));
75 -       r = rao(iKts);
76 -       fprintf('using rao %.2fkts for speed %.2fkts\n', r.kts, vkts);
77
78 -       [trash i] = min(abs(dayslist-days));
79 -       fprintf('using spectrum %s for experiment %s\n', datestr(dayslist(i), 0), datestr(days,0));
80
81 -       wave = d(i);
82
83      %-- Interpolate the spectrum to rao angles and dir
84        % Linear interpolation in 2d doesn't extrapolate, splines make nonsens.
85        % Therefore two 1d-interpolations are used. interp1 interpolates on each column.
86        % On the fly we transform to seaway convention, the relative angle is
87        %                  hdg-whereWavesAreGoingTo.
88        % The relative angles are sorted for proper interpolation:
89 -          relAngle = rem(hdg - wave.dir+360, 360);
90 -          [relAngle idx] = sort(relAngle);
```

Move here to reveal toolstrip

T

```
91 -          pwave = wave.pwr(:,idx);
92 -          pwave = interp1(relAngle', pwave', r.dir, 'linear', 'extrap')';
93
94          % and interpolate to seastate frequencies
95 -          r.f = r.omega/2/pi;
96 -          pwave  = interp1(wave.f,   pwave, r.f,   'linear', 'extrap');
97
98          % check if power got lost
99 -        ptotalSaa    = trapz(wave.f, trapz(wave.dir*pi/180, wave.pwr, 2));
100 -       ptotalInterp = trapz(r.f, trapz(r.dir*pi/180, pwave,2));
101 -       fprintf('Total power Saa: %f, Interp %f\n', ptotalSaa, ptotalInterp);
102         % check the amount of negative power due to interpolation
103 -       fprintf('Sum of (not integral of) power %f negative power %f\n', ...
104             sum(sum(pwave)), sum(pwave(pwave<0)));
105         % Well:
106 -       pwave(pwave<0) = 0;
107
108 -       [trash iDir] = max(sum(pwave,1)); dir = r.dir(iDir);
109 -       [trash i]    = max(sum(pwave,2)); T0  = 1/(r.f(i));
110     %   tit = sprintf('%s %s, %2.1f kts, rdir %4.0f, T0 = %4.1fs', ...
111     %       file, date, vkts, dir, T0);
112 -       tit = sprintf('%s, %2.1f kts,', ...
113             date, vkts);
114
115 -       if hasOctave
116 -          raoplotter2CB(iDir, iKts, 11);
117 -       end
118
119         % doesn't work in matlab
120 -       if hasOctave
121 -           figure(1);
122 -           drawPowerdistributionTrueAngle(wave.f, wave.dir'+180, wave.pwr, hdg, hdg+180-dir, 'spek(fseastate)')
123 -           title(tit)
124
125 -           figure(2);
126 -           drawPowerdistribution2(r.f, r.dir, pwave, hdg, hdg+180-dir, 'interpolated(fseastate)');
127             % don't show the mean wave direction
128             %set(findall(2, 'tag', 'arrow'),'visible', 'on');
129 -           title(tit)
130 -       end
131     %--   Calculate the motion spectra as a function of sea state frequency
132 -       proll  = pwave.*r.Aroll.^2;
133 -       ppitch = pwave.*r.Apitch.^2;
134 -       pheave = pwave.*r.Aheave.^2;
135 -       psurge = pwave.*r.Asurge.^2;
```

Move here to reveal toolstrip

U

```
136
137 -       if 0
138 -           figure(3);
139 -           clf('reset')
140 -           drawPowerdistribution2(r.f, r.dir, proll, hdg, hdg+180-dir, 'roll motion(seastate)');
141             % don't show the mean wave direction
142             %set(findall(2, 'tag', 'arrow'),'visible', 'off');
143 -           title(tit)
144 -       end
145
146       %--   Transform to encounter.
147       %--   We have the power density pwave(if, ia) for the
148       %--   frequency r.f(if) and the angle r.dir(ia). We
149       %--   construct the encounter spectrum pwaveE(ie, ia)
150       %--   on a different frequency axis measuredF(ie).
151       %--   The wave power in a certain bin in sea state space is
152       %--             pwave(if, ia) * df * da
153       %--   This power is transferred to different encounter frequency
154       %--   measuredF(ie) at the same angle r.dir(ia), the power in
155       %--   encounter space is given by
156       %--             pwaveE(ie, ia) * dfm * da
157       %--   So the algorithm is: find ie that corresponds to fe(f)
158       %--   and add the power density suct that the total power is
159       %--   preserved:
160       %--             pwaveE(ie, ia) = pwaveE(ie, ia) + pwave(if, ia)*df/dfe
161       %--   We have to loop over each angle indiviually in the Matlab/Octave implementation
162 -       Nfft = 1024;
163 -       fs   = 8;
164 -       measuredF = (0:Nfft-1)*fs/Nfft;
165 -       measuredF=measuredF(measuredF<.4);
166 -       prollE  = zeros(length(measuredF), length(r.dir));
167 -       ppitchE = prollE;
168 -       pheaveE = prollE;
169 -       psurgeE = prollE;
170 -       pwaveE  = prollE;
171
172 -       g = 9.81;
173 -       q = g/2/pi;
174         % We assume correctly that measuredF has constant spacing, unfortunately
175         % this is not true for the rao frequency axis.
176 -       dfm = measuredF(2)-measuredF(1);
177 -       df  = diff(r.f); df = [df; df(end)];
178
179 -       iemax = length(measuredF);
180 -        tic()
```

```
    for ia = 1:length(r.dir)
       fe    = r.f.*(1-vkts*1852/3600*cos(r.dir(ia)*pi/180)/q*r.f);
       ie    = round(abs(fe)/dfm)+1;
       ie(ie>iemax) = iemax;
         tfr = zeros(length(measuredF), length(r.f));
       for i = 1:length(ie)
          tfr(ie(i), i) = df(i)/dfm;
       end

         pwaveE(:,  ia)  = tfr * pwave(:,ia);
         prollE(:,  ia)  = tfr * proll(:,ia);
         ppitchE(:, ia)  = tfr * ppitch(:,ia);
         pheaveE(:, ia)  = tfr * pheave(:,ia);
         psurgeE(:, ia)  = tfr * psurge(:,ia);
    end % for ia = ...
     toc()

     % calculate the total encounter spectra, density in the wave files
    % are per radian, r.dir is in deg, this is cured by the factor pi/180.
     pwaveEt  = trapz(r.dir, pwaveE, 2)*pi/180;
     prollEt  = trapz(r.dir, prollE, 2)*pi/180;
     ppitchEt = trapz(r.dir, ppitchE, 2)*pi/180;
     pheaveEt = trapz(r.dir, pheaveE, 2)*pi/180;
     psurgeEt = trapz(r.dir, psurgeE, 2)*pi/180;

    %figure(1)
    subplot(2,2,1)
    hndp=plot(measuredF, prollEt, '-');
    xlabel('encounter frequency [Hz]');
    ylabel('PSD [deg^2/Hz]');
    %grid
    set(hndp,'linewidth',2);
    xlim([0 .3]);
    %set(ax(2), 'xtick', []);
    title(tit, 'roll')
    %title([file '    ' date]);

    %figure (2)
    subplot(2,2,2)
    hndp=plot(measuredF, pheaveEt, '-');
    xlabel('encounter frequency [Hz]');
    ylabel('PSD [m^2/Hz]');
    %grid
    set(hndp,'linewidth',2);
    xlim([0 .3]);
```

```
    xlim([0 .3]);
    title(tit,'heave')

    %figure(3)
    subplot(2,2,3)
    hndp=plot(measuredF, ppitchEt, '-');
    xlabel('encounter frequency [Hz]');
    ylabel('PSD [deg^2/Hz]');
    %grid
    set(hndp,'linewidth',2);
    xlim([0 .3]);
    title(tit,'pitch')

    %figure(4)
    subplot(2,2,4)
    hndp=plot(measuredF, psurgeEt, '-');
    xlabel('encounter frequency [Hz]');
    ylabel('PSD [m^2/Hz]');
    %grid
    set(hndp,'linewidth',2);
    xlim([0 .3]);
    title(tit,'surge')
```

UTF-8

W

APPENDIX G: MATLAB CODE FOR VISUAL OBSERVATION

```
% Compute power spectrum
% from single point (visual obs) sea spec
% with Bretschneider spread in frequency
% Adjusted values
%
%
clear
%close all
dtr=pi/180;
format short g

%
% adjusted parameters
alpha_a = 210; % rel. wave heading in [degrees]
Tp_a = 13; % wave peak period in [s]
H13_a=5; % significant wave height
omm_a=2*pi/Tp_a;

% for Bretschneider
BBS_a=5/4*omm_a^4;
ABS_a=BBS_a/4*H13_a^2;
% frequency grid
fs=[0.001:0.001:0.5];
oms=2*pi*fs;
SBS_a=ABS_a./oms.^5.*exp(-BBS_a./oms.^4);
As_a=sqrt(SBS_a);
%
a = 7.5; % ship'speed in [knots]
%a = 8.6; % ship'speed in [knots]
% a = 11.17;
% a = 12;

v = a*1852/3600; % ship'speed in m/s
g  = 9.81;


load('AgulhasNov2018.mat');  % read raos into structures


% choose the proper speed
% (1) = 7; ... (19)= 16

r = rao(2);

[diff angleIndex_a] = min(abs(r.dir-alpha_a));
```

```
47 -    Aroll_a  = As_a.*interp1(r.omega, r.Aroll(:,angleIndex_a), oms);
48 -    Aheave_a = As_a.*interp1(r.omega, r.Aheave(:,angleIndex_a), oms);
49 -    Apitch_a = As_a.*interp1(r.omega, r.Apitch(:,angleIndex_a), oms);
50 -    Asurge_a = As_a.*interp1(r.omega, r.Asurge(:,angleIndex_a), oms);
51
52 -    Scsroll_a = (Aroll_a.^2);
53 -    Scsheave_a = (Aheave_a.^2);
54 -    Scspitch_a = (Apitch_a.^2);
55 -    Scssurge_a = (Asurge_a.^2);
56
57      % transform to encounter freq *oms !!
58 -    Sceroll_a=Scsroll_a./(1-2*oms*cos(alpha_a*dtr)*v/g);
59 -    Sceheave_a=Scsheave_a./(1-2*oms*cos(alpha_a*dtr)*v/g);
60 -    Scepitch_a=Scspitch_a./(1-2*oms*cos(alpha_a*dtr)*v/g);
61 -    Scesurge_a=Scssurge_a./(1-2*oms*cos(alpha_a*dtr)*v/g);
62
63 -    ome_a=oms.*(1-oms*cos(alpha_a*dtr)*v/g);
64 -    fe_a=ome_a/2/pi;
65
66      % as a function of fe, values must be multiplied by 2Pi
67 -    Sceroll_a=Sceroll_a*2*pi;
68 -    Sceheave_a=Sceheave_a*2*pi;
69 -    Scepitch_a=Scepitch_a*2*pi;
70 -    Scesurge_a=Scesurge_a*2*pi;
71
72      % get Chen's spectra
73
74      %load Sm10old.txt
75      %load Sm15old.txt
76      %load Sm24old.txt
77 -    load Sm28old.txt
78      %load Sm36old.txt
79      %load Sm38old.txt
80      %load Sm44old.txt
81      %load Sm55old.txt
82      %load Sm57old.txt
83      %load Sm58old.txt
84      %load Sm59old.txt
85
86 -    Smeas=Sm28old;
87 -    fm=Smeas(1:100,1);
88 -    Smr=Smeas(1:100,2);
89 -    Smp=Smeas(1:100,3);
90 -    Sms=Smeas(1:100,6);
```

Move here

Y

```
Smh=Smeas(1:100,7);
fmi=[0.02:0.001:0.5];
Smri=interp1(fm,Smr,fmi,'cubic');
Smpi=interp1(fm,Smp,fmi,'cubic');
Smsi=interp1(fm,Sms,fmi,'cubic');
Smhi=interp1(fm,Smh,fmi,'cubic');
%
%figure (1)
subplot(2,2,1)
hnda=plot(fe_a,Sceroll_a,'r');
set(hnda,'linewidth',2)
%grid
title('Roll');
xlabel('f [Hz]');
ylabel('deg^2/Hz');
hold off
ax=axis;
ax(2)=0.3;
axis(ax)

%figure (2)
subplot(2,2,2)
hnda=plot(fe_a,Sceheave_a,'r');
set(hnda,'linewidth',2)
%grid
title('Heave');
xlabel('f [Hz]');
ylabel('m^2/Hz');
hold off
ax=axis;
ax(2)=0.3;
axis(ax)

%figure (3)
subplot(2,2,3)
hnda=plot(fe_a,Scepitch_a,'r');
set(hnda,'linewidth',2)
%grid
title('Pitch');
xlabel('f [Hz]');
ylabel('deg^2/Hz');
hold off
ax=axis;
ax(2)=0.3;
```

Z

```
134 -    ax(2)=0.3;
135 -    axis(ax)
136
137      %figure (4)
138 -    subplot(2,2,4)
139 -    hnda=plot(fe_a,Scesurge_a,'r');
140 -    set(hnda,'linewidth',2)
141      %grid
142 -    title('Surge');
143 -    xlabel('f [Hz]');
144 -    ylabel('m^2/Hz');
145 -    hold off
146 -    ax=axis;
147 -    ax(2)=0.3;
148 -    axis(ax)
```

APPENDIX H: MATLAB CODE FOR SHIP MOTION FROM SENSOR

```
% compute motion spectra

%
clear
%close all
dtr=pi/180;
format short g
%
% get Chen's spectra

%load Sm10old.txt
%load Sm15old.txt
%load Sm24old.txt
load Sm28old.txt
%load Sm36old.txt
%load Sm38old.txt
%load Sm44old.txt
%load Sm55old.txt
%load Sm57old.txt
%load Sm58old.txt
%load Sm59old.txt

Smeas=Sm28old;
fm=Smeas(1:100,1);
Smr=Smeas(1:100,2);
Smp=Smeas(1:100,3);
Sms=Smeas(1:100,6);
Smh=Smeas(1:100,7);
fmi=[0.02:0.001:0.5];
Smri=interp1(fm,Smr,fmi,'cubic');
Smpi=interp1(fm,Smp,fmi,'cubic');
Smsi=interp1(fm,Sms,fmi,'cubic');
Smhi=interp1(fm,Smh,fmi,'cubic');
%
%figure (1)
subplot(2,2,1)
hndm=plot(fmi,Smri);
set(hndm,'linewidth',2)
%grid
title('Roll');
xlabel('f [Hz]');
ylabel('deg^2/Hz');
hold off
ax=axis;
ax(2)=0.3;
```

```
    axis(ax)

    %figure (2)
    subplot(2,2,2)
    hndm=plot(fmi,Smhi);
    set(hndm,'linewidth',2)
    %grid
    title('Heave');
    xlabel('f [Hz]');
    ylabel('m^2/Hz');
    hold off
    ax=axis;
    ax(2)=0.3;
    axis(ax)

    %figure (3)
    subplot(2,2,3)
    hndm=plot(fmi,Smpi);
    set(hndm,'linewidth',2)
    %grid
    title('Pitch');
    xlabel('f [Hz]');
    ylabel('m^2/Hz');
    hold off
    ax=axis;
    ax(2)=0.3;
    axis(ax)

    %figure (4)
    subplot(2,2,4)
    hndm=plot(fmi,Smsi,'linewidth',2);
    %set(hndm,'linewidth',2)
    %grid
    title('Surge');
    xlabel('f [Hz]');
    ylabel('m^2/Hz');
    hold off
    ax=axis;
    ax(2)=0.3;
    axis(ax)

```

APPENDIX I: MATLAB CODE - ECMWF COMPARISON

```
% here mit transfermatrix, RAO-plotter, dimensionalisiert ungefragt
more off
clear
hasOctave = 0;

load('output_spectra_SAAGHii.mat');

load('AgulhasNov2018.mat');

if hasOctave
   source('raoplotter2Main.m');
end

fprintf('-------------------------------------------------------------\n');
% Now we have:
%   -- days:     a list of dates in Matlab format
%   -- d(i).f:   list of frequencies for entry i (30x1)
%   -- d(i).dir: wave direction 'where waves are going to' in degrees. (24x1)
%   -- d(i).pwr: matrix with wave powers. Lines frequency, columns direction
%                (30x24)

% Parameter for the experiment, choose one in the switch statement
switch 1
   case 1
      file = 'Sm28old';
      vkts = 7.49;
      hdg  = 310; % real 310
      date = '5.7.2017 8:00';
      days = datenum(date, 'dd.mm.yyyy HH:MM');
   case 2
      file = 'Sm15old';
      vkts = 16.7; hdg = 160; % real 160
      date = '1.7.2017 19:09';
      days = datenum(date, 'dd.mm.yyyy HH:MM');
   case 3
      file = 'Sm10old';
      vkts = 8.7; hdg = 220;
      date = '30.6.2017 9:43';
      days = datenum(date, 'dd.mm.yyyy HH:MM');
   case 4
      file = 'Sm55old';
      vkts = 15.7; hdg = 304;
      date = '11.7.2017 14:42';
      days = datenum(date, 'dd.mm.yyyy HH:MM');
   case 5
```

```
        file = 'Sm57old';
        vkts = 13.5; hdg = 307;
        date = '12.7.2017 06:56';
        days = datenum(date, 'dd.mm.yyyy HH:MM');
    case 6
        file = 'Sm58old';
        vkts = 13.7; hdg = 307;
        date = '12.7.2017 10:20';
        days = datenum(date, 'dd.mm.yyyy HH:MM');
    case 7
        file = 'Sm59old';
        vkts = 13.0; hdg = 307;
        date = '12.7.2017 15:05';
        days = datenum(date, 'dd.mm.yyyy HH:MM');
    otherwise
        error('wrong selection');
end
    Smeas = load([file '.txt']);

%-- Dimensionalize RAOs and make a list of speeds
    ktslist = [];
    for i=1:length(rao);
         ktslist = [ktslist rao(i).kts];
    end;

%-- select data: r for rao, spek for wave spectrum

    [trash iKts] = min(abs(ktslist-vkts));
    r = rao(iKts);
    fprintf('using rao %.2fkts for speed %.2fkts\n', r.kts, vkts);

    [trash i] = min(abs(dayslist-days));
    fprintf('using spectrum %s for experiment %s\n', datestr(dayslist(i), 0), datestr(days,0));

    wave = d(i);

%-- Interpolate the spectrum to rao angles and dir
  % Linear interpolation in 2d doesn't extrapolate, splines make nonsens.
  % Therefore two 1d-interpolations are used. interp1 interpolates on each column.
  % On the fly we transform to seaway convention, the relative angle is
  %                  hdg-whereWavesAreGoingTo.
  % The relative angles are sorted for proper interpolation:
      relAngle = rem(hdg - wave.dir+360, 360);
      [relAngle idx] = sort(relAngle);
      pwave = wave.pwr(:,idx);
```

Move here to reveal toolstrip

```
91 -          pwave = interp1(relAngle', pwave', r.dir, 'linear', 'extrap')';
92
93        % and interpolate to seastate frequencies
94 -          r.f = r.omega/2/pi;
95 -          pwave  = interp1(wave.f,   pwave, r.f,   'linear', 'extrap');
96
97        % check if power got lost
98 -       ptotalSaa    = trapz(wave.f, trapz(wave.dir*pi/180, wave.pwr, 2));
99 -       ptotalInterp = trapz(r.f, trapz(r.dir*pi/180, pwave,2));
100 -      fprintf('Total power Saa: %f, Interp %f\n', ptotalSaa, ptotalInterp);
101       % check the amount of negative power due to interpolation
102 -      fprintf('Sum of (not integral of) power %f negative power %f\n', ...
103 -         sum(sum(pwave)), sum(pwave(pwave<0)));
104       % Well:
105 -      pwave(pwave<0) = 0;
106
107 -      [trash iDir] = max(sum(pwave,1)); dir = r.dir(iDir);
108 -      [trash i]    = max(sum(pwave,2)); T0  = 1/(r.f(i));
109       %   tit = sprintf('%s %s, %2.1f kts, rdir %4.0f, T0 = %4.1fs', ...
110       %       file, date, vkts, dir, T0);
111 -      tit = sprintf('%s, %2.1f kts,', ...
112 -         date, vkts);
113
114 -      if hasOctave
115 -         raoplotter2CB(iDir, iKts, 11);
116 -      end
117
118       % doesn't work in matlab
119 -      if hasOctave
120 -          figure(1);
121 -          drawPowerdistributionTrueAngle(wave.f, wave.dir'+180, wave.pwr, hdg, hdg+180-dir, 'spek(fseastate)');
122 -          title(tit)
123
124 -          figure(2);
125 -          drawPowerdistribution2(r.f, r.dir, pwave, hdg, hdg+180-dir, 'interpolated(fseastate)');
126           % don't show the mean wave direction
127           %set(findall(2, 'tag', 'arrow'),'visible', 'on');
128 -          title(tit)
129 -      end
130       %--   Calculate the motion spectra as a function of sea state frequency
131 -      proll  = pwave.*r.Aroll.^2;
132 -      ppitch = pwave.*r.Apitch.^2;
133 -      pheave = pwave.*r.Aheave.^2;
134 -      psurge = pwave.*r.Asurge.^2;
135
```

FF

```
136 -       if 0
137 -           figure(3);
138 -           clf('reset')
139 -           drawPowerdistribution2(r.f, r.dir, proll, hdg, hdg+180-dir, 'roll motion(seastate)');
140             % don't show the mean wave direction
141             %set(findall(2, 'tag', 'arrow'),'visible', 'off');
142 -           title(tit)
143 -       end
144
145     %--   Transform to encounter.
146     %--   We have the power density pwave(if, ia) for the
147     %--   frequency r.f(if) and the angle r.dir(ia). We
148     %--   construct the encounter spectrum pwaveE(ie, ia)
149     %--   on a different frequency axis measuredF(ie).
150     %--   The wave power in a certain bin in sea state space is
151     %--             pwave(if, ia) * df * da
152     %--   This power is transferred to different encounter frequency
153     %--   measuredF(ie) at the same angle r.dir(ia), the power in
154     %--   encounter space is given by
155     %--             pwaveE(ie, ia) * dfm * da
156     %--   So the algorithm is: find ie that corresponds to fe(f)
157     %--   and add the power density suct that the total power is
158     %--   preserved:
159     %--             pwaveE(ie, ia) = pwaveE(ie, ia) + pwave(if, ia)*df/dfe
160     %--   We have to loop over each angle indiviually in the Matlab/Octave implementation
161 -       Nfft = 1024;
162 -       fs   = 8;
163 -       measuredF = (0:Nfft-1)*fs/Nfft;
164 -       measuredF=measuredF(measuredF<.4);
165 -       prollE  = zeros(length(measuredF), length(r.dir));
166 -       ppitchE = prollE;
167 -       pheaveE = prollE;
168 -       psurgeE = prollE;
169 -       pwaveE  = prollE;
170
171 -       g = 9.81;
172 -       q = g/2/pi;
173         % We assume correctly that measuredF has constant spacing, unfortunately
174         % this is not true for the rao frequency axis.
175 -       dfm = measuredF(2)-measuredF(1);
176 -       df  = diff(r.f); df = [df; df(end)];
177
178 -       iemax = length(measuredF);
179 -        tic()
180 -       for ia = 1:length(r.dir)
```

Move here to reveal toolstrip

GG

```
for ia = 1:length(r.dir)
   fe    = r.f.*(1-vkts*1852/3600*cos(r.dir(ia)*pi/180)/q*r.f);
   ie    = round(abs(fe)/dfm)+1;
   ie(ie>iemax) = iemax;
     tfr = zeros(length(measuredF), length(r.f));
   for i = 1:length(ie)
      tfr(ie(i), i) = df(i)/dfm;
   end

     pwaveE(:,  ia)  = tfr * pwave(:,ia);
     prollE(:,  ia)  = tfr * proll(:,ia);
     ppitchE(:, ia)  = tfr * ppitch(:,ia);
     pheaveE(:, ia)  = tfr * pheave(:,ia);
     psurgeE(:, ia)  = tfr * psurge(:,ia);
end % for ia = ...
 toc()

 % calculate the total encounter spectra, density in the wave files
% are per radian, r.dir is in deg, this is cured by the factor pi/180.
 pwaveEt  = trapz(r.dir, pwaveE, 2)*pi/180;
 prollEt  = trapz(r.dir, prollE, 2)*pi/180;
 ppitchEt = trapz(r.dir, ppitchE, 2)*pi/180;
 pheaveEt = trapz(r.dir, pheaveE, 2)*pi/180;
 psurgeEt = trapz(r.dir, psurgeE, 2)*pi/180;

%figure(1)
subplot(2,2,1);
hold off
%[ax h1 h2] = plotyy(measuredF, prollEt, measuredF, pwaveEt);
%set(h1, 'marker', '+');
%set(h2,    'color', [.5 .5 .5]);
%set(ax(2), 'ycolor', [.5 .5 .5]);
hndm=plot(Smeas(:,1), Smeas(:,2), '-');
hold on
hndp=plot(measuredF, prollEt, '-');
legend('motion measured', 'predicted');
xlabel('encounter frequency [Hz]');
ylabel('PSD [deg^2/Hz]');
%grid
set(hndm,'linewidth',2);
set(hndp,'linewidth',2);
xlim([0 .3]);
%set(ax(2), 'xtick', []);
title(tit,'Roll')
%title([file '   ' date]);
```

HH

```
226         %figure (2)
227 -       subplot(2,2,2);
228 -       hold off
229 -       hndm=plot(Smeas(:,1), Smeas(:,7), '-');
230 -       hold on
231 -       hndp=plot(measuredF, pheaveEt, '-');
232 -       legend('motion measured', 'predicted');
233 -       xlabel('encounter frequency [Hz]');
234 -       ylabel('PSD [m^2/Hz]');
235         %grid
236 -       set(hndm,'linewidth',2);
237 -       set(hndp,'linewidth',2);
238 -       xlim([0 .3]);
239 -       title(tit,'Heave')
240
241         %figure(3)
242 -       subplot(2,2,3);
243 -       hold off
244 -       hndm=plot(Smeas(:,1), Smeas(:,3), '-');
245 -       hold on
246 -       hndp=plot(measuredF, ppitchEt, '-');
247 -       legend('motion measured', 'predicted');
248 -       xlabel('encounter frequency [Hz]');
249 -       ylabel('PSD [deg^2/Hz]');
250         %grid
251 -       set(hndm,'linewidth',2);
252 -       set(hndp,'linewidth',2);
253 -       xlim([0 .3]);
254 -       title(tit,'Pitch')
255
256         %figure(4)
257 -       subplot(2,2,4);
258 -       hold off
259 -       hndm=plot(Smeas(:,1), Smeas(:,6), '-');
260 -       hold on
261 -       hndp=plot(measuredF, psurgeEt, '-');
262 -       legend('motion measured', 'predicted');
263 -       xlabel('encounter frequency [Hz]');
264 -       ylabel('PSD [m^2/Hz]');
265         %grid
266 -       set(hndm,'linewidth',2);
267 -       set(hndp,'linewidth',2);
268 -       xlim([0 .3]);
269 -       title(tit,'Surge')
270
271
```

APPENDIX J: MATLAB CODE - VISUAL OBSERVATION COMPARISON

```
% compute motion spectra
% from single point (visual obs) sea spec
% with Bretschneider spread in frequency
%
% compare measured spectrum with two computed ones
%
clear
%close all
dtr=pi/180;
format short g
%
% original observation
alpha_o = 195; % rel. wave heading in [degrees]
Tp_o = 11; % wave peak period in [s]
H13_o=7; % significant wave height
omm_o=2*pi/Tp_o;

% for Bretschneider
BBS_o=5/4*omm_o^4;
ABS_o=BBS_o/4*H13_o^2;
% frequency grid
fs=[0.001:0.001:0.5];
oms=2*pi*fs;
SBS_o=ABS_o./oms.^5.*exp(-BBS_o./oms.^4);
As_o=sqrt(SBS_o);
%
% adjusted parameters
alpha_a = 210; % rel. wave heading in [degrees]
Tp_a = 13; % wave peak period in [s]
H13_a=5; % significant wave height
omm_a=2*pi/Tp_a;

% for Bretschneider
BBS_a=5/4*omm_a^4;
ABS_a=BBS_a/4*H13_a^2;
% frequency grid
fs=[0.001:0.001:0.5];
oms=2*pi*fs;
SBS_a=ABS_a./oms.^5.*exp(-BBS_a./oms.^4);
As_a=sqrt(SBS_a);
%
a = 10; % ship'speed in [knots]
%a = 8.6; % ship'speed in [knots]
% a = 11.17;
% a = 12;
```

```
46
47 -    v = a*1852/3600; % ship'speed in m/s
48 -    g  = 9.81;
49
50     %load('Agulhas6bNB.mat');  % read raos into structures
51 -    load('AgulhasNov2018.mat');  % read raos into structures
52     %load('AgulhasFeb19C_7,5kts.mat'); % read raos into structures
53     %load('AgulhasFeb19C_7,5kts.mat'); % read raos into structures
54
55     % choose the proper speed
56     % (1) = 7; ... (11)= 12
57
58 -    r = rao(8);
59
60
61 -    [diff angleIndex_o] = min(abs(r.dir-alpha_o));
62
63 -    Aroll_o  = As_o.*interp1(r.omega, r.Aroll(:,angleIndex_o), oms);
64 -    Aheave_o = As_o.*interp1(r.omega, r.Aheave(:,angleIndex_o), oms);
65 -    Apitch_o = As_o.*interp1(r.omega, r.Apitch(:,angleIndex_o), oms);
66 -    Asurge_o = As_o.*interp1(r.omega, r.Asurge(:,angleIndex_o), oms);
67
68 -    Scsroll_o = (Aroll_o.^2);
69 -    Scsheave_o = (Aheave_o.^2);
70 -    Scspitch_o = (Apitch_o.^2);
71 -    Scssurge_o = (Asurge_o.^2);
72
73     % transform to encounter freq *oms !!
74 -    Sceroll_o=Scsroll_o./(1-2*oms*cos(alpha_o*dtr)*v/g);
75 -    Sceheave_o=Scsheave_o./(1-2*oms*cos(alpha_o*dtr)*v/g);
76 -    Scepitch_o=Scspitch_o./(1-2*oms*cos(alpha_o*dtr)*v/g);
77 -    Scesurge_o=Scssurge_o./(1-2*oms*cos(alpha_o*dtr)*v/g);
78
79 -    ome_o=oms.*(1-oms*cos(alpha_o*dtr)*v/g);
80 -    fe_o=ome_o/2/pi;
81
82     % as a function of fe, values must be multiplied by 2Pi
83 -    Sceroll_o=Sceroll_o*2*pi;
84 -    Sceheave_o=Sceheave_o*2*pi;
85 -    Scepitch_o=Scepitch_o*2*pi;
86 -    Scesurge_o=Scesurge_o*2*pi;
87
88 -    [diff angleIndex_a] = min(abs(r.dir-alpha_a));
89
90 -    Aroll_a  = As_a.*interp1(r.omega, r.Aroll(:,angleIndex_a), oms);
```

KK

```
92 -    Apitch_a = As_a.*interp1(r.omega, r.Apitch(:,angleIndex_a), oms);
93 -    Asurge_a = As_a.*interp1(r.omega, r.Asurge(:,angleIndex_a), oms);
94
95 -    Scsroll_a = (Aroll_a.^2);
96 -    Scsheave_a = (Aheave_a.^2);
97 -    Scspitch_a = (Apitch_a.^2);
98 -    Scssurge_a = (Asurge_a.^2);
99
100     % transform to encounter freq *oms !!
101 -    Sceroll_a=Scsroll_a./(1-2*oms*cos(alpha_a*dtr)*v/g);
102 -    Sceheave_a=Scsheave_a./(1-2*oms*cos(alpha_a*dtr)*v/g);
103 -    Scepitch_a=Scspitch_a./(1-2*oms*cos(alpha_a*dtr)*v/g);
104 -    Scesurge_a=Scssurge_a./(1-2*oms*cos(alpha_a*dtr)*v/g);
105
106 -    ome_a=oms.*(1-oms*cos(alpha_a*dtr)*v/g);
107 -    fe_a=ome_a/2/pi;
108
109     % as a function of fe, values must be multiplied by 2Pi
110 -    Sceroll_a=Sceroll_a*2*pi;
111 -    Sceheave_a=Sceheave_a*2*pi;
112 -    Scepitch_a=Scepitch_a*2*pi;
113 -    Scesurge_a=Scesurge_a*2*pi;
114
115     % get Chen's spectra
116     %load Sm10old.txt
117     %load Sm15old.txt
118     %load Sm24old.txt
119     %load Sm28old.txt
120     %load Sm36old.txt
121     %load Sm44old.txt
122     %load Sm55old.txt
123     %load Sm57old.txt
124     %load Sm58old.txt
125     %load Sm59old.txt
126 -    load Sm38old.txt
```

```
    Smeas=Sm38old;
    fm=Smeas(1:100,1);
    Smr=Smeas(1:100,2);
    Smp=Smeas(1:100,3);
    Sms=Smeas(1:100,6);
    Smh=Smeas(1:100,7);
    fmi=[0.02:0.001:0.5];
    Smri=interp1(fm,Smr,fmi,'cubic');
    Smpi=interp1(fm,Smp,fmi,'cubic');
    Smsi=interp1(fm,Sms,fmi,'cubic');
    Smhi=interp1(fm,Smh,fmi,'cubic');
    %
    %figure (1)

    subplot(2,2,1)
    hndo=plot(fe_o,Sceroll_o,'g');
    hold on
    hnda=plot(fe_a,Sceroll_a,'r');
    hndm=plot(fmi,Smri);
    set(hndo,'linewidth',2)
    set(hnda,'linewidth',2)
    set(hndm,'linewidth',2)
    %grid
    title('roll');
    xlabel('f [Hz]');
    ylabel('deg^2/Hz');
    hold off
    ax=axis;
    ax(2)=0.3;
    axis(ax)
    legend('calc. as recorded','calc. modified','measured');

    %figure (2)

    subplot(2,2,2)
    hndo=plot(fe_o,Sceheave_o,'g');
    hold on
    hnda=plot(fe_a,Sceheave_a,'r');
    hndm=plot(fmi,Smhi);
    set(hndo,'linewidth',2)
    set(hnda,'linewidth',2)
    set(hndm,'linewidth',2)
    %grid
    title('heave');
```

```
172 -    xlabel('f [Hz]');
173 -    ylabel('m^2/Hz');
174 -    hold off
175 -    ax=axis;
176 -    ax(2)=0.3;
177 -    axis(ax)
178 -    legend('calc. as recorded','calc. modified','measured');
179
180      %figure (3)
181
182 -    subplot(2,2,3)
183 -    hndo=plot(fe_o,Scepitch_o,'g');
184 -    hold on
185 -    hnda=plot(fe_a,Scepitch_a,'r');
186 -    hndm=plot(fmi,Smpi);
187 -    set(hndo,'linewidth',2)
188 -    set(hnda,'linewidth',2)
189 -    set(hndm,'linewidth',2)
190      %grid
191 -    title('pitch');
192 -    xlabel('f [Hz]');
193 -    ylabel('deg^2/Hz');
194 -    hold off
195 -    ax=axis;
196 -    ax(2)=0.3;
197 -    axis(ax)
198 -    legend('calc. as recorded','calc. modified','measured');
199
200      %figure (4)
201
202 -    subplot(2,2,4)
203 -    plot(fe_o,Scesurge_o,'g','linewidth',2);
204 -    hold on
205 -    hnda=plot(fe_a,Scesurge_a,'r');
206 -    hndm=plot(fmi,Smsi);
207 -    set(hnda,'linewidth',2)
208 -    set(hndm,'linewidth',2)
209      %grid
210 -    title('surge');
211 -    xlabel('f [Hz]');
212 -    ylabel('m^2/Hz');
213 -    hold off
214 -    ax=axis;
215 -    ax(2)=0.3;
216 -    axis(ax)
217 -    legend('calc. as recorded','calc. modified','measured');
```